

Technische Universität München

Fakultät für Chemie

WACKER-Lehrstuhl für Makromolekulare Chemie

**Novel Single-Site Catalysts for the Polymerization
of Polar Monomers – From Aliphatic Poly(ester)s to
Poly(vinylpyridine)s**

Alexander Kronast

Vollständiger Abdruck der von der Fakultät für Chemie der Technischen Universität München zur Erlangung des akademischen Grades eines

Doktors der Naturwissenschaften

genehmigten Dissertation.

Vorsitzender: Prof. Dr. Kai-Olaf Hinrichsen

Prüfer der Dissertation: 1. Prof. Dr. Dr. h.c. Bernhard Rieger

2. Prof. Dr. Fritz E. Kühn

Die Dissertation wurde am 14.02.2017 bei der Technischen Universität München eingereicht und durch die Fakultät für Chemie am 13.03.2017 angenommen.

"Die Wissenschaft fängt eigentlich erst da an interessant zu werden,
wo sie aufhört."

Justus von Liebig

Die vorliegende Arbeit wurde in der Zeit von April 2013 bis April 2016 am WACKER-Lehrstuhl für Makromolekulare Chemie, Technische Universität München, unter Betreuung von Herrn Prof. Dr. Dr. h.c. Bernhard Rieger angefertigt.

I. Acknowledgements

Mein besonderer Dank gilt meinem Doktorvater Herrn **Prof. Dr. Dr. h.c. Bernhard Rieger** für die freundliche Aufnahme in seine Arbeitsgruppe, die herausfordernde Themenstellung und das entgegengebrachte Vertrauen. Im Speziellen danke ich Ihnen für die Förderung einer eigenverantwortlichen Arbeitsweise, auch oder gerade in Industriekooperationen, die vielen fruchtbaren Diskussionen und nicht zuletzt die großartige Vorbereitung auf die bevorstehenden Aufgaben in der chemischen Industrie.

Zusätzlich gebührt mein Dank **Dr. Carsten Troll** und **Dr. Sergei Vagin** für die unermüdlichen Anstrengungen in der Organisation des Lehrstuhls, der Aufrechterhaltung der hervorragenden technischen Ausstattung und die vielen chemischen Diskussionen während meiner Zeit am Lehrstuhl. **Sabine Saul-Hubrich** und **Annette Bauer** danke ich für die Hilfe bei organisatorischen Problemen aller Art.

Der **BASF SE** gilt mein Dank für die Finanzierung meiner Arbeit. Im Speziellen danke ich **Dr. Robert Loos** und **Dr. Peter Deglmann** für die Zusammenarbeit während des PHB-Projekts und die interessanten Diskussionen, sowie die möglichen Einblicke in die Arbeit eines Forschers im größten Chemieunternehmen der Welt.

Allen ehemaligen Kollegen vom WACKER-Lehrstuhl für Makromolekulare Chemie danke ich für die entspannte Arbeitsatmosphäre und die stets gute Zusammenarbeit. Hervorheben möchte ich dabei die folgenden Personen, welche mit fachlichen Diskussionen, auflockernden Gesprächen und Hilfe jeglicher Art die Zeit am Lehrstuhl zu dem gemacht haben, was sie war: **Richard Reithmeier, Stefan Kissling, Marina Reiter, Ignaz Höhle, Peter Altenbuchner, Benedikt Soller, Patrick Werz, Rike Adams, Christina Schwarzenböck** und **Nicole Zollbrecht**. **Peter** und **Benedikt** gilt dabei mein besonderer Dank für viele hilfreiche Diskussionen, das Korrekturlesen dieser Arbeit, wie auch für die andauernden Duelle auf dem Squash Court.

Den Studenten, Bacheloranden und Masteranden, welche ich während meiner Zeit am Lehrstuhl betreuen durfte, danke ich für Ihren Einsatz, der diese Arbeit zum Teil in großen Schritten mit vorangetrieben hat: meinen Forschungspraktikanten **Zeyneb Karatas, Fabian Herz** und **Sebastian Kernbichl**, meiner Bachelorandin **Sandra Wenisch** und meinen Masteranden **Christian Schwaferts** und **Dominik Reiter**.

Folgenden Kollegen aus anderen Lehrstühlen danke ich für Ihre Unterstützung in analytischen Fragen und die Durchführung verschiedener Analysen: **Dr. Alexander Pöthig** für die Einkristallröntgenstrukturanalyse, dem Team des Elementaranalyselabors, insbesondere **Ulrike Ammari**, **Maria Weindl** für Hoch- und Tieftemperatur NMR-Messungen und den Lehrstühlen für Technische Chemie I und II für BET-Messungen an mehr oder weniger porösen Festkörpern.

Großer Dank gilt meinen Freunden, die trotz deutlich verkürzter gemeinsamer Zeiten einen wichtigen Rückhalt für mich dargestellt haben. Im Besonderen möchte ich mich dabei bei **Korbinian Randlinger** und **Peter Schmitz** bedanken.

Meinem Bruder, meinen Eltern und meinen Großeltern danke ich für ihre große Unterstützung während des gesamten Studiums und der Promotion. Ohne euch und euren Rückhalt würde es die folgenden Seiten heute nicht geben.

Meiner Freundin **Stephanie Weicker** gilt mein größter Dank für ihre Geduld, die aufmunternden Worte, ihre Rücksicht während der letzten Jahre und dafür, dass sie nicht aufgehört hat an mich zu glauben.

II. Table of Contents

I.	Acknowledgements	I
II.	Table of Contents	III
III.	List of Abbreviations	V
1.	Introduction	1
1.1	The European chemical industry: A journey through rough waters	1
1.2	Catalysis in Polymer Chemistry: From the supply of simple raw materials to functional solutions	5
2.	Ring-opening Polymerization of Lactones toward Biodegradable Poly(ester)s	7
2.1	Tacticity in the Catalytic Ring-opening Polymerization of Lactones	10
2.2	Metal Based Single-Site Catalysts for the Ring-opening Polymerization of (rac)- β -butyrolactone and (rac)-lactide	12
2.3	Objective: Development of new, highly active Zinc Based Catalysts for the Stereoselective Ring-opening Polymerization of Cyclic Esters	15
3.	Rare Earth Metal-mediated Group Transfer Polymerization of 2-Vinylpyridine	17
3.1	Rare Earth Metal-based Catalysts in the Group Transfer Polymerization of Michael Monomers	17
3.2	Stereospecific Polymerization of Michael-type Monomers	23
3.3	Objective: Development of highly defined and stereoselective Single-Site Catalysts for the REM-GTP of 2-Vinylpyridine	25
4.	Results – Publications	26
4.1	Electron-deficient β -Diiminato-Zinc-Ethyl Complexes: Synthesis, Structure, and Reactivity in Ring-opening Polymerization of Lactones	26
4.2	Manuscript: Electron-deficient β -Diiminato-Zinc-Ethyl Complexes: Synthesis, Structure, and Reactivity in Ring-opening Polymerization of Lactones	28
4.3	2-Methoxyethylamino-bis(phenolate) yttrium catalysts for the synthesis of highly isotactic poly(2-vinylpyridine) by rare-earth metal-mediated group transfer polymerization	35
4.4	Manuscript: 2-Methoxyethylamino-bis(phenolate) yttrium catalysts for the synthesis of highly isotactic poly(2-vinylpyridine) by rare-earth metal-mediated group transfer polymerization	37
5.	Summary and Outlook	46
6.	Appendix	50
6.1	Publications beyond the Scope of this Thesis	50
6.1.1	Gated Channels and Selectivity Tuning of CO ₂ over N ₂ Sorption by Post-Synthetic Modification of a UiO-66-type MOF	50
6.1.2	Functionalization of Metal–Organic Frameworks through the Postsynthetic Transformation of Olefin Side Groups	61

6.1.3	Mechanistic Investigations of the Stereoselective Rare Earth Metal-Mediated Ring-Opening Polymerization of β -Butyrolactone	63
6.1.4	In Situ Generated ABA Block Copolymers from CO ₂ , Cyclohexene Oxide, and Poly(dimethylsiloxane)s	65
6.1.5	Template mediated and solvent-free route to a variety of UiO-66 metal-organic frameworks	66
6.1.6	Stereospecific catalytic precision polymerization of 2-vinylpyridine via rare earth metal-mediated group transfer polymerization with 2-methoxyethylamino-bis(phenolate)-yttrium complexes	67
6.1.7	New Insights into the Ring-opening Polymerization of β -Butyrolactone Catalyzed by Chromium(III) Salphen Complexes	68
6.1.8	Dinuclear zinc catalysts with unprecedented activities for the copolymerization of cyclohexene oxide and CO ₂	70
6.1.9	Versatile 2-Methoxyethylaminobis(phenolate)yttrium Catalysts: Catalytic Precision Polymerization of Polar Monomers via Rare Earth Metal-Mediated Group Transfer Polymerization	71
6.1.10	Next Generation Multiresponsive Nanocarriers for Targeted Drug Delivery to Cancer Cells	73
6.2	Extended Synthetic Procedures and Analytical Data – Supplementary Informations	75
6.2.1	Electron-Deficient β -Diiminato-Zinc-Ethyl Complexes: Synthesis, Structure, and Reactivity in Ring-Opening Polymerization of Lactones	75
6.2.2	2-Methoxyethylamino-bis(phenolate) yttrium catalysts for the synthesis of highly isotactic poly(2-vinylpyridine) by rare-earth metal-mediated group transfer polymerization	91
6.2.3	Gated Channels and Selectivity Tuning of CO ₂ over N ₂ Sorption by Post-Synthetic Modification of a UiO-66-type MOF	105
6.3	Reprint Permissions	120
6.3.1	Electron-Deficient β -Diiminato-Zinc-Ethyl Complexes: Synthesis, Structure, and Reactivity in Ring-Opening Polymerization of Lactones	120
6.3.2	2-Methoxyethylamino-bis(phenolate) yttrium catalysts for the synthesis of highly isotactic poly(2-vinylpyridine) by rare-earth metal-mediated group transfer polymerization	121
6.3.3	Gated Channels and Selectivity Tuning of CO ₂ over N ₂ Sorption by Post-Synthetic Modification of a UiO-66-type MOF	122
7.	Literature	123

III. List of Abbreviations

2VP	<i>2-Vinylpyridine</i>
<i>at</i>	<i>Atactic</i>
BDC	<i>Benzene dicarboxylic acid</i>
BDI	<i>β-Diiminato</i>
BET	<i>Brunauer-Emmett-Teller</i>
BL	<i>β-Butyrolactone</i>
CA	<i>Conjugate addition</i>
Cp	<i>Cyclopentadienyl</i>
Cp*	<i>1,2,3,4,5-Pentamethyl-cyclopentadienyl</i>
DAVP	<i>Dialkyl vinylphosphonate</i>
DEVP	<i>Diethyl vinylphosphonate</i>
DMAA	<i>N,N-Dimethyl acrylamide</i>
DMDO	<i>Dimethyl dioxirane</i>
DSC	<i>Differential Scanning Calorimetry</i>
<i>e.g.</i>	<i>For example</i>
EA	<i>Elemental Analysis</i>
ESI-MS	<i>Electron-Spray Ionization - Mass Spectroscopy</i>
Et	<i>Ethyl</i>
EWG	<i>Electron-withdrawing group</i>
GDP	<i>Gross domestic product</i>
GPC	<i>Gel Permeation Chromatography</i>
GTP	<i>Group Transfer Polymerization</i>
h	<i>Hour</i>
HPPO	<i>Hydrogen peroxide propylene oxide</i>
<i>i, it, iso</i>	<i>Isotactic</i>
<i>I*</i>	<i>Initiator efficiency</i>
IPOx	<i>iso-Propenyloxazoline</i>

<i>ⁱPr</i>	<i>iso-Propyl</i>
IUPAC	<i>International Union of Pure and Applied Chemistry</i>
LA	<i>Lactide</i>
LCST	<i>Lower Critical Solution Temperature</i>
<i>m</i>	<i>Meso</i>
MA	<i>Meth acrylate</i>
Me	<i>Methyl</i>
MI	<i>Migratory insertion</i>
MMA	<i>Methyl methacrylate</i>
M_n	<i>Number average molar mass</i>
MOF	<i>Metal Organic Framework</i>
MTP	<i>Methanol to propylene</i>
M_w	<i>Mass average molar mass</i>
NAFTA	<i>North American Free Trade Agreement</i>
<i>n</i> Bu	<i>n-Butyl</i>
NMP	<i>Nitroxide Mediated Polymerization</i>
NMR	<i>Nuclear Magnetic Resonance</i>
Nu	<i>Nucleophile</i>
PDI	<i>Polydispersity</i>
PHB	<i>Poly(3-hydroxybutyrate)</i>
PLA	<i>Poly(lactide)</i>
P_m	<i>propability of meso linkage</i>
PP	<i>Poly(propylene)</i>
P_r	<i>Propability of racemic linkage</i>
PSM	<i>Post-Synthetic Modification</i>
<i>r, rac</i>	<i>Racemic</i>
RAFT	<i>Reversible Addition-Fragmentation Chain Transfer</i>
ROP	<i>Ring-opening polymerization</i>

s	<i>Second</i>
SKA	<i>Silyl Ketene Acetal</i>
<i>syndio, st</i>	<i>Syndiotactic</i>
^t Bu	<i>tert-Butyl</i>
T _c	<i>Crystallization temperature</i>
TDC	<i>Triptycene dicarbocyclic acid</i>
T _g	<i>Glass transition temperature</i>
TGA	<i>Thermogravimetric Analysis</i>
THF	<i>Tetrahydrofuran</i>
T _m	<i>Melting temperature</i>
TOF	<i>Turn Over Frequency</i>
TOF*	<i>Normalized Turn Over Frequency</i>
T _p	<i>Polymerization temperature</i>
UiO	<i>University of Oslo</i>
UV	<i>Ultra Violet</i>
XRD	<i>X-Ray Diffraction</i>

1. Introduction

1.1 The European chemical industry: A journey through rough waters

The industry in Europe and North America experiences the largest change in its history through economic growth, market opportunities abroad, and value chain movement to Asia. Most of the value is not created anymore in western countries of Europe or North America but in the eastern hemisphere and thereof especially in China and India, where gross domestic product (GDP) growth rates are still double as high as in the western hemisphere (**Figure 1**).

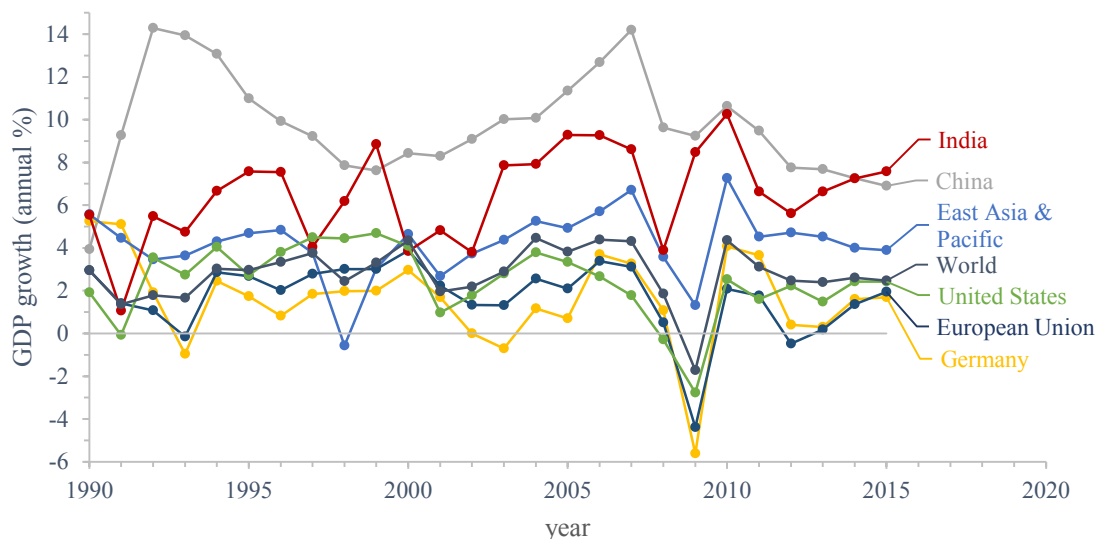


Figure 1. Economic growth rates (GDP) over the last 25 years based on worldbank.org search results (accessed on April 26th, 2016).

The prevailing markets for chemical products are no more located close to the European global players' headquarters but rise in a round trip around the globe. Although the Chinese market does not provide growth rates of up to 15% per year anymore, as it was used to in the near past (2007), it grew to the number one chemical sales country in the world with a major lead (**Figure 1**).

In 2014, the overall chemical sales were calculated to be 3,232 billion € and China holds a market share of 1,111 billion €, what equates with over one third of the overall sales in value terms.^[1] This is even more than the market share of the European (551 billion €) and the NAFTA (North American Free Trade Agreement; 528 billion €) countries together. A trend is becoming apparent that this gap widens further in the next

decades through predicted economic growth rates of 1% for Europe and 3% for Chinese sales.^[2] On a long term the energy-intensity of the chemical industry is another major drawback for the European producers, especially in times where the US players benefit of the shale gas revolution on the North-American continent creating a competitive advantage.^[3] This development of cheap raw material and energy resource has to be observed with caution by the European competitors, although the reentry of Iran in the market and the price decline induced by Saudi Arabia brought the prices back to levels of around 50 US\$/barrel at the end of 2015 (**Figure 2**). Thus this may not be a major problem on a short term, as the decline end of 2015 totally devastated the market. But on a long term raw material, regulatory, and labour costs tend to force changes in terms of energy demand reduction and productivity in the European companies.

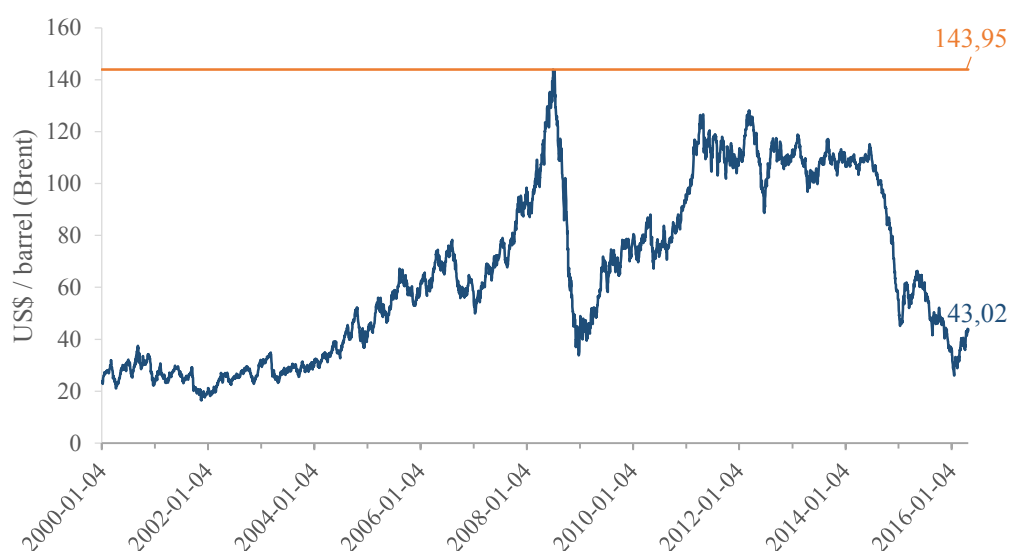


Figure 2. Oil prize chart (Brent in US\$) from 2000 to 2016 (fred.stlouisfed.org; accessed on April 28th, 2016).

China recently pronounced the “13th Five-Year Plan” on the development of its chemical industry and stated the need of further technology innovation. In this context it is expected that state controlled giants *PetroChina* and *ChemChina* are meant to play an even more important role in the world market until the year 2030.^[4] In 1985, ten out of ten of the biggest global players in the chemistry business came from Europe or the US. AT Kearney now predicts five to eight chemical companies from Asia and the Middle East to be part of the global top ten players until 2030 compared to only three in 2010.^[2]

As the goals of state-owned companies are not dominated by the classical shareholder claims of maximized profits, other values like employment, market share and especially the serving of the domestic market and industry play crucial roles. These changes force the long-established companies to widen their horizon and to adapt to the needs of the customers and the fast-growing emerging markets.^[2] Although the European companies are well positioned in their slowly growing home markets, their market share in overseas is significantly lower and is predicted to decrease further.^[1] Especially the movement of value chains, the potential, and growth rates make Asia an interesting market for European companies. Different industries such as automotive, construction, and electronics continuously increase the demand on chemicals for the domestic Asian market and therefore simplify an entrance.^[1]

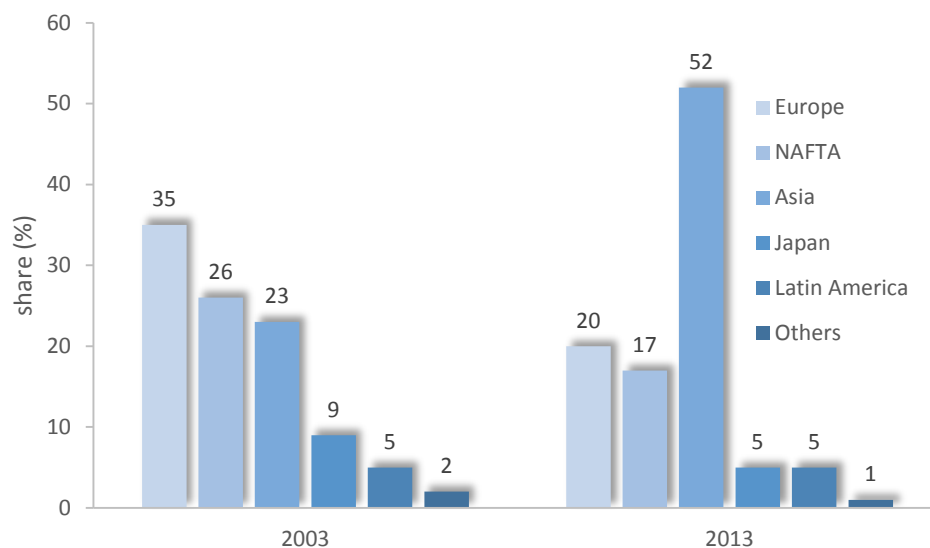


Figure 3. Comparison of world sales from 2003 and 2013 in percent of the total market volume.^[4]

The major tasks that should be addressed by the well-established European players in the upcoming years may be summarized as following: protect and increase market shares in the home market, join in the persisting Asian growth, and develop and establish growth fields or so called “mega trends”.^[5]

The defense of the home market focuses on preventing a possible migration of key customers or suppliers to Asia. Mainly they move to ensure continuous value chains close to the consumer. This represents a major argument for companies to turn their back on home markets, as half of the global population lives in Asia and therefore the majority of

the sales is made in this region. This point maybe cannot be addressed by one company alone but if the value chains stay intact and the production costs competitive the European market will not be ruined by imported products produced elsewhere.

As the economy in Asia is still growing with a speed unrivaled all over the world European producers should hold on to participate. A great part of the consumer goods industries already moved to Asia and large amounts of fabrics, textiles, cars, food, and industrial equipment is produced on site. European chemical companies should therefore move in careful steps into the market evaluating the pros and cons and align the strategy accordingly.

The development of possible growth fields by the European chemical industry strongly depends on the R&D departments of the different companies in close collaboration with the western universities, what can be seen as one of the major advantages compared to Asian giants. Different “mega trends” have been identified by AT Kearney that may play key roles in the future:^[2]

- Natural resources and environment
- Demographics
- Globalization
- Regulation and activism
- Technology and innovation
- Consumption patterns

1.2 Catalysis in Polymer Chemistry: From the supply of simple raw materials to functional solutions

The aforementioned trends are driven by the basic needs of society such as nutrition, energy storage, functional materials, and alternative energy sources. By providing system solutions instead of simple materials, the chemical companies can evolve from a raw material supplier to a technology provider role along the value chain of the future.^[6]

“Plastics have become the ubiquitous workhorse material of the modern economy – combining unrivalled functional properties with low cost”^[7]

This statement comes along with an evolution of over 150 years starting with the first identified polymeric material and cumulating in a row of commodity polymers being cheap enough to use them in single-use applications, like plastic bags or packaging material. During the last fifty years the production of polymeric materials ran through a twentyfold increase and is still expected to double in the next twenty years. Along this way the products responsible for substantial growth in European companies changed during the last years. European suppliers started to transform their strategy facing a prize pressure for commodity materials through *e.g.*, low energy costs in the Middle East and the US. They started to evolve their portfolio and sell enhanced functional systems instead of single polymeric materials.^[5, 8] Long runners of great volume and low margins (*e.g.*, commodity polymers, inorganics) have been sold to competitors or finally closed down in the European sites to maximize profits and especially shareholder returns. This low profit production mainly moved to Asia. Plastics paved the way into our modern society, but the future rises questions and problems in *e.g.* transportation, nutrition, energy sources, and storage that cannot be easily answered with our today’s material feedstock.

Catalysis entered and shaped polymeric material chemistry already in an early stage and was one of the main reasons for the steep rise of polymers in our daily live. The development of a catalytic system for the controlled linear polymerization of ethylene and the *isospecific* polymerization of prochiral propylene led not only to the Nobel Prize for *Karl Ziegler* and *Giulio Natta* in 1963,^[9-10] but produced for the first time polymeric material that was competitive against classical, heavier metal based structural components in many applications.

The demand in innovations of polymeric materials to achieve steadily improvements cannot easily be covered with simple improvements of existing products anymore, but contrary needs completely new materials with unique properties and therefore a more profound research, especially on catalytic solutions to produce the materials of the future.^[4]
^{6]} This most impressively reflects in the number of chemical and pharmaceutical companies present in the list of 50 most innovative companies in 2015 with an amount of roughly 20%.^[11]

Especially the role of functional groups incorporated in the polymeric backbone or sidechain promise specific materials properties incomparable to most nowadays used plastics. Heteroatoms like oxygen, sulfur, phosphorous, and nitrogen can address a vast series of functionalities from biodegradability to high performance stimuli responsive materials.

The availability of these materials hardly relies on the accessible monomers and production pathways. Polymerization techniques in heterogeneous or homogeneous catalysis once again offer possibilities, which are not reachable with standard procedures based on free radical, anionic, or cationic processes. Catalysis thereby offers a plethora of different structures capable to perform reactions from “simple” Ring-opening polymerization of cyclic monomers to the – in theory – more complex group transfer polymerization of polarized olefins. This gives access to completely new polymeric materials from “inspired by nature” biodegradable polyesters to highly complex pH or temperature switchable functional plastics, fulfilling the needs of modern material research. Biodegradable and/or bio based polymers thereby have the chance to open a new chapter in commodity business and are essential revolutions of today’s polymer business heading to a sustainable future.^[6]

Both types of catalyzed polymerization and the obtained functional materials will be the main subjects of the following thesis.

2. Ring-opening Polymerization of Lactones toward Biodegradable Poly(ester)s

Synthetic bio-based and biodegradable polymers are contemplated for a long time as the ecological and economical alternatives for synthetic polymers on a petrochemical basis. Especially the substitution of fossil raw materials is essential and would represent a leap to sustainable commodity products.^[12] The progress made in the field of biodegradable polymers in the last decades led to various applications from ordinary packaging in the commodity sector to demanding biomedical products. Among this complex group, linear aliphatic polyesters always held a special position and are therefore the most present sub group in literature. Especially poly(lactide) (PLA) and poly(3-hydroxybutyrate) (PHB) came into focus in the last years due to their outstanding characteristics (**Figure 4**).^[13-22]

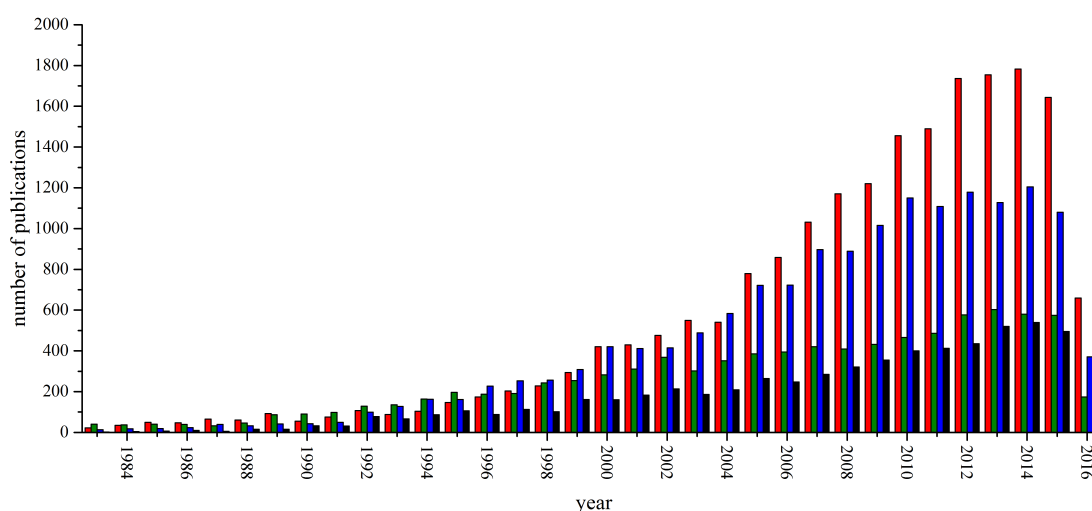


Figure 4. Number of contributions published since 1983 based on scifinder.cas.org search results (accessed on April 20th, 2016) using the keywords poly(lactide) ■, poly(3-hydroxybutyrate) ■, PLA ■, and PHB ■.

The linear aliphatic polyester (*R*)-*iso*-poly(3-hydroxybutyrate) (*n*PHB) is naturally produced as carbon and energy storage material by numerous bacteria. First described by Maurice Lemoigne in 1925 after the extraction of PHB out of *bacillus megaterium* the thermoplastic polyester shows remarkable characteristics in density, tensile strength, temperature resistance, UV stability, and as oxygen barrier.^[23-24] These features, excluding oxygen permeability and UV resistance, are comparable to *isotactic* poly(propylene) (*i*PP) and promise therefore a possible substitution of *i*PP as commodity polymer for packaging applications.^[24-26] Especially, the high density of *n*PHB is a major advantage in packaging as plastic trash assembling in marine systems could be avoided through sink and subsequent degradation even under anaerobic conditions (**Figure 5**).^[27-29]

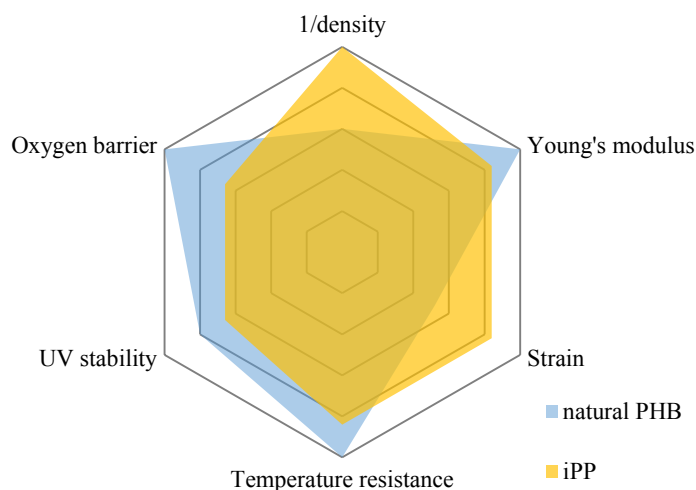


Figure 5. Relative comparison of characteristics of *n*PHB and *i*PP.^[24]

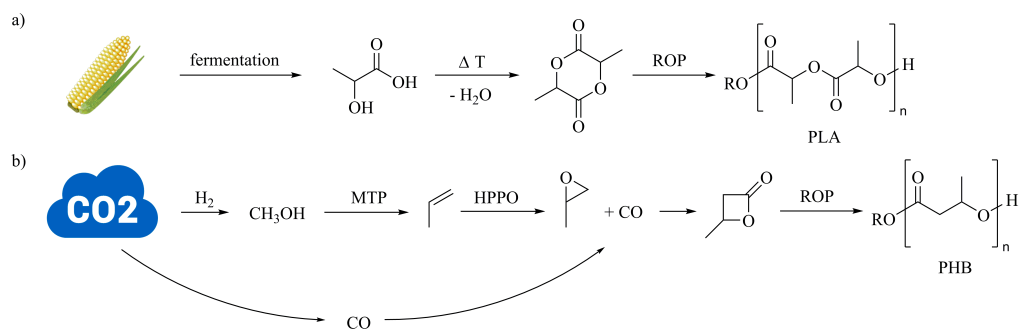
The currently predominant route to PHBs is based on fermentative production and therefore competes with the production of nutriment and is of high cost.^[30-31] Thus PHB is still only of interest for niche applications. The chemical alternative of homogenous catalysis using Ring-opening polymerization (ROP) of the cyclic ester β -butyrolactone (BL) offers excellent preconditions in catalyst design and therefore the variation of the polymer microstructure, but still lacks of a breakthrough in stereocontrol to afford *isotactic* PHB.^[24, 32-33]

PLA contrary to PHB does not only show biodegradability but also bio-assimilability. Hydrolysis of PLA in physiological media, like *e.g.*, human tissue, produces lactic acid

which is converted into water and carbon dioxide in the *Krebs cycle* and allows the use of PLA based implants in medical applications or sutures.^[16] The usage of PLA based orthopedic devices makes precautions and removal surgeries redundant. PLA is among the biobased and biodegradable plastics the one that already made it into the large scale industrial synthesis and is *e.g.*, part of the BASF product line *ecovio*[®] or is produced as *NatureWorks*[™] by Cargill Dow LLC.^[8, 34-35]

As the poly-condensation reaction of lactic acid lacks control, ROP of the cyclic diester lactide as monomer is the most widely used method for the production of highly defined polymeric PLAs. Although tin(II) bis(2-ethylhexanoate) is the most common spread catalyst in the coordinative-insertion ROP of LA, providing high activities and molecular weights, the toxicity of most tin compounds prohibits biomedical applications and shows the demand in further research in high active polymerization catalysts based on other metal cations.^[36] Alternative metal salts of aluminum and zinc were successfully tested. Al(O^{*i*}Pr)₃ shows only moderate activities and Al(III) cations are suspected to support *Alzheimer's* disease^[16, 36], which prohibits residues of the catalyst in medical products. Zinc(II) lactate contrary is highly active and shows great reaction control compared to the use of ordinary zinc powder.^[37-39]

PHB and PLA can theoretically be prepared *via* completely oil-independent routes, which would pave the way to a new era of feedstocks for commodity polymers considering the fact of inevitable vanishing of global oil reserves (**Scheme 1**).^[24, 40-42] PHB can thereby be synthesized starting from the greenhouse gas CO₂ *via* reduction to methanol, a consecutive methanol to propylene process (MTP) followed by an oxidation using *e.g.*, the HPPO process, ending up in propylene oxide. The latter one can be carbonylated to butyrolactone using CO, and finally be ring-opened to PHB.^[24]



Scheme 1. Synthesis of lactide (a) and β -butyrolactone (b) using sustainable resources and subsequent Ring-opening polymerization to aliphatic polyesters PLA and PHB.

2.1 Tacticity in the Catalytic Ring-opening Polymerization of Lactones

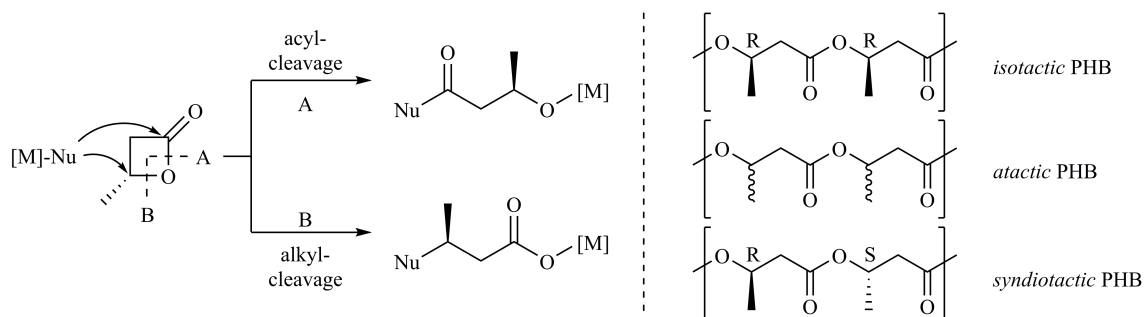
Stereochemistry plays the crucial role in the application of PHBs. The probability of *racemic* (P_r) or *meso* (P_m) linkages along the polymer backbone thereby quantifies the degree of stereoregularity. Besides mechanical drawbacks for especially *atactic* PHB the microstructure dramatically influences the biodegradability of the polymer. This explains the only minor degrading behavior of *atactic* and *syndiotactic* PHB in degradation experiments. Enzymatic investigations of different PHB depolymerases like *e.g.*, PhaZ_{Afa} from *Alcaligenes faecalis* and PhaZ_{Rpi} from *Ralstonia picketti* point out, that most depolymerases are selective for the cleavage of *R,R* linkages inside the polymer backbone.^[43-47]

The biodegradable natural highly *isotactic* PHB suffers of some drawbacks as well, such as a low strain elongation and brittleness through ongoing crystallization while ageing and the high melting point of around 180 °C. This is close to the decomposition temperature and therefore limits the thermal processability *via e.g.*, extrusion. These points were shown to be radically improved by decreasing the *isotacticity* to values between 70 and 80%, whereby an *iPP* like material with a melting transition between 100 and 130 °C can be obtained.^[25] Highly *syndiotactic* PHB exhibits high melting points of up to 183 °C ($P_r = 0.94$) but lacks of the required biodegradability.^[48]

The desired *isotactic* PHB can chemically either be accessed by ROP of enantiopure BL or stereoselective polymerization of (*rac*)-BL. As enantiopure BL through carbonylation of propyleneoxide or *via* hydration of diketene are out of range for an economically profitable process, ROP of (*rac*)-BL seems to be the most promising route and provides a vast number of available polymerization catalysts that can be altered.^[40, 49-50]

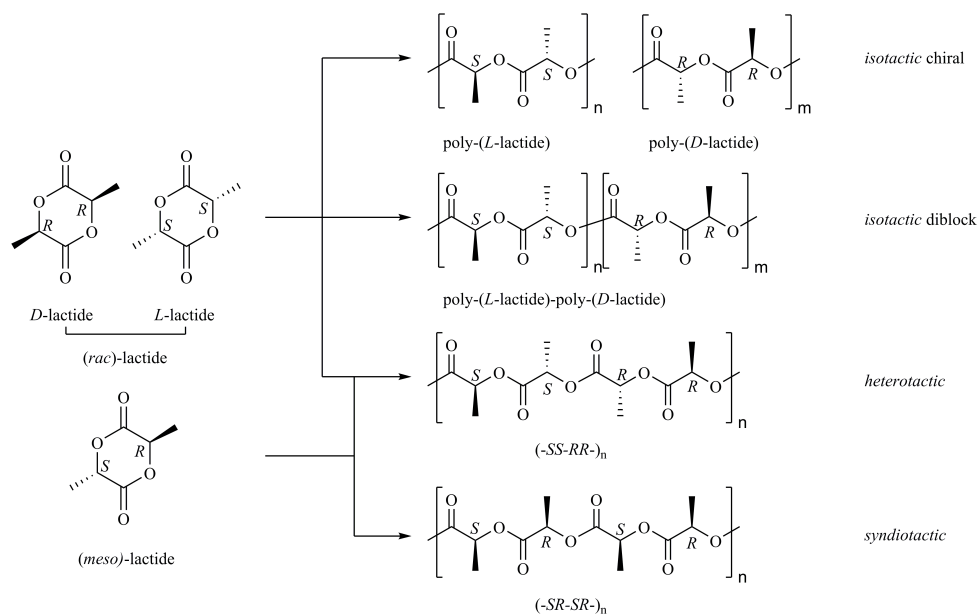
Most metal based catalysts reported in literature operate *via* a coordination-insertion mechanism and can thereby proceed *via* an acyl or an alkyl-cleavage depending *e.g.*, on the initiating nucleophile. An acyl cleavage thereby leads to a retention of the stereoinformation of the incorporated monomer, whereas an alkyl cleavage proceeds through inversion at the stereogenic centre (**Scheme 2**). Side reactions, such as elimination of the alkoxy coordinated polymer chain as crotonate, often lead to a loss of control during the polymerization and have to be suppressed if possible. Thus metal-based homogenous

single-site catalysts present an optimal platform for understanding the ongoing processes and tuning the catalysts behavior.^[24]



Scheme 2. ROP of R -BL in coordination-insertion polymerization (left) and the possible microstructures of polymers made from (rac) -BL (right).

Similar to PHB the tacticity influences the thermal and mechanic behavior of PLA. Whereas *heterotactic* PLA melts at about $T_m = 130$ °C, the melting point of *syndiotactic* PLA is increased to about $T_m = 150$ °C, and even up to $T_m = 180$ °C for *isotactic* PLA.^[51-52] The formation of stereocomplexes of *isotactic* poly(*L*-lactide) and poly(*D*-lactide) further increases the melting transition to $T_m \approx 230$ °C and was impressively evaluated and elucidated by different groups (**Scheme 3**).^[53]



Scheme 3. Different microstructures accessible *via* ROP of (rac) - and $(meso)$ -lactide.^[53]

2.2 Metal Based Single-Site Catalysts for the Ring-opening Polymerization of (*rac*)- β -butyrolactone and (*rac*)-lactide

A variety of single-site catalysts have been applied in the homogenous ROP of BL and LA in the last decades (**Figure 6**). Due to the similarity in the coordination-insertion mechanism taking place for both monomers, most of the catalysts are applicable for PHB and PLA synthesis. Various groups concentrated on the development of tunable, highly active catalysts for the stereoselective polymerization of cyclic esters. Although PHB and PLA still show increasing interest in literature only a short introduction in the most promising ligand and catalyst structures is shown in here.

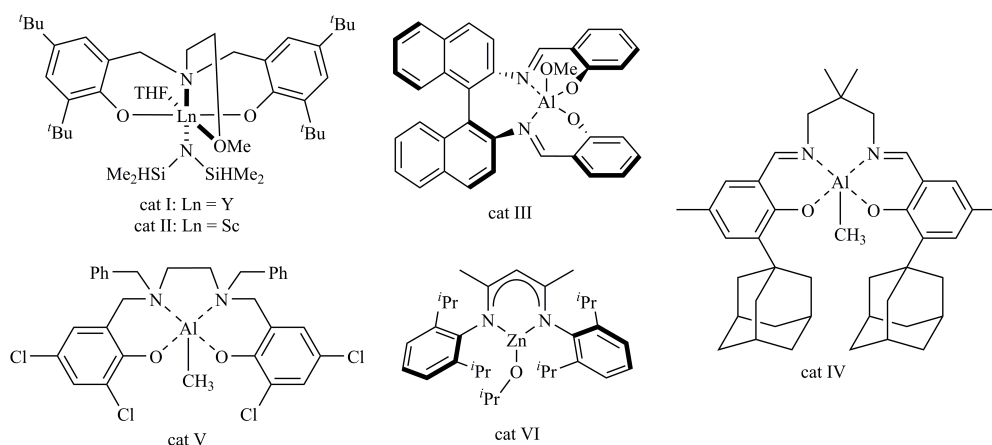
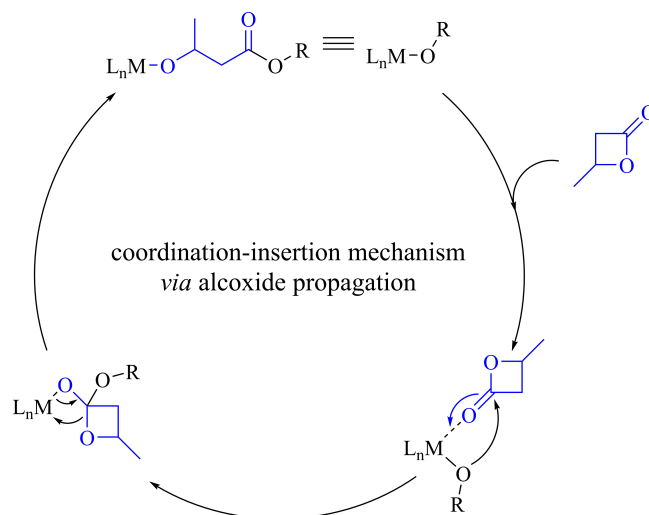


Figure 6. Commonly applied catalyst structures with high reputation in literature applicable for both, the ROP of BL and LA.

The group of *Carpentier* reported on alkoxy-amino-bisphenolate yttrium and scandium complexes in the ROP of BL and LA (cat I-II). For the yttrium complexes the polymerization already proceeds at room temperature with high activities and a high degree of control (PHB: PDI < 1.9; PLA: PDI < 2.0) combined with a living character for the polymerization of both monomers in coordinating (THF) and non-coordinating (toluene) solvents.^[54] The addition of up to one equivalent of chain transfer reagent *i*PrOH per metal center allows an immortal ROP with these systems. Besides the high controlled fashion the catalysts show stereoselective polymerization in both cases.^[54]

Mechanistic considerations revealed a monometallic coordination-insertion mechanism proceeding *via* acyl-oxygen cleavage of the four membered lactone ring (**Scheme 4**). The nature of the solvent showed an influence on the obtained tacticity in ROP. While in the ROP of (*rac*)-BL THF lowered the syndioselectivity of the

polymerization from $P_r = 0.94$ in toluene to $P_r = 0.83$ the trend reversed for the ROP of (*rac*)-LA with an increase of *heterotacticity* ($P_{r,(toluene)} = 0.54$; $P_{r,(THF)} = 0.73$). These findings in combination with *Bernoullian* analysis using ^{13}C NMR spectroscopy validate a *chain end control* as origin of the syndioselectivity.^[54-55]



Scheme 4. Similarity in the monometallic coordination insertion mechanism for catalysts I-VI proceeding *via* the same major steps during ROP of BL.

Different groups reported on Aluminium salen- and salan-type complexes for the controlled ROP of (*rac*)-BL and (*rac*)-LA. Besides narrow molecular weight distributions and high molecular weights sterically altered ligand structures led to a high degree of control in the stereoselectivity for PLA. *Spassky* used the enantiopure complex III for the isoselective ROP of (*rac*)-LA discriminating the incorporation of L-lactide with a 19 times lower polymerization rate than for D-lactide.^[56] Also the use of achiral aluminium salen complexes allowed the isoselective ROP of (*rac*)-LA as *e.g.* demonstrated by *Shaver* using complexes IV and V.^[57-58] He additionally investigated the ROP of (*rac*)-BL and found a high control in the polymerization without any influence on the stereoselectivity ending up in *atactic* PHB.

Coates introduced β -diiminate based zinc catalysts in the controlled ROP of cyclic esters BL and LA at mild conditions. Besides high activities the catalyst structure (cat VI) provides stereoselective polymerization of (*rac*)-LA to highly *heterotactic* PLA ($P_r = 0.94$) at 0 °C.^[52] The high control in stereoregularity is not transferable to the smaller cyclic ester

BL providing a longer distance between the attacked carbonyl atom and the stereogenic centre. Thus, only *atactic* polymer is obtained.^[33]

2.3 Objective: Development of new, highly active Zinc Based Catalysts for the Stereoselective Ring-opening Polymerization of Cyclic Esters

As obvious from the latter chapters, new catalysts for the stereoselective and highly active Ring-opening polymerization of cyclic esters are of profound interest to satisfy the rising demand for biodegradable polyesters *e.g.*, PLA and PHB as an economically viable alternative to nowadays commodity polymers. As fermentative production is of high cost, homogenous catalysis, especially for the production of functional PHB, can mark a leap in this movement. Although there has not been a major breakthrough for the isoselective polymerization of (*rac*)-BL, mechanistic understanding and addressing the catalytic activity of zinc based initiators has the potential to forward this field of research in a massive manner. The literature known principle of β -diiminato (BDI) zinc (II) offers variable structures and was successfully investigated in the ROP of BL and the stereoselective polymerization of LA to PLA.

However further improvements on this structural motive especially concerning the activity of the complexes was not further focused in the past. Electron withdrawing groups (EWG) and particularly trifluoromethyl (CF₃) groups have often been modifications in ligand design to increase the electrophilicity of the metal cation and are therefore expected to increase the Lewis acidity of BDI ligated zinc (II) ions. The influence of these alterations plays an important role on the catalyst activity. Enhanced activity as well as the interplay with steric alterations inside the BDI ligated zinc (II) complexes were investigated in **chapter 4.2** to gain a deeper understanding for future catalyst systems.

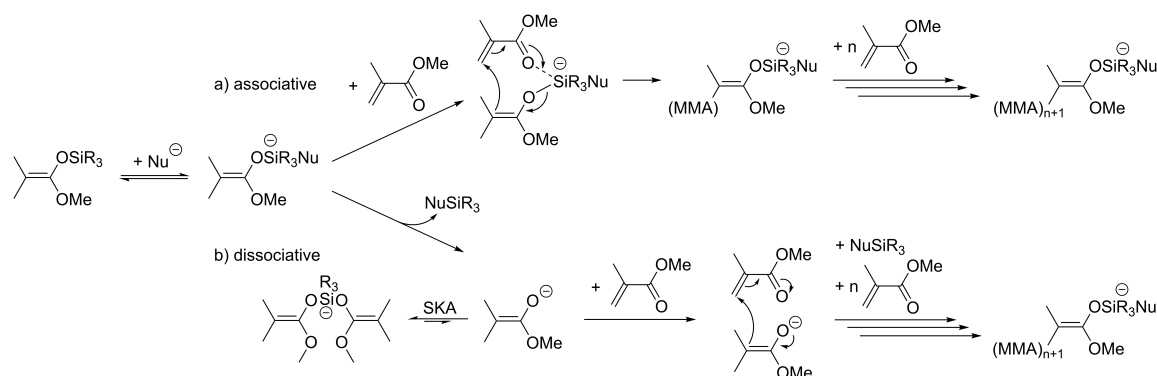
The promising potential of biodegradable polymers, *e.g.* PHB or PLA in packaging and medical applications, can only be fully accessed by utilizing cutting edge catalysis to add an additional layer of functionality to those materials.

Rare earth metal-mediated group transfer polymerization, as a synergistic combination of living anionic and coordination polymerization, represents a versatile tool for the synthesis of functional materials of the future. REM-GTP has not received a lot of attention during the course of the last years, however the introduction of new *Michael* type monomers, *e.g.* dialkyl vinylphosphonates and 2-vinylpyridine, combined with the development of new catalyst structures revived researchers' attention. Versatile 2-methoxyethylamino-bis(phenolate) yttrium catalysts are a remarkable example for these developments, as they have their origin in the successful syndioselective ROP of (*rac*)-BBL but evolved through a simple initiating ligand exchange to a capable catalyst for the REM-GTP of various *Michael* systems.^[55, 59]

Especially the elevated levels of precision in terms of molecular weight and polydispersity offer opportunities for material design. These aspects and advantages of REM-GTP will be elucidated in the following chapter focused on stereospecific polymerization towards pH sensitive poly(2-vinylpyridine).

3. Rare Earth Metal-mediated Group Transfer Polymerization of 2-Vinylpyridine

The terminology of group transfer polymerization (GTP) was established in the early 1980s by *Webster et al.* They described the living polymerization of *Michael*-type monomers through initiating silyl ketene acetal (SKA) addition to vinylic monomers followed by a transfer of the silyl group to the next monomer under polymer growth.^[60-61] Using this principle the group was able to polymerize a row of vinylic monomers (methyl methacrylate, *n*-butyl methacrylate, ethyl acrylate, allyl methacrylate, glycidyl methacrylate, methyl vinylketone, *N,N*-dimethyl acrylamide) to well defined homo- and block-*co*-polymers (PDI = 1.0 – 1.9; $M_w \leq 25 \text{ kg mol}^{-1}$).^[61] The underlying mechanism was discussed over the following years^[62-64] distinguishing between an associative and a dissociative mechanism, whereas the latter was supported by experimental results (**Scheme 5**).^[65-69]



Scheme 5. Associative and dissociative mechanism for silyl ketene acetal addition followed by GTP. Nu⁻ can be any out of the following anions: HF₂⁻, F₂⁻, cyanide, azide, oxyanions, or bioxyanions.

3.1 Rare Earth Metal-based Catalysts in the Group Transfer Polymerization of Michael Monomers

In 1992, two independent contributions in *JACS* marked a leap in the development of discrete metallocene catalysts for the controlled polymerization of acrylic monomers. *Collins* and *Ward* developed dimeric *bis*-cyclopentadienyl (Cp) ligated zirconium complexes for the GTP of MMA in a transition metal-mediated GTP to *syndiotactic* PMMA.^[70] Simultaneously, rare earth metals paved their way into the group transfer polymerization of polar vinylic monomers. The group of *Yasuda* used a dimeric, 1,2,3,4,5-

pentamethyl-cyclopentadienyl (Cp*) based samarium catalyst (**Figure 7**) for the syndiospecific polymerization of methyl methacrylate (MMA) providing narrow polydispersities (PDI = 1.0) and high molecular weights ($M_n = 56 \text{ kg mol}^{-1}$).^[71]

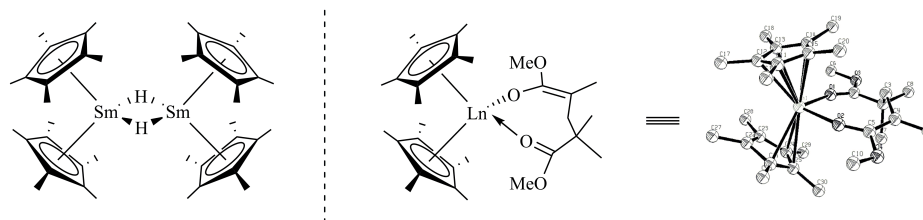
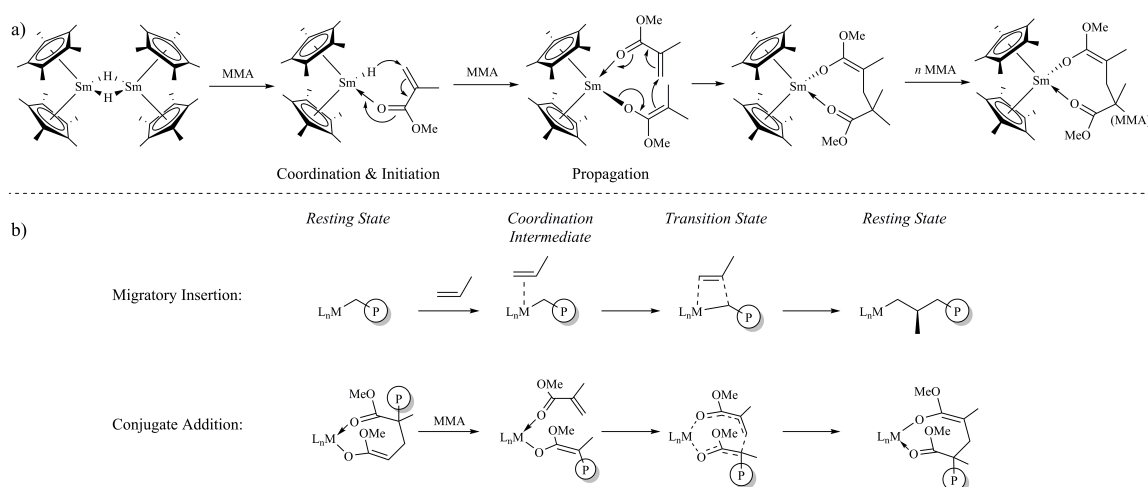


Figure 7. Dimeric $[\text{Cp}^*_2\text{SmH}]_2$ catalyst (left) and eight membered resting state after initiation and first insertion of REM-GTP of MMA (incl. X-ray structure, reproduced with permission from ^[83]; Copyright 2016 American Chemical Society; right).

The dimeric samarium hydride complex thereby acts as initiator and catalyst. In a first step the hydride ligand attacks in a nucleophilic fashion the pre-coordinated and activated monomer. In a second step the formed ester-enolate adds in a conjugate addition to a second pre-coordinated MMA forming the propagating species as an eight-membered ring, which was finally proven *via* single crystal X-ray analysis (**Figure 7**).^[71-72] The propagation continues through repeated *Michael*-additions of the preformed enolate to an activated monomer following an eight-membered ring intermediate. The resting state of conjugate-addition (coordination-addition) mechanism as well as the eight-membered ring transition state is of sharp contrast to the migratory-insertion of non-polar and polar olefins (**Scheme 6**).^[72-73]



Scheme 6. (a) REM-GTP mechanism of initiation and chain propagation of MMA using dimeric Sm catalyst $[\text{Cp}^*_2\text{SmH}]_2$; (b) mechanistic differences between migratory insertion (MI, top) and conjugate addition (CA, bottom).

Methacrylate and Acrylate Polymerization

Starting with the polymerization of MMA by *Yasuda et al.* as the origin of REM-GTP a variety of groups worked on the basis of these groundbreaking findings and achieved remarkable results for REM-GTP as well as for a row of other metal centers, which will not be presented herein.

Methyl methacrylate stayed for a long time the preferred workhorse in REM-GTP research due to the possibilities the highly defined REM-GTP offers.^[73-74]

The group of *Yasuda* developed a plethora of catalysts for MMA polymerization on the basis of their original findings and found methyl lanthanocenes ($\text{Cp}^*_2\text{LnMe}(\text{THF})$ ($\text{Ln} = \text{Sm}, \text{Y}, \text{Yb}, \text{Lu}$)) as well as AlMe_3 complexes of lanthanocenes ($\text{Cp}^*_2\text{Ln}(\mu\text{-Me})_2\text{AlMe}_2$ ($\text{Ln} = \text{Y}, \text{Yb}, \text{Lu}$)) to be active in a comparable fashion to the originally used complex. Accompanied with these results a dependence of the catalyst activity on the ionic radius of the metal center was found, showing an increase in activity for increased ionic radii ($\text{Sm} > \text{Y} > \text{Yb} > \text{Lu}$).^[72, 75] Additionally the polymerization of other methacrylates was successful using this catalyst topology showing an anticipated decrease in activity for an increase of the steric bulk of the alkyl-ester moiety. The degree of stereospecificity surprisingly decreases for bulkier alkyl moieties, which is in sharp contrast to the expectations based on a chain-end control mechanism but may be explained through the unique and sterically demanding transition state (**Table 1**; for information about the stereoselection event see **3.2**).^[72]

Table 1: Results for the polymerization of different methacrylates using $[\text{Cp}^*_2\text{SmH}]_2$ as catalyst.^(a)

$\text{CH}_2=\text{CH}(\text{Me})\text{COOR}$	TOF (h^{-1}) ^(b)	rr (%) ^(c)	PDI ^(d)
$R = \text{Me}$	500	82.4	1.02
$R = \text{Et}$	490	80.9	1.03
$R = \textit{i}Pr$	450	77.3	1.03
$R = \textit{t}Bu$	125	78.2	1.05

^(a) Polymerization in toluene at 0 °C for 1 h. $[\text{M}]/[\text{Cat}] = 500/1$. ^(b) TOF = TON/t. ^(c) rr(%) is determined *via* ^{13}C NMR.

^(d) PDI = M_w/M_n determined by GPC.

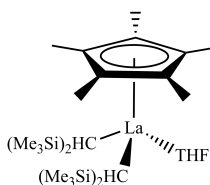
Another remarkable finding is the resistance of stereocontrol against coordinating solvents like THF and diethylether for lanthanocene based REM-GTP.^[72] Using classic anionic polymerization a switch from non-coordinating to coordinating solvents results in a competing coordination of the counter ion and the monomer to the chain-end. Thus the

solvation of the counter ion in coordinating solvents can switch the obtained PMMA tacticity from *isotactic* (e.g., toluene) to *syndiotactic* placement (e.g., THF).^[73]

Beside this manifold lanthanocene catalyst and many more variations a few more catalysts have been developed for the REM-GTP of MMA. A series of C_s-symmetric *ansa*-lanthanocenes have been tested and found to be less active, syndiospecific and efficient than their unbridged analogues.^[76-79]

The half-sandwich lanthanocene Cp*La[CH(SiMe₃)₂]₂(THF) on the other hand polymerizes MMA highly controlled at low temperatures to highly *syndiotactic* PMMA with the drawback of low activities. An increase of the reaction temperature from – 78 °C results in higher activities but also decreases control in means of PDI and syndiotacticity.^[80]

Table 2: Results for the polymerization of MMA using Cp*La[CH(SiMe₃)₂]₂(THF) at different polymerization temperatures.^(a)



T_P (°C)	TOF (h^{-1}) ^(b)	<i>rr</i> (%) ^(c)	PDI ^(d)
– 78	3	91	1.11
0	100	80	1.18
25	200	74	1.23

^(a) Polymerization in toluene for 1 h. [M]/[Cat] = 500/1. ^(b) TOF = TON/t. ^(c) *rr*(%) is determined via ¹³C NMR. ^(d) PDI = M_w/M_n determined by GPC.

The polymerization of acrylates represents a special challenge when using anionic initiators due to the potential H abstraction in α -position. This might be the reason for only sparsely found metal mediated polymerization of acrylates in literature. Nevertheless it was once again the catalyst structure introduced by *Yasuda* in the REM-GTP of vinylic monomers that can handle this issue also at elevated temperatures. Cp*₂LnMe(THF) (Ln = Sm, Y) catalyzes highly active – in a comparable initiation and propagation mechanism to the MMA polymerization – the polymerization of alkyl acrylates (R = Me (MA), Et (EA), ⁿBu (ⁿBA), ^tBu (^tBA)) at 0 °C.^[81-82]

To get deeper in touch with the catalyzed GTP of vinylic monomers especially for acrylate- and acrylamide-based monomers the extensive review of *Chen* can be

recommended and contains additionally to the examples mentioned herein a plethora of catalysts based on other metals *e.g.*, group 4 metallocenes.^[73]

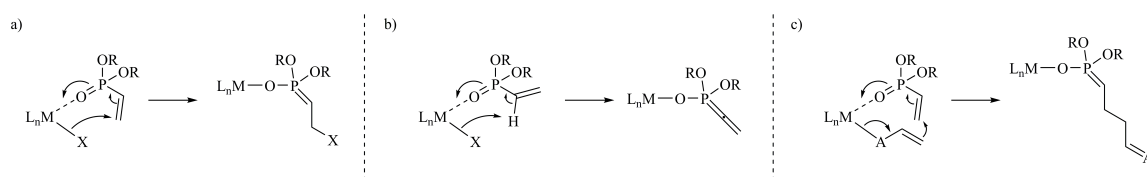
Other Monomers in REM-GTP

These first REM-GTP findings mark a leap in the development of new catalyst structures for the highly defined polymerization of vinylic monomers and served as foundation for new catalysts and accessible monomers. GTP thereby combines the advantages of a living polymerization with those of a coordinative polymerization, which allow in principle high molecular homo- and block-*co*-polymers and stereocontrol through adapted ligand design.^[83]

Consequently the feedstock of applicable monomers widened over the years resulting in new highly defined functional polymeric materials. Already in the early years simple Cp-based catalysts were successfully tested for a row of new monomers besides the acrylate and acrylamide long-runners.

Vinylphosphonates in particular had been challenging monomers for radical and anionic polymerization over the years and were either unable to polymerize or ended up in low molecular weight polymers and high degrees of side product impurities. In 2010, *Rieger et al.* reported on the controlled synthesis of poly(diethyl vinylphosphonate) (PDEVVP) *via* REM-GTP using simple lanthanocene based initiators (Cp₂YbMe, Cp₂YbCl).^[84]

The initiation step was clarified to proceed *via* a nucleophilic transfer of the initiating ligand (Cp, thiolates) to a coordinated monomer molecule (a). Other initiating mechanisms, like deprotonation of the acidic α -proton through the alkyl initiators (b) or a ligand exchange (c) could be excluded for these types of initiating ligands through end group analysis using ESI mass spectroscopy (**Scheme 7**). Profound studies on the mechanism of REM-GTP of dialkyl vinylphosphonates (DAVP) in 2013 by the group of *Rieger* revealed a monometallic conjugate addition mechanism comparable to that already proposed for the polymerization of MMA using the *Yasuda* catalyst.^[74, 85]



Scheme 7. Possible initiation mechanisms for REM-GTP of DAVPs.

The obtained PDEVp exhibits a lower critical solution temperature (LCST) in aqueous media between 40 and 46 °C, depending on molecular weight, concentration and media. The solubility of poly(dialkyl vinylphosphonates) (PDAVP) depends on the alkyl-substituents and can therefore be tuned by the random *co*-polymerization of diethyl vinylphosphonate (DEVp) with *e.g.* dimethyl vinylphosphonate (DMVP), to increase the LCST, and di-*n*-propyl vinylphosphonate (DIVP), to decrease the LCST.^[86]

Besides acrylates and DAVPs *iso*-propenyloxazoline (IPOx), 2-vinylpyridine (2VP), and *N,N*-dimethyl acrylamide (DMAA) can be polymerized in a controlled fashion *via* REM-GTP catalysis using simple Cp-based systems like Cp₂YbMe. Although the underlying method is thereby applicable for these monomers, low activities (especially for 2VP) and a missing influence on the polymer microstructure point out the need for a broader catalyst feedstock to tune the material properties.^[86-88]

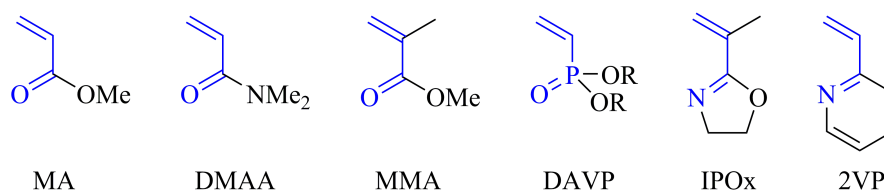


Figure 8. Selection of monomers applicable for REM-GTP (*Michael*-system highlighted).

2-Methoxyethylamino-bis(phenolate) yttrium catalysts bearing amido and alkyl initiating ligands have been first tested in 2003 by the group of *Carpentier* for the REM-GTP of MMA. Although the amido complex, known for its high activity in ROP of cyclic esters, produced some polymeric material at a low yield the alkyl complex (CH₂TMS) failed in initiating the polymerization.^[89] In 2014, the group of *Rieger* revived this catalyst principle in the REM-GTP of different monomers and was able to successfully polymerize DMAA, IPOx, DAVP, and 2VP with moderate to high activities in a highly controlled fashion. In depth investigations have been carried out to reveal the ongoing mechanism and prove the monometallic conjugate-addition mechanism.^[59]

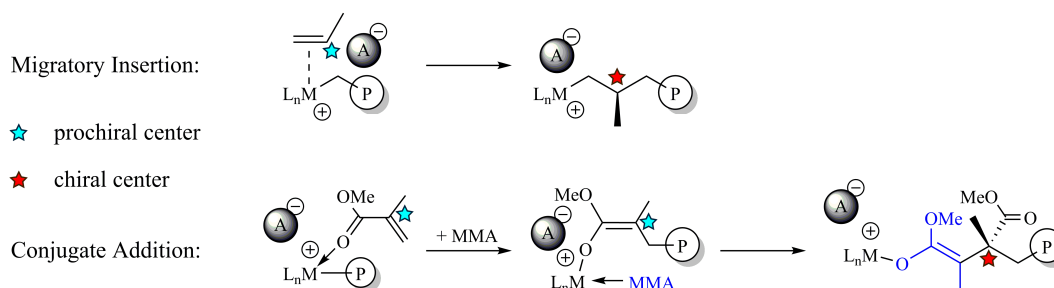
3.2 Stereospecific Polymerization of *Michael*-type Monomers

The conversion of prochiral *Michael* monomers can lead to the same kind of tacticities (*isotactic* (*it*), *atactic* (*at*), *syndiotactic* (*st*)) as the stereoselective polymerization of chiral monomers, like (*rac*)-BL or (*rac*)-LA, but is according to the recommendation of IUPAC defined as stereospecific instead. Different levels of tacticity can be obtained determining the thermal and mechanical properties of the polymeric material (**Table 3**).

Table 3. Ranges of tacticities theoretically available through polymerization of chiral and prochiral monomers.^[73]

$rr > 0.90$	$89 > rr > 70$	$69 > rr > 55$	$rr \sim mm$	$55 < mm < 69$	$70 < mm <$	$90 < mm$
highly <i>st</i>	<i>st</i>	<i>st</i> -rich	<i>at</i>	<i>it</i> -rich	<i>it</i>	highly <i>it</i>

In sharp divergence to the stereoselection event in a migratory insertion mechanism of *e.g.* α -olefines, the chirality of the monomer in GTP is not yet determined when enchained in the polymer. The final selection is made one step later, after the addition of the next monomer, between the enantiofaces of the prochiral latter incorporated monomer, the chiral chain and the next monomer (**Scheme 8**).^[73]



Scheme 8. Difference in the stereoselection event between migratory insertion and conjugate addition.

In 2011, the group of *Mashima* developed an active ene-diamido yttrium catalyst for the isospecific synthesis of poly(2-vinylpyridine) (**Figure 9**).^[90-91] Among this widening of the applicable ligand structures for REM-GTP he was able to introduce new end group functionalities in the polymers *via* utilization of C–H bond activation of alkynes and heteroaromatic precursors and thus opened another chapter in REM-GTP, already applied in different investigations.^[74, 92-93]

In 2015, our group has been successful in even broadening the applicability of the 2-methoxyethylamino-bis(phenolate) yttrium catalyst (**Figure 9**) by varying the steric

surrounding of the metal center and therefore creating for the first time, using this ligand system, *isotactic* enriched poly(2-vinylpyridine). We have not only been able to achieve a variety of different ligand structures and tacticities but in a further step unmasked the origin of stereocontrol as an *enantiomorphic site control* mechanism using profound NMR studies on the triad level of the quaternary aromatic carbon atom of P2VP.^[94]

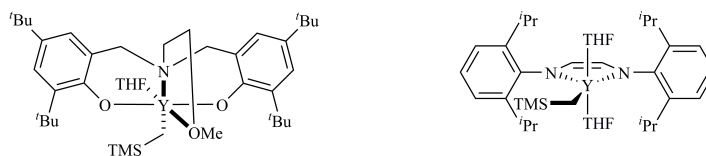


Figure 9. Basic structure of 2-methoxyethylamino-bis(phenolate) yttrium catalyst used for REM-GTP of different monomers by *Rieger et al.* (left); ene-diamido REM-GTP catalyst developed by *Mashima* (right).

3.3 Objective: Development of highly defined and stereoselective Single-Site Catalysts for the REM-GTP of 2-Vinylpyridine

This work was motivated through some recent findings on the possibility to influence the stereospecificity in the polymerization of prochiral 2-vinylpyridine using different catalyst systems based on rare earth metals that just have been mentioned in **chapter 3.2**.

Polymers and especially co-polymers of 2VP promise a multitude of fields of applications in *e.g.*, electrochemistry, optics, medicine, nanotechnology, and membranes. Nevertheless until this point there is a lack in the opportunities to test highly defined and stereoregular copolymer-based materials for further improvements of materials' characteristics. Different architectures have already been accessible through highly defined polymerization techniques like RAFT or NMP, but no stereoinformation can be included in the polymers using this track. Thus the influence of tacticity on the different applications of *e.g.* copolymers in micelles was unable to be observed until now.

Nevertheless previous findings in our group pointed the way to highly defined and stereoregular homopolymers of 2VP but only with low tacticities of up to $P_m = 0.74$ using steric variations of well-known 2-methoxyethylamino-bis(phenolate) ligated yttrium catalysts. Following the examples in *e.g.*, the polymerization of prochiral propylene to highly tactic poly(propylene) further adjustments were planned and executed to maximize the steric bulk around the metal center and therefore increase the maximum reachable tacticities in the isoselective polymerization of 2VP.

These steric alterations, their influence on polymerization kinetics and especially reachable tacticities, the origin of the *isotactic* nature, and deeper understanding of ^{13}C pentad assignments have been investigated in detail in **chapter 4.4**.

4. Results – Publications

4.1 Electron-deficient β -Diiminato-Zinc-Ethyl Complexes: Synthesis, Structure, and Reactivity in Ring-opening Polymerization of Lactones

Alexander Kronast, Marina Reiter, Peter T. Altenbuchner, Christian Jandl, Alexander Pöthig, and Bernhard Rieger

published as Full Paper in *ORGANOMETALLICS*, 2016, 35 (5), 681–685

The condensation of 1,1,1,5,5,5-hexafluoro-acetylacetone with 2,6-disubstituted anilines, creating a reactive titanium species using TiCl_4 , led to a new class of *bis*- CF_3 -substituted β -diiminato ligands. The literature unknown pre-ligands (BDI^{CF_3} -II)H ($\text{CH}(\text{CCF}_3\text{NC}_6\text{H}_4\text{-2,6- C}_2\text{H}_5)_2$) and (BDI^{CF_3} -III)H ($\text{CH}(\text{CCF}_3\text{NC}_6\text{H}_4\text{-2,6-CH}_3)_2$) were synthesized and effectively ligated the zinc(II)-ethyl metal precursor in quantitative yields (**Figure 10**). The structures of the complexes, including complex I of the literature known pre-ligand (BDI^{CF_3} -I)H ($\text{CH}(\text{CCF}_3\text{NC}_6\text{H}_4\text{-2,6-CH}(\text{CH}_3)_2)_2$), in the solid state were elucidated using SC-XRD measurements and revealed differences in bond lengths and symmetry, especially when compared to a literature known analogue of I, BDI-1-ZnEt, bearing CH_3 instead of CF_3 groups in the ligand backbone.

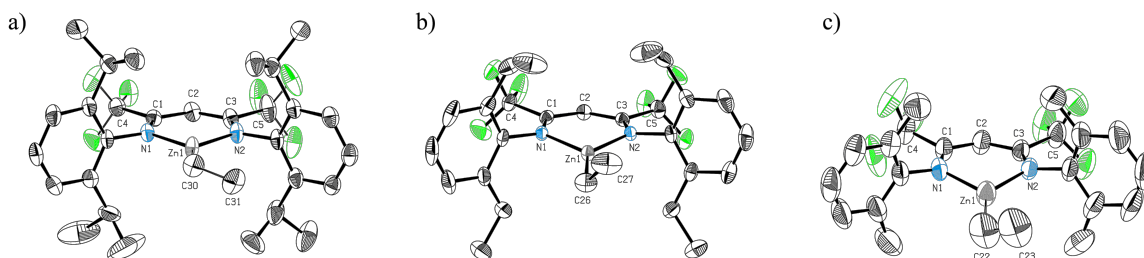


Figure 10: ORTEP style representations of the pre-catalysts I (BDI^{CF_3} -I-ZnEt; a), II (BDI^{CF_3} -II-ZnEt; b), and III (BDI^{CF_3} -III-ZnEt; c) with ellipsoids drawn at the 50% probability level.

The resulting pre-catalysts I–III were tested in the Ring-opening polymerization of cyclic esters BL and LA and showed an increase in activity in comparison to the literature known BDI-1-ZnEt. The improved activity originates from enhanced Lewis acidity of the metal center and thereby the activation of the coordinated lactone. The activity in the Ring-opening polymerization of (*rac*)- β -butyrolactone was observed using *in situ* IR measurements, revealing III as the most active zinc-ethyl-based initiator. II and III were also highly active in the ROP of (*rac*)-lactide and showed a high dependency of the

resulting polymer microstructure on the phenyl substituents in the *ortho* position of the aniline moiety, resulting in higher degrees of *heterotactic* PLA for steric more bulky alkyl moieties.

4.2 Manuscript: Electron-deficient β -Diiminato-Zinc-Ethyl Complexes: Synthesis, Structure, and Reactivity in Ring-opening Polymerization of Lactones

Bibliographic Data


Status	Published online: February 17 th , 2016
Journal	<i>Organometallics</i> Volume 35, issue 5, pages 681–685
Publisher	American Chemical Society
Article type	Full Paper
DOI	10.1021/acs.organomet.5b00983
Authors	<u>Alexander Kronast</u> , Marina Reiter, Peter T. Altenbuchner, Christian Jandl, Alexander Pöthig, and Bernhard Rieger

Electron-Deficient β -Diiminato-Zinc-Ethyl Complexes: Synthesis, Structure, and Reactivity in Ring-Opening Polymerization of Lactones

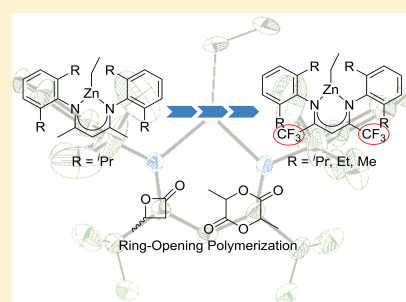
Alexander Kronast,^{†,§} Marina Reiter,^{†,§} Peter T. Altenbuchner,[†] Christian Jandl,[‡] Alexander Pöthig,[‡] and Bernhard Rieger^{*,†}

[†]WACKER-Lehrstuhl für Makromolekulare Chemie, Technische Universität München, Lichtenbergstraße 4, 85747 Garching bei München, Germany

[‡]Zentralinstitut für Katalyseforschung, Technische Universität München, Ernst-Otto-Fischer Straße 1, 85747 Garching bei München, Germany

 Supporting Information

ABSTRACT: A series of β -diiminato zinc(II) complexes bearing two electron-withdrawing trifluoromethyl groups in the pentane ligand backbone were successfully isolated ((BDI^{CF₃}-I)H = [CH(CCF₃NC₆H₄-2,6-CH(CH₃)₂)₂]; (BDI^{CF₃}-II)H = [CH(CCF₃NC₆H₄-2,6-C₂H₅)₂], and (BDI^{CF₃}-III)H = [CH(CCF₃NC₆H₄-2,6-CH₃)₂]). The solid-state structures illustrate differences in the ligation of the Zn atom compared to a literature known BDI-ZnEt complex. All catalysts show good activities in the ring-opening polymerization of the cyclic ester (*rac*)- β -butyrolactone (BL), whereas only BDI^{CF₃}-II-ZnEt and BDI^{CF₃}-III-ZnEt are active initiators for the polymerization of (*rac*)-lactide (LA).



Ring-opening polymerization of cyclic esters offers an easy access to biodegradable polyester structures.^{1–5} Cheap, available, and biocompatible metal-based initiators are of high interest as a postpolymerization removal of the catalyst is not necessary. Zinc(II) as a colorless metal ion and not dispensable trace element is applied as ligated catalyst center with a plethora of different ligands in the ring-opening polymerization of cyclic esters as well as in the copolymerization of carbon dioxide and epoxides. Among these ligands, the class of β -diiminato (BDI) structures assumes a special position due to its ease in accessibility and variability.^{6–20} The BDI as bidentate ligand bearing one delocalized negative charge was originally reported by Holm and co-workers.²¹ It has been synthesized with a multitude of substituents and metal ions all over the periodic table.^{22–24}

Electron-withdrawing substituents have been introduced by different groups into BDI or BDI related catalyst structures, primarily to increase the Lewis acidity of the metal center and thereby the activity of the catalyst for the copolymerization of carbon dioxide and epoxide and the ring-opening polymerization (ROP) of lactones.^{12,25} Tolman and co-workers extensively investigated the effect of electron-withdrawing groups on different catalysts for the ROP of cyclic esters, revealing opposing trends on activity for salen- and aminobisphenolate-based Al catalysts.^{26–28}

BDI ligands based on a 1,1,1,5,5,5-hexafluoro-acetylacetonone are scarcely reported in the literature and, to our knowledge, not applied to Zn(II) metal ions and ring-opening polymer-

ization catalysts until now.^{29–33} BDI^{CF₃}-I complexes of Cu(I) and Ti(IV) are some of these rare examples. The BDI^{CF₃}-I-Cu(I)-CO complex was tested in oxidation experiments comparing the reactivity of different BDI ligated Cu(I) complexes in correlation with the increased Lewis acidity of the metal center.³⁰ The group of Hill et al. discovered a double μ -F-bridged Ca dimeric complex bearing BDI^{CF₃}-I ligands at each Ca(II)-center, observing an intramolecular C–F-bond activation during synthetic procedures.³⁴ A BDI^{CF₃}-I analogue bearing unsubstituted phenyl moieties at the nitrogen atoms was used to increase the activity in the Ti(IV)-catalyzed polymerization of ethylene.³³ Although there are few examples for the use of 1,1,1,5,5,5-hexafluoro-acetylacetonone-based BDI ligands in the literature, the influence of two electron-withdrawing CF₃-groups on BDI-based initiators for the ring-opening polymerization of cyclic esters is still a white spot on the map.

Herein, we present the synthesis, characterization, and application of BDI^{CF₃}-Zn-Ethyl complexes as highly active initiators for the ROP of BL and LA. Aniline moieties of different steric demand were applied and revealed interesting differences in activity and stereoselectivity especially for LA.

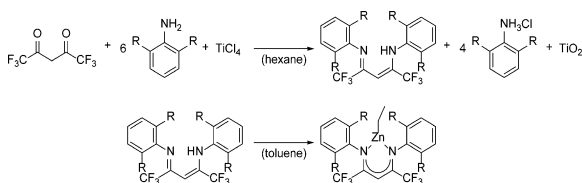
Syntheses. The preligands BDI^{CF₃}-H (I–III) can be synthesized by a modified literature procedure.²⁹ Because of

Received: December 2, 2015

Published: February 17, 2016

the low boiling point of 1,1,1,5,5,5-hexafluoro-2,4-pentadione, a simple acid-catalyzed condensation using a Dean–Stark apparatus to remove the produced water is not applicable. Rather, the reaction was performed by creating a reactive condensation mixture of the corresponding aniline and titanium tetrachloride. The amine forms a mixture of amido–titanium and imido–titanium species, as it was characterized for other amines in the reaction with titanium tetrachloride.^{35,36} Six equivalents of the amine have to be used for the double condensation with hexafluoro-acetylacetone as well as for the removal of HCl and the accompanied titanium dioxide precipitation driving the reaction to product formation (Scheme 1).

Scheme 1. Ligand and Complex Synthesis for BDI^{CF₃}-I-ZnEt (R = *i*Pr), BDI^{CF₃}-II-ZnEt (R = Et), and BDI^{CF₃}-III-ZnEt (R = Me)



The reaction of 1 equiv of the preligand BDI^{CF₃}-H (I–III) with an excess of 1.5 equiv of diethyl zinc in toluene at 100 °C over adjusted reaction times gave the complexes BDI^{CF₃}-I-ZnEt (I), BDI^{CF₃}-II-ZnEt (II) and BDI^{CF₃}-III-ZnEt (III) in quantitative yields after removal of the solvent, byproduct (ethane), and surplus metal precursor *in vacuo*. The highly moisture- and air-sensitive complexes can be recrystallized from toluene at –35 °C to obtain crystals in single-crystal X-ray diffraction (SC-XRD) quality (Figures 1–3).

An ORTEP style representation of the solid-state structure of I is given in Figure 1, including selected bond lengths and

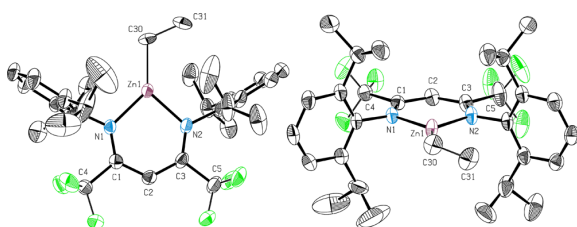


Figure 1. ORTEP style representation of I (hydrogen atoms omitted for clarity) with ellipsoids drawn at the 50% probability level. Disordered groups are indicated by thin bonds. Selected bond lengths (Å) and bond angles (deg): Zn1–N1 1.982(2), Zn1–N2 1.982(2), Zn1–C30 1.963(15), N1–Zn1–N2 94.28(8), N2–Zn1–C30 131.1(6), N1–Zn1–C30 134.4(6).

angles. Zn complexes of sterically less demanding BDI ligands are well-known to tend to the formation of dimeric structures in the case of alkoxide or amide ligands. This μ -bridging can be hampered through the choice of diethyl zinc as metal precursor, whereby I crystallizes in its monomeric form comparable to a BDI-ZnEt complex known in the literature (BDI-1-ZnEt).⁷ The metal center has a trigonal-planar coordination geometry with a Zn1–C30 bond length matching the value for BDI-1-ZnEt (1.963 Å) bearing methyl instead of trifluoro-methyl groups in

the pentane backbone. The Zn1–N1 and Zn1–N2 bond lengths are exactly equal with a value of 1.982(2) Å, and the metal is in plane with the ligand. The phenyl rings are almost perpendicular to the coordination plane.

The molecular structure of II is depicted in Figure 2. The 2,6-diethylphenyl moieties show little influence on the solid-

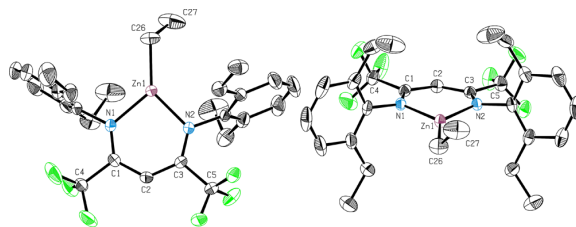


Figure 2. ORTEP style representation of II (hydrogen atoms omitted for clarity) with ellipsoids drawn at the 50% probability level. Selected bond lengths (Å) and bond angles (deg): Zn1–N1 1.985(2), Zn1–N2 1.975(2), Zn1–C26 1.947(2), N(1)–Zn(1)–N(2) 95.21(6), N(2)–Zn(1)–C(26) 136.08(8), N1–Zn(1)–C26 128.70(8).

state structure compared to I. The metal core adopts a similar distorted trigonal-planar geometry with a shortening of the Zn1–C26 bond to 1.947(2) Å. The Zn1–N1 (1.985(1) Å) and Zn1–N2 (1.975(1) Å) bonds show a slight difference in length in contrast to I. The N1–Zn1–C26 angle (128.70(8)°) and the N2–Zn1–C26 angle (136.08(8)°) show a larger difference between the two values in comparison to I.

In the solid-state structure of complex III, the Zn1–N1 (1.971(2) Å) and Zn1–N2 (1.969(2) Å) bonds differ only within their standard deviation, whereas the difference is 0.036 Å for BDI-1-ZnEt (Figure 3). The metal center adopts a

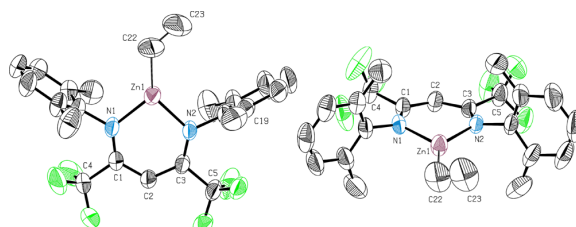


Figure 3. ORTEP style representation of III (hydrogen atoms omitted for clarity) with ellipsoids drawn at the 50% probability level. Disordered groups are indicated by thin bonds. Selected bond lengths (Å) and bond angles (deg): Zn1–N1 1.971(2), Zn1–N2 1.969(2), Zn1–C22 1.94(1), N1–Zn1–N2 95.24(9), N2–Zn1–C22 135.9(4), N1–Zn1–C22 128.8(4).

distorted trigonal-planar surrounding as in I and II. The Zn atom sits slightly above the mean plane of the ligand defined by N1, N2, C1, C2, C3 (0.183 Å), and the phenyl rings of the aniline moieties are almost aligned perpendicular to this plane and span angles of 89.4° and 82.5°. The N(1)–Zn1–C(22) angle (136.3(3)°) is slightly increased in comparison to BDI-1-ZnEt (133.9°), whereas, correspondingly, the N2–Zn(1)–C22 angle (128.4(3)°) is decreased. The crystals of compound III fragmented at low temperatures and, therefore, had to be measured at 200 K, causing a lower quality than for the other samples. A detailed discussion of further values will, therefore, be omitted, but it can be seen that there are no significant differences to the other structures.

Polymerization Results. Complexes I–III were tested in the ring-opening polymerization (ROP) of the cyclic esters (*rac*)- β -butyrolactone (BL) and (*rac*)-lactide (LA). Whereas II and III were active initiators in the polymerization of BL and LA, I was only active in the ring-opening polymerization of BL. This may be mainly attributed to sterical reasons, as the demanding *iso*-propyl groups in I hamper the coordination of the bulkier LA monomer. In comparison to BDI-1-ZnEt with the same substitution pattern, the bulkier CF₃ groups align the phenyl moieties almost vertically to the N1–Zn1–N2 plane and hamper rotational freedom around the *N*-phenyl bonds. This way, the nucleophilic attack of the attached initiator or alkoxide chain end at the monomer cannot proceed or is energetically unfavored.

The polymerizations of BL using the new initiators I–III show higher activities in comparison with (BDI-1-ZnEt) as an analogue of I, a living character (see Figure S2), and were observed via *in situ* IR (see Figure S1) (Table 1). Comparable

Table 1. Polymerization Results for the Polymerization of BL Using Complexes I–III and BDI-1-ZnEt^{37a}

entry	catalyst	conv. ^b	$M_{n,theo}$ ^c	$M_{n,exp}$ ^d	PD ^d	P_r ^e
1	BDI-1-ZnEt	>99	51.6	99.3	1.3	52
2	I	>99	51.6	66.6	1.2	52
3	II	>99	51.6	107.3	1.7	54
4	III	>99	51.6	120.8	1.8	53

^aReactions performed with $M = 17.4$ mmol, cat. = $29.0 \mu\text{mol}$ at 60°C in 5.0 g of toluene in an *in situ* IR autoclave. ^b[%] Conversion determined by ¹H NMR spectroscopy. ^c $M_{n,theo}$ [kg mol⁻¹]. ^d $M_{n,exp}$ [kg mol⁻¹] and PD determined by GPC in CHCl₃ versus polystyrene standards. ^e P_r is the probability of racemic linkages between monomer units and is determined by ¹³C NMR resonances of the carbonyl C atom.

to these results of increasing the catalyst activity by decreasing the electron density around the metal center, similar effects for salen-based Al initiators were found.²⁷ Under consideration of these investigations, the activity in ROP of cyclic esters of BDI-based Zn catalysts can be accelerated via introducing electron-withdrawing groups in the ligand backbone. Although all initiators indicate no stereoselectivity in the polymerization studies, activity trends can be deduced from the obtained experimental results. The lower the sterical demand of the substituent, the higher the resulting activity. Moreover, the obtained polymers point out a high degree of control during the polymerization, resulting in narrow PDs from 1.2 (I) to 1.8 (III).

The cyclic diester LA can also be successfully ring-opened by II and III (Table 2). After 20 h polymerization time, nearly quantitative conversion (>95%) of LA was observed, whereas the literature example shows only 83% conversion. The PD is comparable to literature results with (BDI-I-ZnEt) (2.1). The polymer microstructure was under closer scrutiny, as literature examples show a dependency of the heterotacticity on the aniline substituents. Lower sterical demand in the *ortho* position was found to reduce the control in stereoselectivity to heterotactic polymer.³⁷ Thus, the substitution pattern affects the possibility to control the monomer enchainment. This trend can also be transferred to our results, which mirrors in a drop from 66% heterotactic linkages for II (R = ethyl) to 60% for III (R = methyl).

Table 2. Polymerization Results for the Polymerization of LA Using Complexes I–III and BDI-1-ZnEt^{37a}

entry	catalyst	conv. ^b	$M_{n,theo}$ ^c	$M_{n,exp}$ ^d	PD ^d	P_r ^e
5	BDI-1-ZnEt	83	24.9	9.3	2.1	84
6	I	7	2.0	n.d.	n.d.	n.d.
7	II	96	27.7	18.8	2.1	66
8	III	95	27.4	13.1	2.1	60

^aReactions performed with $M = 3.20$ mmol, cat. = $16.0 \mu\text{mol}$ at 25°C in 10.64 g of dichloromethane. ^b[%] Conversion determined by ¹H NMR spectroscopy. ^c $M_{n,theo}$ [kg mol⁻¹]. ^d $M_{n,exp}$ [kg mol⁻¹] and PD determined by GPC in CHCl₃ versus polystyrene standards. ^e P_r is the probability of racemic linkages between monomer units and is determined by homodecoupled ¹H NMR resonances of the methine H atom.

CONCLUSION

We successfully introduced a new class of bis-CF₃-substituted β -diiminate Zn catalysts as initiators for the ring-opening polymerization of cyclic esters. The literature unknown preligands (BDI^{CF₃}-I)H and (BDI^{CF₃}-II)H were synthesized and effectively ligated the zinc-ethyl metal precursor to the active catalysts in quantitative yields. The structure of the complexes in the solid state was elucidated using SC-XRD measurements. The resulting catalysts I–III were tested in the ring-opening polymerization of cyclic esters BL and LA and showed an increase in activity in comparison to the literature known BDI-1-ZnEt. The improved activity originates from enhanced Lewis acidity of the metal center and thereby the activation of the coordinated lactone. The activity in the ROP of BL was observed using *in situ* IR measurements, revealing I as the most active zinc-ethyl-based initiator. II and III were also highly active in the ROP of LA and showed a high dependency of the resulting polymer microstructure on the phenyl substituents in the *ortho* position of the aniline moiety, resulting in different degrees of heterotactic PLA.

EXPERIMENTAL SECTION

General. All reactions containing air- and/or moisture-sensitive compounds were performed under dry argon using standard Schlenk or glovebox techniques. All chemicals were purchased from Aldrich, ABCR, or Acros. Solvents were obtained from an MBraun MB-SPS-800 solvent purification system.

Monomers were dried over calcium hydride and distilled prior to polymerization. NMR spectra were recorded on a Bruker AVIII-300 and AVIII-500 Cryo spectrometer. ¹H NMR spectroscopic chemical shifts δ are reported in ppm relative to tetramethylsilane and calibrated to the residual proton signal of the deuterated solvent. Deuterated solvents were obtained from Sigma-Aldrich and dried over 3 Å molecular sieves. ESI-MS analytical measurements were performed in acetonitrile solutions on a Varian 500 MS spectrometer. Gel permeation chromatography (GPC) analysis was performed on a Varian PL-GPC 50. As eluent, chloroform (HPLC grade) with 1.5 g L⁻¹ tetrabutylammonium tetrafluoroborate was used. Polystyrene standards were used for calibration. Elemental analysis was performed at the microanalytical laboratory of the Department of Inorganic Chemistry at the Technical University of Munich.

Ligand Synthesis. The ligands are synthesized according to a modified literature procedure for (BDI^{CF₃}-I)H.²⁹

N-((2Z,4Z)-4-((2,6-Di-isopropylphenyl)imino)-1,1,1,5,5,5-hexafluoropent-2-en-2-yl)-2,6-di-isopropylaniline ((BDI^{CF₃}-I)H). ¹ *N*-((2Z,4Z)-4-((2,6-Diethylphenyl)imino)-1,1,1,5,5,5-hexafluoropent-2-en-2-yl)-2,6-diethylaniline ((BDI^{CF₃}-II)H). 2,6-Diethylaniline (6.25 mL, 40.2 mmol, 8.40 equiv) was diluted in 40 mL of dry hexane under argon. A solution of TiCl₄ (1.44 mL, 13.1 mmol, 2.70 equiv) in 7 mL of dry hexane was added dropwise to a stirred solution of 2,6-

diethylaniline at 0 °C, while immediately a dense brown precipitate was formed. The mixture was left to stir for 2 h at 80 °C. After cooling to room temperature, 1,1,1,5,5,5-hexafluoro-2,4-pentanedione (0.67 mL, 4.78 mmol, 1.00 equiv) was added, and the mixture was stirred at 90 °C overnight. TiO₂ was removed by filtration, and the yellow solution was washed with water and brine. After hexane was removed *in vacuo*, MeOH was added to the oily residue, whereby yellow crystals (1.38 g, 2.93 mmol, 61%) were obtained overnight at 5 °C.

Anal. Calcd for C₂₅H₂₈F₆N₂: C, 63.82; H, 6.00; N, 5.95. Found: C, 63.77; H, 6.13; N, 5.95. ¹H NMR (300 MHz, CDCl₃, 298 K): δ (ppm) = 11.74 (br s, 1H, NH), 7.19–7.06 (m, 6H, H_{Aromat}), 5.86 (s, 1H, CH), 2.62–2.43 (m, 8H, CH₂), 1.18 (t, ³J = 7.6 Hz, 12H, CH₃). ¹³C NMR (75 MHz, CDCl₃, 298 K) δ (ppm) = 150.7 (q, ²J_{CF} = 29.5 Hz, NC(CF₃)CHC(CF₃)N), 139.41 (C_{Aromat}), 136.94 (C_{Aromat}), 126.40 (C_{Aromat}), 125.71 (C_{Aromat}), 119.1 (¹J_{CF} = 281 Hz, NC(CF₃)CHC(CF₃)N), 87.04 (NC(CF₃)CHC(CF₃)N), 24.32 (CH₂CH₃), 14.12 (CH₂CH₃).

N-(2*Z*,4*Z*)-4-((2,6-Dimethylphenyl)imino)-1,1,1,5,5,5-hexafluoro-2-en-2-yl)-2,6-dimethylaniline ((*BDI*^{CF₃}-III)*H*). 2,6-Dimethylaniline (6.10 mL, 49.5 mmol, 6.00 equiv) was diluted in 30 mL of dry hexane under argon. A solution of TiCl₄ (1.99 mL, 18.15 mmol, 2.20 equiv) in 7 mL of dry hexane was added dropwise to a stirred solution of 2,6-dimethylaniline at 0 °C, while immediately a dense brown precipitate was formed. The mixture was left to stir for 2 h at 80 °C. After cooling to room temperature, 1,1,1,5,5,5-hexafluoro-2,4-pentanedione (1.15 mL, 8.25 mmol, 1.00 equiv) was added, and the mixture was stirred at 90 °C overnight. TiO₂ was removed by filtration, and the yellow solution was washed with water and brine. After hexane was removed *in vacuo*, MeOH was added to the oily residue, whereby yellow crystals (1.12 g, 2.70 mmol, 33%) were obtained overnight at 5 °C.

Anal. Calcd for C₂₁H₂₀F₆N₂: C, 60.87; H, 4.86; N, 6.76. Found: C, 60.80; H, 5.11; N, 6.73. ¹H NMR (300 MHz, CDCl₃, 298 K): δ (ppm) = 11.89 (br s, 1H, NH), 7.11–7.06 (m, 6H, H_{Aromat}), 5.92 (s, 1H, CH), 2.19 (s, 12H, CH₃). ¹³C NMR (126 MHz, CDCl₃, 298 K) δ (ppm) = 151.06 (q, ²J_{CF} = 29.7 Hz, NC(CF₃)CHC(CF₃)N), 140.80 (C_{Aromat}), 131.44 (C_{Aromat}), 127.96 (C_{Aromat}), 126.03 (C_{Aromat}), 118.94 (¹J_{CF} = 283.5 Hz, NC(CF₃)CHC(CF₃)N), 86.83 (NC(CF₃)CHC(CF₃)N), 18.37 (ArCH₃).

Complex Synthesis. 1.00 equiv of the ligand and 1.50 equiv of a 1 M ZnEt₂ solution were dissolved in dry toluene and stirred at 100 °C under an inert atmosphere for 3 days. After cooling to room temperature, the solvent was removed under vacuum, and a pure yellow solid was obtained.

Complex I. Yield 80%. Anal. Calcd for C₃₁H₄₀F₆N₂Zn: C, 60.05; H, 6.50; N, 4.52. Found: C, 59.76; H, 6.21; N, 4.54. ¹H NMR (300 MHz, C₆D₆, 298 K): δ (ppm) = 7.10–7.01 (m, 6H, H_{Aromat}), 6.19 (s, 1H, CH), 3.04–2.90 (m, 4H, CH), 1.21 (d, ³J = 6.7 Hz, 12H, CH₃), 1.16 (d, ³J = 6.7 Hz, 12H, CH₃), 0.66 (t, ³J = 8.1 Hz, 3H, CH₃), 0.16 (q, ³J = 8.1 Hz, 2H, CH₂). ¹³C NMR (75 MHz, C₆D₆, 298 K) δ (ppm) = 155.7 (q, ²J_{CF} = 26.5 Hz, NC(CF₃)CHC(CF₃)N), 142.2 (C(CH₃)(Me)₂), 140.9 (C–N, aromatic C), 127.2 (C_{Aromat}), 123.92 (C_{Aromat}), 120.3 (¹J_{CF} = 285.0 Hz, NC(CF₃)CHC(CF₃)N), 86.0 (NC(CF₃)CHC(CF₃)N), 29.0 (MeCHMe), 24.7 (MeCHMe), 23.0 (MeCHMe), 11.0 (ZnCH₂CH₃), 0.6 (ZnCH₂CH₃).

Complex II. Yield 85%. Anal. Calcd for C₂₇H₃₂F₆N₂Zn: C, 57.51; H, 5.72; N, 4.97. Found: C, 57.63; H, 5.74; N, 5.02. ¹H NMR (300 MHz, C₆D₆, 298 K): δ (ppm) = 7.06–6.96 (m, 6H, H_{Aromat}), 6.21 (s, 1H, CH), 2.53–2.39 (m, 8H, CH₂), 1.09 (t, ³J = 7.6 Hz, 12H, CH₃), 0.70 (t, ³J = 8.1 Hz, 3H, CH₃), 0.11 (q, ³J = 8.1 Hz, 2H, CH₂). ¹³C NMR (75 MHz, C₆D₆, 298 K) δ (ppm) = 155.7 (q, ²J_{CF} = 28.0 Hz, NC(CF₃)CHC(CF₃)N), 143.6 (C_{Aromat}), 136.3 (C_{Aromat}), 126.7 (C_{Aromat}), 126.1 (C_{Aromat}), 120.1 (¹J_{CF} = 281.3 Hz, NC(CF₃)CHC(CF₃)N), 85.8 (NC(CF₃)CHC(CF₃)N), 24.8 (CH₂CH₃), 14.2 (CH₂CH₃), 11.3 (ZnCH₂CH₃), –1.7 (ZnCH₂CH₃).

Complex III. Yield 82%. Anal. Calcd for C₂₃H₂₄F₆N₂Zn: C, 54.40; H, 4.76; N, 5.52. Found: C, 54.21; H, 4.96; N, 5.46. ¹H NMR (300 MHz, C₆D₆, 298 K): δ (ppm) = 6.90 (s, 6H, H_{Aromat}), 6.18 (s, 1H, CH), 2.03 (s, 12H, ArCH₃), 0.73 (t, ³J = 9.0 Hz, 3H, CH₃), 0.09 (q, ³J = 9.0 Hz, 2H, CH₂). ¹³C NMR (126 MHz, C₆D₆, 298 K) δ (ppm) =

155.55 (q, ²J_{CF} = 27.2 Hz, NC(CF₃)CHC(CF₃)N), 144.66 (C_{Aromat}), 130.48 (C_{Aromat}), 128.20 (C_{Aromat}), 126.01 (C_{Aromat}), 119.70 (q, ¹J_{CF} = 286.2 Hz, NC(CF₃)CHC(CF₃)N), 85.61 (NC(CF₃)CHC(CF₃)N), 18.33 (ArCH₃), 10.87 (ZnCH₂CH₃), –3.40 (ZnCH₂CH₃).

General Polymerization Procedure for (*rac*)-β-Butyrolactone. A solution of the respective catalyst (29.0 μmol, 1 equiv) was dissolved in 5.0 g of toluene and transferred in a mechanically stirred 30 mL steel autoclave with an *in situ* IR diamond window and preheated to the polymerization temperature (60 °C). (*rac*)-BL (1.50 g, 17.4 mmol, 600 equiv) was added to the catalyst solution, and the polymerization progress was monitored via *in situ* IR. After the reaction is at a standstill, as no more increase of the polymer carbonyl stretching is observed, a small aliquot was taken to determine the conversion using ¹H NMR spectroscopy. The polymerization was quenched by addition of hydrous chloroform. The polymer was precipitated by the addition of 50 mL of an Et₂O/pentane (1:1) mixture and dried under vacuum to constant weight.

General Polymerization Procedure for (*rac*)-Lactide. (*rac*)-Lactide (0.461 g, 3.20 mmol, 200 equiv) was dissolved in 9.0 g of dichloromethane. A solution of the respective catalyst (16.0 μmol, 1 equiv) in 1.64 g of dichloromethane was prepared and added to the lactide solution. After 20 h stirring at room temperature, a small aliquot was taken to determine the conversion using ¹H NMR spectroscopy. The polymerization was quenched by addition of hydrous methanol. Afterward, the polymer was precipitated by the addition of 50 mL of an Et₂O/pentane (1:1) mixture and dried under vacuum to constant weight.

■ ASSOCIATED CONTENT

● Supporting Information

The Supporting Information is available free of charge on the ACS Publications website at DOI: 10.1021/acs.organomet.5b00983.

Crystallographic data for complexes I–III (CIF)

Experimental procedures, *in situ* IR data, GPC data, NMR data for microstructure determination of PHB and PLA, and SC-XRD data (CCDC 1439897–1439899) (PDF)

■ AUTHOR INFORMATION

Corresponding Author

*E-mail: rieger@tum.de. Tel: +49-89-289-13570. Fax: +49-89-289-13562.

Author Contributions

§These authors contributed equally.

Notes

The authors declare no competing financial interest.

■ ACKNOWLEDGMENTS

The authors thank BASF SE for financial support. The authors thank Richard Reithmeier for proofreading the manuscript.

■ REFERENCES

- (1) Thomas, C. M. *Chem. Soc. Rev.* **2010**, *39*, 165.
- (2) Dechy-Cabaret, O.; Martin-Vaca, B.; Bourissou, D. *Chem. Rev.* **2004**, *104*, 6147.
- (3) Bouyahy, M.; Ajellal, N.; Kirillov, E.; Thomas, C. M.; Carpentier, J.-F. *Chem.–Eur. J.* **2011**, *17*, 1872.
- (4) Coulembier, O.; Degée, P.; Hedrick, J. L.; Dubois, P. *Prog. Polym. Sci.* **2006**, *31*, 723.
- (5) Altenbuchner, P. T.; Kronast, A.; Kissling, S.; Vagin, S. I.; Herdtweck, E.; Pöthig, A.; Deglmann, P.; Loos, R.; Rieger, B. *Chem.–Eur. J.* **2015**, *21*, 13609.
- (6) Cheng, M.; Attygalle, A. B.; Lobkovsky, E. B.; Coates, G. W. *J. Am. Chem. Soc.* **1999**, *121*, 11583.

- (7) Cheng, M.; Moore, D. R.; Reczek, J. J.; Chamberlain, B. M.; Lobkovsky, E. B.; Coates, G. W. *J. Am. Chem. Soc.* **2001**, *123*, 8738.
- (8) Dunn, E. W.; Coates, G. W. *J. Am. Chem. Soc.* **2010**, *132*, 11412.
- (9) Ovitt, T. M.; Coates, G. W. *J. Am. Chem. Soc.* **1999**, *121*, 4072.
- (10) Rieth, L. R.; Moore, D. R.; Lobkovsky, E. B.; Coates, G. W. *J. Am. Chem. Soc.* **2002**, *124*, 15239.
- (11) Kissling, S.; Altenbuchner, P. T.; Lehenmeier, M. W.; Herdtweck, E.; Deglmann, P.; Seemann, U. B.; Rieger, B. *Chem.–Eur. J.* **2015**, *21*, 8148.
- (12) Kissling, S.; Lehenmeier, M. W.; Altenbuchner, P. T.; Kronast, A.; Reiter, M.; Deglmann, P.; Seemann, U. B.; Rieger, B. *Chem. Commun.* **2015**, *51*, 4579.
- (13) Lehenmeier, M. W.; Kissling, S.; Altenbuchner, P. T.; Bruckmeier, C.; Deglmann, P.; Brym, A.-K.; Rieger, B. *Angew. Chem., Int. Ed.* **2013**, *52*, 9821.
- (14) Wang, Y.; Zhao, W.; Liu, D.; Li, S.; Liu, X.; Cui, D.; Chen, X. *Organometallics* **2012**, *31*, 4182.
- (15) Mou, Z.; Liu, B.; Wang, M.; Xie, H.; Li, P.; Li, L.; Li, S.; Cui, D. *Chem. Commun.* **2014**, *50*, 11411.
- (16) Darensbourg, D. J.; Karroonnirun, O. *Inorg. Chem.* **2010**, *49*, 2360.
- (17) Darensbourg, D. J.; Karroonnirun, O. *Macromolecules* **2010**, *43*, 8880.
- (18) Williams, C. K.; Breyfogle, L. E.; Choi, S. K.; Nam, W.; Young, V. G.; Hillmyer, M. A.; Tolman, W. B. *J. Am. Chem. Soc.* **2003**, *125*, 11350.
- (19) Sarazin, Y.; Schormann, M.; Bochmann, M. *Organometallics* **2004**, *23*, 3296.
- (20) Darensbourg, D. J.; Choi, W.; Richers, C. P. *Macromolecules* **2007**, *40*, 3521.
- (21) Parks, J. E.; Holm, R. H. *Inorg. Chem.* **1968**, *7*, 1408.
- (22) Bourget-Merle, L.; Lappert, M. F.; Severn, J. R. *Chem. Rev.* **2002**, *102*, 3031.
- (23) Chisholm, M. H.; Gallucci, J. C.; Phomphrai, K. *Inorg. Chem.* **2005**, *44*, 8004.
- (24) Lazarov, B. B.; Hampel, F.; Hultzsck, K. C. Z. *Anorg. Allg. Chem.* **2007**, *633*, 2367.
- (25) Allen, S. D.; Moore, D. R.; Lobkovsky, E. B.; Coates, G. W. *J. Am. Chem. Soc.* **2002**, *124*, 14284.
- (26) Miranda, M. O.; DePorre, Y.; Vazquez-Lima, H.; Johnson, M. A.; Marell, D. J.; Cramer, C. J.; Tolman, W. B. *Inorg. Chem.* **2013**, *52*, 13692.
- (27) Ding, K.; Miranda, M. O.; Moscato-Goodpaster, B.; Ajellal, N.; Breyfogle, L. E.; Hermes, E. D.; Schaller, C. P.; Roe, S. E.; Cramer, C. J.; Hillmyer, M. A.; Tolman, W. B. *Macromolecules* **2012**, *45*, 5387.
- (28) Alcazar-Roman, L. M.; O'Keefe, B. J.; Hillmyer, M. A.; Tolman, W. B. *Dalton Trans.* **2003**, 3082.
- (29) Carey, D. T.; Cope-Eatough, E. K.; Vilaplana-Mafe, E.; Mair, F. S.; Pritchard, R. G.; Warren, J. E.; Woods, R. J. *Dalton Trans.* **2003**, 1083.
- (30) Hill, L. M. R.; Gherman, B. F.; Aboeella, N. W.; Cramer, C. J.; Tolman, W. B. *Dalton Trans.* **2006**, 4944.
- (31) Radwan, Y. K.; Maity, A.; Teets, T. S. *Inorg. Chem.* **2015**, *54*, 7122.
- (32) Schreiber, D. F.; Ortin, Y.; Müller-Bunz, H.; Phillips, A. D. *Organometallics* **2011**, *30*, 5381.
- (33) Tang, L.-M.; Duan, Y.-Q.; Li, X.-F.; Li, Y.-S. *J. Organomet. Chem.* **2006**, *691*, 2023.
- (34) Barrett, A. G. M.; Crimmin, M. R.; Hill, M. S.; Hitchcock, P. B.; Procopiou, P. A. *Angew. Chem., Int. Ed.* **2007**, *46*, 6339.
- (35) Nielson, A. J. *Inorg. Chim. Acta* **1988**, *154*, 177.
- (36) Zambrano, C. H.; Profflet, R. D.; Hill, J. E.; Fanwick, P. E.; Rothwell, I. P. *Polyhedron* **1993**, *12*, 689.
- (37) Chamberlain, B. M.; Cheng, M.; Moore, D. R.; Ovitt, T. M.; Lobkovsky, E. B.; Coates, G. W. *J. Am. Chem. Soc.* **2001**, *123*, 3229.

From Aliphatic Poly(ester)s to Poly(vinylpyridine)s

After some effort was taken to reach the ambitious goals for a stereoselective and highly active zinc (II) based catalysis for the Ring-opening polymerization of BBL and LA to biodegradable plastics, the possibilities in catalyst alterations were exhausted. Though a stereoselectivity was not reached for the ROP of BBL an enhanced polymerization activity of BDI based catalysts *via* introducing electron-withdrawing groups was achieved. Despite the use in ROP catalysis, BDI zinc (II) complexes are well known to catalyze the copolymerization of carbon dioxide and different epoxides, such like propylene oxide, cyclohexene oxide, or limonene oxide. In following work on the basis of the herein presented electron-deficient complexes ensuing investigations in other projects lead to insights and remarkable improvements for this kind of catalysis. Beside improved activity the catalysts thereby distinguished themselves as being the only capable system to allow the use of poly(siloxane) based chain transfer agents in the copolymerization of propylene oxide and CO₂ (see *e.g.* **chapter 6.1.4**).

Parallel progress in the field of REM-GTP offered an alternative approach for the synthesis of functional polymers taking advantage of recent findings in- and outside our group. The widening of the assortment of addressable monomers promised tremendous possibilities to enhance materials characteristics through a high degree of control combined with catalyst induced stereospecificity. Especially the introduction of versatile 2-methoxyethylamino-bis(phenolate) yttrium catalysts offers the introduction of steric alterations being powerful enough to influence the stereochemistry of REM-GTP significantly. Thus the second part of this thesis was dedicated to the stereospecific rare earth metal-mediated group transfer polymerization of 2-vinylpyridine.

4.3 2-Methoxyethylamino-bis(phenolate) yttrium catalysts for the synthesis of highly isotactic poly(2-vinylpyridine) by rare-earth metal-mediated group transfer polymerization

Alexander Kronast, Dominik Reiter, Peter T. Altenbuchner, Sergei I. Vagin, and Bernhard Rieger

published as Full Paper in *MACROMOLECULES* **2016**, *49* (17), 6260–6267

C_1 -asymmetric 2-methoxyethylamino-bis(phenolate)yttrium catalysts of the type (ONOO)RY(CH₂Si(CH₃)₃) (THF) have been developed and successfully tested for the living and highly *isoselective* group transfer polymerization of prochiral 2-vinylpyridine. The steric bulk introduced into the new ligand structures influenced the stereospecificity of the catalysts. Isotacticities varying from $P_m = 0.60$ (2, **Figure 11**) up to $P_m = 0.92$ (4, **Figure 11**), narrow molecular weight distributions (PDI < 1.19), and high molecular weights were achieved by steric modifications of the variable bisphenolate ligand structure.

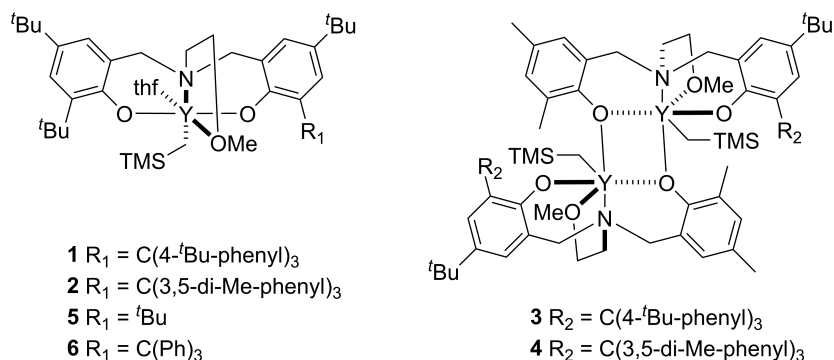


Figure 11: Catalyst structures developed for the highly *isoselective* REM-GTP of 2VP (1-4) including literature known complexes 5 and 6.

The melting transition temperatures of the obtained polymers depended on their *isotactic* content and thermal history. To observe crystalline domains *via* DSC and XRD a thermal treatment of the highly *isotactic* polymer samples was inevitable and the optimum crystallization temperature for highly *isotactic* P2VP was determined to be at around 170 °C, providing the sharpest melting transition in DSC measurements.

The underlying mechanism of the polymerization was examined in greater detail by ¹³C NMR, which excluded a *Bernoulli chain end control* mechanism and confirmed an *enantiomorphic site control* mechanism. The unique characteristics of this *enantiomorphic site mechanism* in the polymerization of 2VP allowed additional microstructure

information to be deduced and two previously misassigned pentads of P2VP to be correctly assigned.

4.4 Manuscript: 2-Methoxyethylamino-bis(phenolate) yttrium catalysts for the synthesis of highly isotactic poly(2-vinylpyridine) by rare-earth metal-mediated group transfer polymerization

Bibliographic Data

Status	Published online: August 29 th , 2016
Journal	<i>Macromolecules</i> Volume 49, issue 17, pages 6260–6267
Publisher	American Chemical Society
Article type	Full Paper
DOI	10.1021/acs.macromol.6b01179
Authors	<u>Alexander Kronast</u> , Dominik Reiter, Peter T. Altenbuchner, Sergei I. Vagin, and Bernhard Rieger

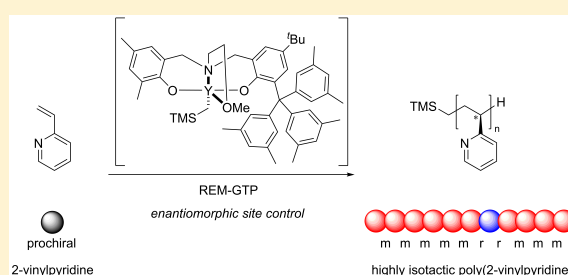
2-Methoxyethylamino-bis(phenolate)yttrium Catalysts for the Synthesis of Highly Isotactic Poly(2-vinylpyridine) by Rare-Earth Metal-Mediated Group Transfer Polymerization

Alexander Kronast, Dominik Reiter, Peter T. Altenbuchner, Sergei I. Vagin, and Bernhard Rieger*

WACKER-Lehrstuhl für Makromolekulare Chemie, Technische Universität München, Lichtenbergstraße 4, 85748 Garching b. München, Germany

Supporting Information

ABSTRACT: Highly isotactic poly(2-vinylpyridine) (P2VP) was synthesized by the group transfer polymerization of the prochiral 2-vinylpyridine (2VP) with 2-methoxyethylamino-bis(phenolate)yttrium complexes. Isotacticities of up to $P_m = 0.92$, narrow molecular weight distributions, and high molecular weights were achieved by steric modifications of the variable bisphenolate ligand structure. The resulting polymer samples were characterized by thermoanalysis (DSC, TGA), GPC, and ^{13}C NMR. The origin of the isotactic microstructure was attributed to an enantiomorphic site control mechanism based on ^{13}C NMR mechanistic studies and allowed new insights into ^{13}C pentad assignments.



INTRODUCTION

Stereocontrol in polymerization chemistry was first achieved in the 1950s through the remarkable findings of Giulio Natta's group, who reported the isoselective polymerization of prochiral propylene and other α -olefinic monomers.¹ Many other publications on the stereoselective polymerization of propylene followed, and interest in polymer microstructures spread to all vinylic monomers.^{2–7} The polymer microstructure has tremendous effects on the macromolecular characteristics such as the mechanical and physical properties. For example, atactic poly(propylene) (aPP) lacks crystalline domains, whereas isotactic poly(propylene) (iPP) coils into a helical shape, allowing crystallization of the helices with a higher melting temperature ($T_m = 185\text{--}220\text{ }^\circ\text{C}$) compared with syndiotactic poly(propylene) (sPP; $T_m = 160\text{--}180\text{ }^\circ\text{C}$).^{8,9}

Poly(2-vinylpyridine) (P2VP) and its copolymers have been studied for applications in electrochemistry, optics, medicine, nanotechnology, and membrane technology.^{10–34} The isospecific polymerization of 2-vinylpyridine (2VP) was also discovered by Natta's group in the early 1960s through the polymerization of 2VP with magnesium amides in non-coordinating solvents.^{35,36} Subsequent studies by Soum and Fontanille concerning the chain propagation mechanism and thus the source of its stereoselectivity excluded Bernoulli chain end control.^{37–39} Supported by ^{13}C NMR analysis, these researchers proposed a Markov chain end control with two coordinated monomers in a *gauche* conformation at the metal cation. Unfortunately, the use of magnesium amides always produces a certain proportion of atactic byproduct and prevents further fine-tuning of the tacticity to lower or higher values of the *meso* diads (P_m) in the respective polymers.

Recently, the use of rare-earth metal-mediated group transfer polymerization (REM-GTP), e.g., by the group of Rieger and Mashima, enabled the polymerization of 2VP.^{40–42} Different catalyst systems based on yttrium metal ions were employed for the isoselective polymerization of 2VP with varying degrees. Group transfer polymerization using group 3 metal ions itself was originally developed by the group of Yasuda using samarium Cp* complexes for the polymerization of methyl methacrylate.⁴³ The advantages of GTP include its production of strictly linear polymers and narrow molecular weight distributions ($\text{PDI} < 1.1$). Based on the originally easily accessible amine-bis(phenolate) ligands invented by Kol's group,⁴⁴ a new class of 2-methoxyethylamino-bis(phenolate) yttrium catalysts was successfully tested for the homo- and copolymerization of several monomers, namely 2VP, diethyl vinyl phosphonate (DEVp), 2-isopropenyl-2-oxazoline (IPOx), and *N,N'*-dimethylacrylamide (DMAA).⁴¹

Variation in the steric environment of the metal center in this class allowed isospecific polymerization of 2VP with P_m values up to 0.74. Contrary to the polymerization using magnesium amides, the elucidated mechanism for the stereospecific GTP of 2VP is enantiomorphic site control.⁴⁵ This difference represents a breakthrough in stereospecific GTP and opens a multitude of new possibilities, comparable with the introduction of metallocenes in propylene polymerization. In parallel to the on hand work the group of Lu developed an bis(phenolate) ether-based yttrium catalyst based on literature known ligand structures

Received: June 2, 2016

Revised: August 14, 2016

Published: August 29, 2016

Table 1. REM-GTP Results for Catalysts 1–4 of 2VP^a

entry	catalyst	temp [°C]	solvent	time [h]	conv [%]	$M_{n,theo}^b$ [kg/mol]	$M_{n,exp}$ [kg/mol]	I^*c	M_w/M_n	P_m^d
1	1	-10	toluene	22	38	8.3	15.0	0.55	1.06	0.82
2	2	-10	toluene	22	73	15.8	30.4	0.52	1.05	0.60
3	1	r.t.	toluene	2	>99	21.5	35.7	0.60	1.06	0.82
4	2	r.t.	toluene	2.6	>99	21.7	33.0	0.66	1.05	0.60
5	3	r.t.	toluene	22	28	6.2	368.1	0.02	1.19	0.64
6	4	r.t.	toluene	22	99	21.9	355.4	0.06	1.14	0.92
7	4	r.t.	THF	22	>99	21.1	175.2	0.12	1.12	0.92
8	4	r.t.	pyridine	22	<1	n.d.	n.d.	n.d.	n.d.	n.d.
9	1	50	toluene	1	>99	21.4	41.1	0.52	1.05	0.82
10	2	50	toluene	1	>99	21.6	39.2	0.55	1.05	0.60
11	3	50	toluene	4	<1	n.d.	n.d.	n.d.	n.d.	n.d.
12	4	50	toluene	4	64	14.1	491.7	0.03	1.13	0.92

^aPolymerizations performed with [2VP] = 2.7 mmol, [2VP]/[Cat.] = 200/1, at 25 °C in 2 mL of solvent, conversions determined by ¹H NMR spectroscopy and $M_{n,exp}$ determined by GPC-MALS. ^b $M_{n,theo} = M(2VP) \cdot ([2VP]/[Cat.] \cdot \text{conversion})$. ^c $I^* = M_{n,theo}/M_{n,exp}$. ^d P_m is the probability of *meso* linkages between monomer units and is determined by ¹³C NMR spectroscopy. n.d. = not determined due to low conversion.

producing P2VP with high molecular weights and tacticities of $P_m > 0.95$.⁴⁶

Herein, we present the application of ligand-tuned 2-methoxyethylamino-bis(phenolate)yttrium catalysts (ONOO)^RY(CH₂Si(CH₃)₃)₂ (THF) in the isoselective polymerization of 2VP to *i*P2VP. Variation of the substitution pattern of the ligands in the *ortho* position provides a broad range of tacticities with a maximum P_m of over 0.90. These findings lead to a detailed discussion of the mechanistic considerations and more profound insights into the ¹³C pentad assignments for microstructure analysis.

RESULTS AND DISCUSSION

In our previous publication, we reported the synthesis of C₁-symmetric 2-methoxyethylamino-bis(phenolate)yttrium catalysts and their application in the polymerization of 2VP to isotactically enriched P2VP.⁴⁵ Asymmetrically substituted ligands were accessible by a seven-step synthesis utilizing an alternative approach (see Supporting Information). In the final step, a secondary amine participates in an S_N-type reaction with a bromomethyl phenol to produce the desired asymmetric ligand structures in good yields (64–68%). Subsequent reaction of the proligands H₂(ONOO)^R (L1–L4) with 1 equiv of the metal precursor Y(CH₂TMS)₃(THF)₂ at low temperature, followed by recrystallization in pentane, yields the desired catalysts.

The complexes were characterized by NMR spectroscopy and elemental analysis (EA), whereby complexes 3 and 4 revealed dimeric structures comparable to previously described symmetrically and unsymmetrically substituted complexes.⁴⁷ The newly developed asymmetric complexes 1–4 were successfully applied in the GTP of 2VP in toluene at room temperature, producing P2VP in a highly controlled fashion (PDI < 1.19, Table 1), which is somehow surprising due to low initiator efficiencies.

The initiation mechanism had previously been elucidated and entails precoordination of 2VP followed by a six-membered intermediate and insertion of the vinylic double bond into the Y-CH₂TMS bond (see Supporting Information).

The initiator efficiency (I^*) ensures comparable values for the different catalyst activities in kinetic investigations. The normalized turnover frequency (TOF*) can be calculated as TOF/ I^* , where I^* is the average value of I^* during the linear growth of the polymerization.

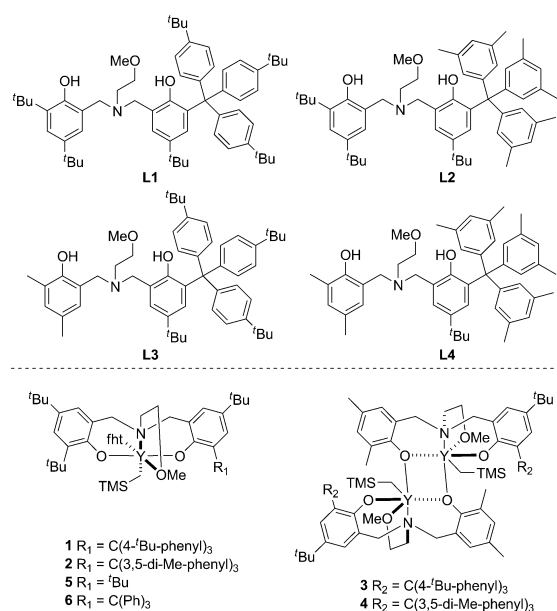


Figure 1. Proligand and catalyst structures for the REM-GTP of 2VP, including the literature complexes 5 and 6.⁴⁵

Steric crowding around the metal center and dimerization of the complexes have previously been found to dramatically influence I^* , whereas the normalized activities of the evaluated catalysts remain comparable. Consequently, the I^* values for catalysts 1 (65%) and 2 (60%) are lower than for complex 6 from the literature. Kinetic investigations show that catalysts 1 and 2 have no initiation period and activities of TOF* = 239 h⁻¹ and TOF* = 330 h⁻¹, respectively (Figure 2). Despite being lower than those of complex 6, these moderate activities are still applicable for kinetic investigations. Catalysts 3 and 4 were not subjected to further kinetic investigation due to their low activities and slow initiation processes.

Although the activities of complexes 1 and 2 are only moderate, the steric bulk around the metal center is noticeably higher than that for the highly active bis(phenolate)-based complex 5 (TOF* = 1100 h⁻¹).

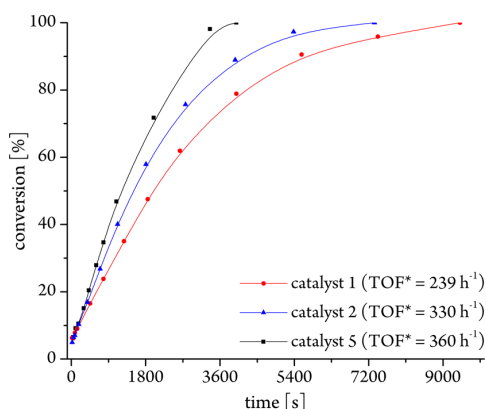


Figure 2. Catalytic activity of catalysts **1**, **2**, and **5** (catalyst 135 μmol , 2VP 27 mmol, toluene 20 mL, $T = 25\text{ }^\circ\text{C}$).

The variation of the polymerization parameters led to differences in initiation and activity, as expected based on the breaking up of the dimeric structures and energetic arguments. At low polymerization temperatures ($-10\text{ }^\circ\text{C}$), catalysts **3** and **4** showed no conversion after 22 h, while catalysts **1** (38%) and **2** (73%) showed moderate conversions.

As expected, the I^* values decreased slightly to 52% (**1**) and 55% (**2**) at lower polymerization temperatures. Increasing the polymerization temperature to $50\text{ }^\circ\text{C}$ led to higher activities for complexes **1** and **2**, full conversion of 200 equiv of 2VP in 1 h, and comparable I^* values of 55% (**1**) and 52% (**2**). Meanwhile, **3** only showed low conversion (<1%) after 4 h, whereas catalyst **4** showed 64% conversion and an unchanged I^* value of 3%.

The influence of the coordinating solvents was evaluated by substituting toluene for pyridine and THF with complex **3**. Whereas the pyridine-solvated reaction mixture showed no conversion after 22 h, the THF-solvated mixture still showed full conversion of the monomer, a higher I^* (12%) due to the breaking up of the dimeric structures, and a slightly broadened PDI (1.12).

Catalyst **6** paved the way for the stereoselective GTP of 2VP using asymmetric 2-methoxyethylamino-bis(phenolate)yttrium catalysts. Steric repulsion of the triphenylmethyl (trityl) group in the *ortho* position leads to an enantiomorphic site control mechanism, providing an isotacticity of $P_m = 0.74$, calculated based on the triad level of the aromatic quaternary resonances in the ^{13}C NMR spectra.

An increase of this steric bulk under the restraining influence of the second coordinating phenol led to complexes **1** and **2**. Complex **1** showed the expected increase in stereoselectivity to a P_m value of 0.82 and mmmm as main pentad in the ^{13}C NMR spectrum; however, contrary to our expectations these features were not found for complex **2**. Although the activity of **2** ($\text{TOF}^* = 330\text{ h}^{-1}$) was lower than that of **6**, the tacticity indicates only a minimal shift to isotactically enriched P2VP, including a clear increase of the mmmm pentad ($P_m = 0.60$). Thus, the results of the kinetic investigations and the obtained tacticities do not permit any context.

These contradictory results were also found when comparing complexes **3** and **4**. While complex **3** shows the lowest activity of all the tested complexes and a P_m of only 0.62, complex **4** produces a highly isotactic P2VP with a P_m value of 0.92, which is the highest value reported for 2-methoxyethylamino-bis(phenolate)yttrium catalysts to date.

The influence of coordinating solvents, such as THF and pyridine, on the stereoselectivity was investigated (Table 1, entries 7 and 8). While polymerization in pyridine shows no conversion, that in THF preserves the stereoselectivity ($P_m = 0.92$).

In summary, the steric environment around the active metal center must exactly match the requirements of the polymerization mechanism to exert a stereospecific influence. These findings therefore support a more targeted synthesis of ligand structures for the stereoselective GTP of 2VP.

The origin of stereocontrol was further investigated by considering the two possible regimes: chain end control and enantiomorphic site control. Because of insufficient resolution of the pentad resonances in the quaternary aromatic region of the ^{13}C NMR polymer spectra, the interpretation was conducted on the triad level (Figure 3). The prevailing

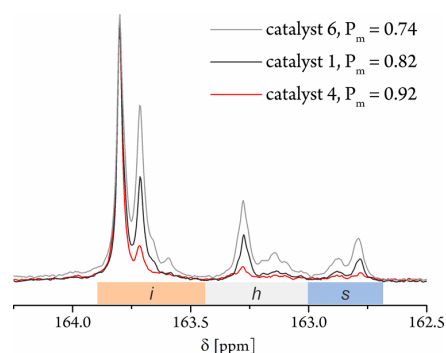


Figure 3. Aromatic quaternary ^{13}C NMR resonances (*i*, *h*, and *s* represent isotactic, heterotactic, and syndiotactic triads, respectively) of 30 mg of poly(2-vinylpyridine) (P2VP) in 0.6 mL of CD_3OD for catalysts **1**, **4**, and **6** ($[\text{2VP}]:[\text{Cat.}] = 200:1$, $[\text{M}] = 2.7\text{ mmol}$, 2 mL of toluene, $25\text{ }^\circ\text{C}$).

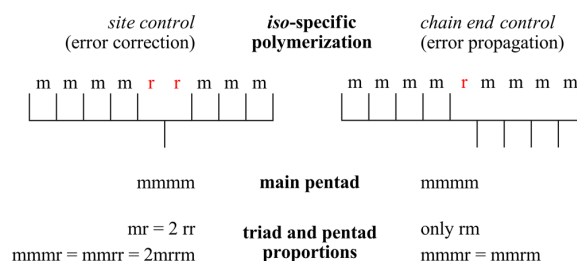


Figure 4. Stereoerrors in enantiomorphic site vs Bernoullian chain end control.

mechanism of the isospecific polymerization of prochiral 2VP can be assigned by Bernoullian chain end (1) and enantiomorphic site control (2) tests:

$$B = \frac{4(\text{mm})(\text{rr})}{(\text{mr})^2} = 1 \quad (1)$$

$$E = \frac{2(\text{rr})}{(\text{mr})} = 1 \quad (2)$$

Accordance is achieved for a triad test if the calculated value is 1. The obtained triad proportions and corresponding triad test values are summarized in Table 2, revealing that the stereocontrol follows an enantiomorphic site control mecha-

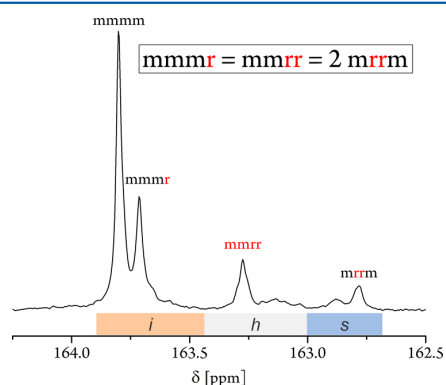
Table 2. Isotactic (*i*), Heterotactic (*h*), and Syndiotactic (*s*) Triad Distributions Determined from the ^{13}C NMR Resonances of the Aromatic Quaternary Carbon Atom of Poly(2-vinylpyridine) for Catalysts 1–4

catalyst	triad distributions						triad tests		tacticity
	experimental ^a			theoretical ^b			B^c	E^d	P_m^e
	<i>i</i>	<i>h</i>	<i>s</i>	<i>i</i>	<i>h</i>	<i>s</i>			
1	0.73	0.18	0.09	0.73	0.18	0.09	8.11	1.00	0.82
2	0.40	0.40	0.20	0.40	0.40	0.20	2.00	1.00	0.60
3	0.46	0.36	0.18	0.46	0.36	0.18	2.56	1.00	0.64
4	0.87	0.09	0.05	0.87	0.90	0.05	21.48	1.00	0.92

^a30 mg of P2VP in 0.6 mL of CD_3OD ; NMR AV500C; ^{13}C NMR resonances of poly(2-vinylpyridine) produced with catalysts 1–4 at 25 °C ($[\text{2VP}]:[\text{Cat.}] = 200:1$, $[\text{M}] = 2.7$ mmol, 2 mL of toluene). ^bTheoretical triad distributions calculated based on the enantiomorphic site control model (see Supporting Information). ^cBernoulli model triad test B , where $B = (4[\text{mm}][\text{rr}])/[\text{mr}]^2$. ^dEnantiomorphic site control triad test E , where $E = (2[\text{rr}])/[\text{mr}]$. ^e P_m is the probability of *meso* linkages between monomer units and is determined by ^{13}C NMR spectroscopy.

nism. Polymerization at different temperatures reinforces these findings: a temperature-dependent stereoselectivity would be expected for a chain end control mechanism but was not observed (Table 1, entries 1, 2, and 9–12).

A closer look into the pentad assignments in the literature reveals inconsistencies with our findings. Although Dimov extensively studied the pentad structure using different literature examples and existing assignments, a conclusive attribution was not possible until now.⁴⁸ Enantiomorphic site control features an error correction approach with defined relative probabilities of mmmr, mmrr, and mrrm pentads. This unique pentad distribution allows the precise assignment of the pentads shown in Figure 5 for the first time.

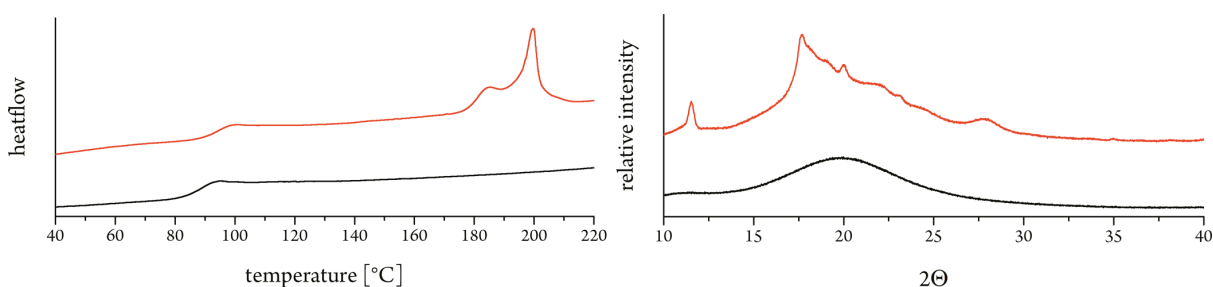
**Figure 5.** Correction of pentad assignments using the pentad distributions for the enantiomorphic site control mechanism (polymer: entry 1, Table 1).

The highly isotactic P2VP, with values above 90%, allows the crystallization of the polymer samples and therefore a change in their thermal behavior. However, the polymer of entry 6 (Table 1) did not exhibit a melting transition temperature without further thermal treatment comparable to isotactic poly(styrene). Only glass transitions were found from 90 to 100 °C for all the samples (atactic and isotactic). To evaluate the optimal crystallization temperature (T_c), the highly isotactic polymer ($P_m = 0.92$) was crystallized for 150 min at 130, 150, and 170 °C (see Supporting Information). The optimal T_c was found to be 170 °C, as this T_c corresponded to the sharpest T_m at approximately 195 °C. Longer crystallization times at this high temperature should be avoided because of thermal degradation of the polymer, which can be observed as discoloration. Applying these crystallization conditions to the other polymer samples failed to induce any crystalline domains measurable by differential scanning calorimetry (DSC).

Nevertheless, the crystallization of a sample of lower isotacticity ($P_m = 0.84$) for 16 h at 130 °C induces a broad melting transition, occurring between 180 and 200 °C (see Supporting Information).

TGA analysis of the thermal degradation of the polymer samples revealed that the polymer tacticity and crystallinity were unaffected by the degradation onset temperature. The atactic polymer, isotactic noncrystalline polymer ($P_m = 0.92$), and crystallized polymer ($P_m = 0.92$; $T_c = 170$ °C; 150 min) exhibited coincident degradation curves and an onset point at approximately 386 °C (see Supporting Information).

For completeness, the same samples were analyzed using powder X-ray diffraction (XRD). Only the crystallized sample produced XRD patterns comparable to those in the literature, whereas the patterns for the noncrystallized and atactic samples lacked any reflections.

**Figure 6.** DSC curves (left, first heating cycle) and XRD patterns (right) of amorphous (black) and crystallized (red, $T_c = 170$ °C, 150 min) P2VP samples (catalyst 4, $[\text{2VP}]:[\text{Cat.}] = 200:1$, $[\text{M}] = 2.7$ mmol, 2 mL of toluene, 25 °C).

CONCLUSION

In conclusion, we successfully developed (C_1) asymmetric 2-methoxyethylamino-bis(phenolate)yttrium catalysts of the type $(\text{ONOO})^R\text{Y}(\text{CH}_2\text{Si}(\text{CH}_3)_3)$ (THF) for the living and highly isoselective group transfer polymerization of prochiral 2-vinylpyridine. The steric bulk introduced into the new ligand structures influenced the stereoselectivity of the catalysts. Isotacticities varying from 60% to 92% and a high degree of control ($\text{PDI} < 1.19$) were achieved. The improvement of the initiator efficiencies will be of high interest in future work especially as narrow PDIs are paradoxical to these findings. The melting transition temperatures of the obtained polymers depended on their isotactic content and thermal history. Crystalline domains were observed by DSC and XRD.

The underlying mechanism was examined in greater detail by ^{13}C NMR, which excluded a Bernoulli chain end control mechanism and confirmed an enantiomorphic site control mechanism. The unique enantiomorphic site mechanism of our catalysts with 2VP allowed additional microstructure information to be deduced and two previously misassigned pentads of P2VP to be correctly assigned.

The results of this study underscore the high versatility of bis(phenolate)-based yttrium initiators for the stereoselective GTP of polar monomers and widen the horizon of stereoselective GTP.

EXPERIMENTAL SECTION

General. All air- and moisture-sensitive reactions were conducted under an argon atmosphere using standard Schlenk or glovebox techniques. All glassware was heat-dried under vacuum prior to use. Unless otherwise stated, all chemicals were purchased from Acros Organics, Sigma-Aldrich, or ABCR and used as received. Dichloromethane, pentane, THF, and toluene were dried using an MBraun SPS-800 solvent purification system. The precursor complex $[\text{Y}(\text{CH}_2\text{SiMe}_3)_3(\text{THF})_2]$ was prepared following literature procedures.⁴⁹ Triethylamine and 2-vinylpyridine were dried over calcium hydride and distilled prior to use. 2-(((2-Methoxyethyl)amino)methyl)-4,6-dimethylphenol and 2,4-di-*tert*-butyl-6-(((2-methoxyethyl)amino)methyl)phenol were also synthesized according to literature procedures.⁴⁵

NMR spectra were recorded on Bruker AVIII-300 and AVIII-500C spectrometers. ^1H NMR spectroscopic chemical shifts δ are reported in ppm relative to the residual proton signals of deuterated solvents. Unless otherwise stated, ^{13}C NMR spectroscopic chemical shifts δ are referenced to the carbon atoms of the solvent. Coupling constants J are given as averaged values in hertz (Hz) and refer to couplings between protons. The following abbreviations are used to describe signal multiplicities: s (singlet), d (doublet), t (triplet), m (multiplet), dd (doublet of doublets), dt (doublet of triplets), br (broad signal). Deuterated solvents were obtained from Sigma-Aldrich and dried over 3 Å molecular sieves.

Quantitative elemental analysis (EA) was conducted at the Laboratory for Microanalysis, Institute of Inorganic Chemistry, Technische Universität München. Low-resolution mass spectrometry (LRMS) measurements were obtained using electrospray ionization (ESI) with acetonitrile and toluene solutions on a Varian LC/MS 500-MS spectrometer. Gel permeation chromatography (GPC) measurements were conducted on a Varian 920-LC HPLC equipped with two PL Polargel columns. Powder X-ray diffractograms were recorded on a PANalytical Empyrean system. DSC was carried out on a Texas Instruments DSC Q2000 with a heating rate of 5 K min^{-1} . TGA was carried out on a Texas Instruments TGA Q5000 with a heating rate of 10 K min^{-1} .

The initiator efficiency ($I^* = M_{n,\text{calc}}/M_{n,\text{exp}}$) was determined from aliquots taken during and after the polymerization. For polymerization kinetics, I^*_t is determined as the average initiator efficiency I^* at the

maximum reaction rate (maximum slope of the conversion–reaction time plot).

Proligand Synthesis. A solution of 2-(bromomethyl)phenol (1.0 equiv) in dry THF (12 mL) was added dropwise to a stirred solution of (2-methoxyethylamino)methylphenol derivative (1.0 equiv) in dry THF (12 mL). The reaction mixture was stirred for 1 h at room temperature. Subsequently, freshly distilled triethylamine (1.5 equiv) was added slowly, and the solution was heated under reflux for 20 h. After cooling to room temperature, the solid was filtered off, and the solvent removed *in vacuo* to yield the crude product.

2,4-Di-*tert*-butyl-6-(((5-*tert*-butyl-2-hydroxy-3-(tris(4-*tert*-butylphenyl)methyl)benzyl)(2-methoxyethyl)amino)methyl)phenol (L1). Batch size: 1.19 mmol. The residue was purified by silica gel column chromatography (*n*-hexane:EtOAc = 20:1) and consecutive recrystallization from ethanol to afford proligand L1 as a white powder (673 mg, 777 μmol , 65%). TLC: R_f = 0.30 (silica gel, *n*-hexane:EtOAc = 20:1, [UV]). ^1H NMR (500 MHz, CDCl_3 , 300 K): δ [ppm] = 1.12 (s, 9H, $\text{C}(\text{CH}_3)_3$), 1.29 (s, 9H, $\text{C}(\text{CH}_3)_3$), 1.32 (s, 27H, $\text{C}(\text{CH}_3)_3$), 1.45 (s, 9H, $\text{C}(\text{CH}_3)_3$), 2.63 (t, $^3J = 5.7$ Hz, 2H, CH_2), 3.22 (s, 3H, OCH_3), 3.43 (t, $^3J = 5.7$ Hz, 2H, CH_2), 3.67 (s, 2H, Ar- CH_2), 3.82 (s, 2H, Ar- CH_2), 6.81 (d, $^4J = 2.5$ Hz, 1H, Ar-H), 6.87 (d, $^4J = 2.4$ Hz, 1H, Ar-H), 7.12 (d, $^3J = 8.6$ Hz, 6H, Trit-H), 7.22 (d, $^4J = 2.5$ Hz, 1H, Ar-H), 7.23 (d, $^4J = 2.5$ Hz, 1H, Ar-H), 7.29 (d, $^3J = 8.6$ Hz, 6H, Trit-H). ^{13}C NMR (126 MHz, CDCl_3 , 300 K): δ [ppm] = 29.8, 31.5, 31.5, 31.9, 34.3, 34.3, 34.5, 35.1, 51.7, 53.0, 58.8, 58.9, 62.0, 70.6, 121.9, 122.9, 124.0, 124.0, 124.6, 127.6, 127.8, 130.8, 133.4, 135.7, 140.4, 141.7, 141.8, 149.2, 151.2, 154.4. LRMS (ESI, toluene): m/z = 866.6 [M^+]. EA [%]: calculated: C 83.19, H 9.66, N 1.62; found: C 83.32, H 9.78, N 1.73.

2,4-Di-*tert*-butyl-6-(((5-*tert*-butyl-2-hydroxy-3-(tris(3,5-dimethylphenyl)methyl)benzyl)(2-methoxyethyl)amino)methyl)phenol (L2). Batch size: 1.36 mmol. The residue was recrystallized from methanol to afford proligand L2 as a white powder (684 mg, 875 μmol , 64%). ^1H NMR (500 MHz, CDCl_3 , 300 K): δ [ppm] = 1.18 (s, 9H, $\text{C}(\text{CH}_3)_3$), 1.27 (s, 9H, $\text{C}(\text{CH}_3)_3$), 1.41 (s, 9H, $\text{C}(\text{CH}_3)_3$), 2.22 (s, 18H, CH_3), 2.64 (t, $^3J = 5.7$ Hz, 2H, CH_2), 3.22 (s, 3H, OCH_3), 3.39 (t, $^3J = 5.7$ Hz, 2H, CH_2), 3.66 (s, 2H, Ar- CH_2), 3.79 (s, 2H, Ar- CH_2), 6.77 (s, 6H, Trit-H), 6.84–6.85 (m, 4H, Trit-H + Ar-H), 7.07 (d, $^4J = 2.4$ Hz, 1H, Ar-H), 7.19 (d, $^4J = 2.4$ Hz, 1H, Ar-H), 7.23 (d, $^4J = 2.5$ Hz, 1H, Ar-H). ^{13}C NMR (126 MHz, CDCl_3 , 300 K): δ [ppm] = 21.8, 29.8, 31.6, 31.9, 34.2, 34.3, 35.0, 51.5, 52.3, 58.7, 58.9, 62.8, 70.6, 122.0, 122.8, 123.9, 123.9, 127.5, 127.8, 128.1, 129.0, 133.1, 135.6, 136.8, 140.2, 141.7, 144.7, 151.4, 154.4. LRMS (ESI, toluene): m/z = 782.6 [M^+]. EA [%]: calculated: C 82.92, H 9.15, N 1.79; found: C 83.10, H 9.23, N 1.81.

4-*tert*-Butyl-2-(((2-hydroxy-3,5-dimethylbenzyl)(2-methoxyethyl)amino)methyl)-6-(tris(4-*tert*-butylphenyl)methyl)phenol (L3). Batch size: 1.31 mmol. The crude product was recrystallized from ethanol to afford proligand L3 as a white powder (710 mg, 907 μmol , 69%). ^1H NMR (500 MHz, CDCl_3 , 300 K): δ [ppm] = 1.10 (s, 9H, $\text{C}(\text{CH}_3)_3$), 1.31 (s, 27H, $\text{C}(\text{CH}_3)_3$), 2.21 (s, 3H, CH_3), 2.24 (s, 3H, CH_3), 2.61 (t, $^3J = 5.6$ Hz, 2H, CH_2), 3.21 (s, 3H, OCH_3), 3.41 (t, $^3J = 5.6$ Hz, 2H, CH_2), 3.68 (s, 2H, Ar- CH_2), 3.75 (s, 2H, Ar- CH_2), 6.65 (d, $^4J = 2.2$ Hz, 1H, Ar-H), 6.80 (d, $^4J = 2.4$ Hz, 1H, Ar-H), 6.86 (d, $^4J = 2.1$ Hz, 1H, Ar-H), 7.12 (d, $^3J = 8.6$ Hz, 7H, Trit-H + Ar-H), 7.29 (d, $^3J = 8.6$ Hz, 6H, Trit-H). ^{13}C NMR (126 MHz, CDCl_3 , 300 K): δ [ppm] = 16.1, 20.6, 31.4, 31.5, 34.2, 34.5, 51.7, 54.0, 57.2, 58.7, 62.0, 70.7, 121.4, 123.6, 124.5, 127.4, 127.5, 127.7, 128.0, 130.6, 130.7, 130.8, 133.6, 141.5, 141.7, 149.2, 151.4, 153.6. LRMS (ESI, toluene): m/z = 782.5 [M^+]. EA [%]: calculated: C 82.92, H 9.15, N 1.79; found: C 82.79, H 9.36, N 1.69.

4-*tert*-Butyl-2-(((2-hydroxy-3,5-dimethylbenzyl)(2-methoxyethyl)amino)methyl)-6-(tris(3,5-dimethylphenyl)methyl)phenol (L4). Batch size: 1.43 mmol. The crude product was recrystallized from methanol to afford proligand L4 as a white powder (677 mg, 970 μmol , 68%). ^1H NMR (500 MHz, CDCl_3 , 300 K): δ [ppm] = 1.17 (s, 9H, $\text{C}(\text{CH}_3)_3$), 2.21 (s, 6H, CH_3), 2.22 (s, 18H, CH_3), 2.62 (t, $^3J = 5.6$ Hz, 2H, CH_2), 3.22 (s, 3H, OCH_3), 3.38 (t, $^3J = 5.6$ Hz, 2H, CH_2), 3.66 (s, 2H, Ar- CH_2), 3.76 (s, 2H, Ar- CH_2), 6.64 (d, $^4J = 2.2$ Hz, 1H, Ar-H), 6.79 (s, 6H, Trit-H), 6.84–6.86 (m, 4H, Trit-H + Ar-

H), 7.09 (d, $^4J = 2.4$ Hz, 1H, Ar–H), 7.14 (d, $^4J = 2.4$ Hz, 1H, Ar–H). ^{13}C NMR (126 MHz, CDCl_3 , 300 K): δ [ppm] = 16.0, 20.6, 21.8, 31.5, 34.3, 51.5, 53.1, 57.4, 58.7, 62.9, 70.6, 121.5, 123.5, 124.9, 127.4, 127.5, 127.6, 128.1, 129.0, 130.6, 133.2, 136.8, 137.0, 141.5, 144.8, 151.5, 153.6. LRMS (ESI, toluene): $m/z = 698.5$ [M^+]. EA [%]: calculated: C 82.60, H 8.52, N 2.01; found: C 81.82, H 8.60, N 1.96.

Synthesis of Complexes. A solution of $[\text{Y}(\text{CH}_2\text{SiMe}_3)_3(\text{THF})_2]$ (200 mg, 404 μmol , 1.0 equiv) in dry pentane (5 mL) was cooled to -40 °C in a glovebox. A solution of the corresponding proligand **L1–L4** (404 μmol , 1.0 equiv) in dry toluene (3 mL) was added dropwise. The resulting reaction mixture was stirred for 1 h at this temperature and then for 17 h at room temperature. The solvent was removed *in vacuo*, and the residue was washed with cold pentane. The crude product was recrystallized from pentane to afford catalysts **1–4** as white crystalline powders in good yields.

$[\text{Y}(\text{ONOC}^{\text{tBu}}\text{Bu}^{\text{tBu}}\text{Bu}^{\text{tBu}}\text{Tr}^{\text{t}})(\text{CH}_2\text{SiMe}_3)(\text{THF})] (\mathbf{1})$. The crude product was recrystallized from pentane to afford **1** as a white powder (253 mg, 227 μmol , 56%). ^1H NMR (500 MHz, C_6D_6 , 300 K): δ [ppm] = -1.26 (dd, $^2J_{\text{YH}} = 3.5$ Hz, $^2J = 10.7$ Hz, 1H, CH_2SiMe_3), -0.99 (dd, $^2J_{\text{YH}} = 3.2$ Hz, $^2J = 10.8$ Hz, 1H, CH_2SiMe_3), 0.30 (s, 9H, SiMe_3), 1.21–1.27 (m, 32H, $\text{C}(\text{CH}_3)_3 + \text{THF-H}$), 1.41 (s, 9H, $\text{C}(\text{CH}_3)_3$), 1.46 (s, 9H, $\text{C}(\text{CH}_3)_3$), 1.76 (s, 9H, $\text{C}(\text{CH}_3)_3$), 2.04–2.12 (m, 1H, CH_2), 2.44–2.52 (m, 1H, CH_2), 2.57 (m, 1H, CH_2), 2.56–2.72 (m, 1H, CH_2), 2.84 (d, $^2J = 12.5$ Hz, 1H, Ar– CH_2), 2.91 (s, 3H, OCH_3), 2.92 (d, $^2J = 12.1$ Hz, 1H, Ar– CH_2), 3.57–3.58 (m, 4H, THF–H), 3.67 (d, $^2J = 12.4$ Hz, 1H, Ar– CH_2), 3.71 (d, $^2J = 12.4$ Hz, 1H, Ar– CH_2), 7.09 (d, $^4J = 2.7$ Hz, 1H, Ar–H), 7.13–7.33 (m, 6H, Trit–H), 7.22 (d, $^4J = 2.7$ Hz, 1H, Ar–H), 7.50–7.75 (m, 6H, Trit–H), 7.58 (d, $^4J = 2.7$ Hz, 1H, Ar–H), 7.59 (d, $^4J = 2.7$ Hz, 1H, Ar–H). ^{13}C NMR (126 MHz, C_6D_6 , 300 K): δ [ppm] = 5.0, 24.8, 25.2, 30.5, 31.6, 32.1, 32.3, 34.3, 34.3, 34.3, 35.7, 49.6, 61.8, 63.2, 64.9, 65.2, 71.6, 74.1, 124.2, 124.3, 124.3, 124.4, 124.5, 125.3, 126.8, 130.8, 131.6, 135.1, 136.0, 136.6, 136.6, 147.3, 161.8, 161.8. Doublet for CH_2TMS cannot clearly be observed through overlapping signals. EA [%]: calculated: C 73.41, H 9.06, N 1.26; found: C 73.33, H 9.18, N 1.37.

$[\text{Y}(\text{ONOC}^{\text{tBu}}\text{Bu}^{\text{tBu}}\text{Bu}^{\text{tBu}}\text{Me}^{\text{t}}\text{Tr}^{\text{t}})(\text{CH}_2\text{SiMe}_3)(\text{THF})] (\mathbf{2})$. The crude product was recrystallized from pentane to afford **2** as a white powder (221 mg, 215 μmol , 53%). ^1H NMR (500 MHz, C_6D_6 , 300 K): δ [ppm] = -1.09 (dd, $^2J = 10.7$, $^2J_{\text{YH}} = 3.4$ Hz, 1H, CH_2SiMe_3), -0.94 (dd, $^2J = 10.8$, $^2J_{\text{YH}} = 3.1$ Hz, 1H, CH_2SiMe_3), 0.25 (s, 9H, CH_2SiMe_3), 1.21–1.29 (m, 4H, THF), 1.38 (s, 9H, $\text{C}(\text{CH}_3)_3$), 1.47 (s, 9H, $\text{C}(\text{CH}_3)_3$), 1.77 (s, 9H, $\text{C}(\text{CH}_3)_3$), 2.14 (br, 18H, Ar– CH_3), 2.40–2.52 (m, 1H), 2.71 (s, 3H, OCH_3), 2.83–2.97 (m, 3H, CH_2), 3.48–3.83 (m, 6H, 2 Ar– $\text{CH}_2 + 4$ THF–H), 6.68 (s, 3H), 7.07 (d, $^4J = 2.5$ Hz, 1H), 7.20 (d, $^4J = 2.6$ Hz, 1H), 7.59 (d, $^4J = 2.6$ Hz, 1H), 7.77 (d, $^4J = 2.6$ Hz, 1H). ^{13}C NMR (126 MHz, C_6D_6 , 300 K): δ [ppm] = 4.8, 21.9, 24.6 (d, $J_{\text{YC}} = 46.3$ Hz), 25.2, 30.6, 32.1, 32.2, 32.3, 34.2, 34.2, 35.7, 48.8, 60.5, 64.0, 64.9, 71.5, 73.6, 124.2, 124.3, 124.4, 125.6, 126.5, 127.2, 128.0, 128.2, 128.3, 129.8, 131.2, 135.2, 135.9, 136.5, 161.8, 161.9. EA [%]: calculated: C 72.41, H 8.63, N 1.36; found: C 73.41, H 8.69, N 1.38.

$[\text{Y}(\text{ONOC}^{\text{Me}}\text{Me}^{\text{tBu}}\text{Bu}^{\text{tBu}}\text{Tr}^{\text{t}})(\text{CH}_2\text{SiMe}_3)_2] (\mathbf{3})$. The crude product was recrystallized from pentane to afford **3** as a white powder (239 mg, 125 μmol , 62%). ^1H NMR (500 MHz, $\text{THF-}d_8$, 300 K, monomeric species): δ [ppm] = -1.76 (dd, $^2J = 11.1$, $^2J_{\text{YH}} = 3.1$ Hz, 1H, CH_2SiMe_3), -1.49 (dd, $^2J = 11.1$, $^2J_{\text{YH}} = 2.5$ Hz, 1H, CH_2SiMe_3), -0.16 (s, 9H, CH_2SiMe_3), 1.21 (s, 9H, $\text{C}(\text{CH}_3)_3$), 1.30 (s, 36H, $\text{C}(\text{CH}_3)_3$), 1.92–1.98 (m, 1H), 2.28 (br, 6H, Ar CH_3), 2.44–2.51 (m, 2H, CH_2), 2.69 (s, 3H, OCH_3), 2.90–3.03 (m, 2H, CH_2), 3.03–3.07 (m, 2H), 3.90–3.96 (m, 2H, Ar– CH_2), 7.02–7.16 (m, 12H, Ar–H), 7.17–7.20 (m, 4H, Ar–H). ^{13}C NMR (126 MHz, $\text{THF-}d_8$, 300 K, monomeric species): δ [ppm] = 5.4, 17.6, 20.7, 23.2, 25.3, 31.9, 32.0, 32.1, 34.5, 34.8, 50.2, 61.0, 61.2, 63.3, 64.8, 75.0, 123.2, 124.5, 125.0, 125.3, 126.2, 127.1, 127.2, 128.9, 129.7, 130.2, 131.6, 132.1, 135.2, 136.1, 147.6, 161.5. Doublet for CH_2TMS cannot clearly be observed through overlapping signals. EA [%]: calculated: C 72.85, H 8.43, N 1.46; found: C 73.27, H 8.37, N 1.57.

$[\text{Y}(\text{ONOC}^{\text{Me}}\text{Me}^{\text{tBu}}\text{Bu}^{\text{tBu}}\text{Me}^{\text{t}}\text{Tr}^{\text{t}})(\text{CH}_2\text{SiMe}_3)_2] (\mathbf{4})$. The crude product was recrystallized from pentane to afford **4** as a white powder (207 mg, 119 μmol , 59%). ^1H NMR (500 MHz, $\text{THF-}d_8$, 300 K, monomeric

species): δ [ppm] -1.55 (dd, $^2J = 11.3$, $^2J_{\text{YH}} = 3.1$ Hz, 1H, CH_2SiMe_3), -1.46 (dd, $^2J = 11.3$, $^2J_{\text{YH}} = 2.7$ Hz, 1H, CH_2SiMe_3), -0.14 (s, 9H, CH_2SiMe_3), 1.16 (s, 9H, $\text{C}(\text{CH}_3)_3$), 2.14 (br, 18H, Ar– CH_3), 2.31 (br, 6H, Ar– CH_3), 2.47–2.52 (m, 2H, CH_2), 2.86–2.91 (m, 2H, CH_2), 3.21 (s, 3H, OCH_3), 3.28–3.37 (m, 2H, Ar– CH_2), 3.60–3.65 (m, 2H), 6.60–6.90 (m, 9H, Ar–H), 7.05–7.14 (m, 2H, Ar–H), 7.18–7.23 (m, 2H, Ar–H). ^{13}C NMR (126 MHz, $\text{THF-}d_8$, 300 K, monomeric species): δ [ppm] = 4.5, 20.7, 21.5, 25.4, 26.4, 32.4, 34.4, 35.1, 58.8, 59.9, 63.9, 64.2, 65.3, 74.6, 123.3, 124.8, 126.1, 126.2, 126.8, 127.2, 128.9, 129.1, 129.7, 130.2, 130.4, 132.1, 136.0, 138.5, 161.3, 162.6. Doublet for CH_2TMS cannot clearly be observed through overlapping signals. EA [%]: calculated: C 71.62, H 7.86, N 1.61; found: C 72.02, H 7.90, N 1.51.

Polymerization Procedure. To a stirred solution of 13.5 μmol catalyst (1.0 equiv) in 2 mL of toluene, 2.7 mmol of monomer (200 equiv; $c = 1.35$ mol/L) was added in one portion at room temperature. The polymerization was quenched by the addition of methanol after predefined polymerization durations. The conversion was determined by ^1H NMR spectroscopy. The polymers were precipitated by addition of the reaction mixture to 50 mL of cold pentane, and the solution was decanted off. Residual solvent was removed under vacuum at elevated temperatures.

Kinetic Measurements by the Aliquot Method. To a stirred solution of 135 μmol of catalyst (1.0 equiv) in 20 mL of toluene, 27 mmol of monomer (200 equiv; $c = 1.35$ mol/L) was added in one portion at room temperature. Aliquots were removed from the reaction mixture and quenched by the addition of MeOH. Toluene and surplus monomer were removed under vacuum at elevated temperatures overnight. The conversion was determined gravimetrically, and the molecular weight was determined by GPC-MALS analysis.

Characterization of P2VP Samples. The P2VP microstructure was determined using ^{13}C NMR spectroscopy at room temperature with a minimum of 1024 scans and a relaxation delay of 4 s. Spectra for P2VP samples (6% (w/v; 30 mg/0.6 mL CD_3OD)) were recorded on a Bruker AVIII 500 Cryo spectrometer for microstructure analysis at a triad level and analyzed according to the literature.^{45,48}

GPC was conducted using samples with a concentration of 5 mg/mL on a Varian LC-920 equipped with two PL Polargel columns. THF/water (1:1; v/v), 9 g/L tetrabutylammonium bromide (TBAB), and 680 mg/L_{THF} 3,5-di-*tert*-butyl-4-hydroxytoluene (BHT) were used as eluents. The absolute molecular weights were determined online by multiangle light scattering (MALS) analysis using a Wyatt Dawn Helels II in combination with a Wyatt Optilab rEX concentration source.

■ ASSOCIATED CONTENT

● Supporting Information

The Supporting Information is available free of charge on the ACS Publications website at DOI: 10.1021/acs.macromol.6b01179.

Additional experimental procedures and analytical data (PDF)

■ AUTHOR INFORMATION

Corresponding Author

*E-mail riege@tum.de; Fax +49-89-289-13562; Tel +49-89-289-13570 (B.R.).

Author Contributions

A.K. and D.R. contributed equally.

Notes

The authors declare no competing financial interest.

■ ACKNOWLEDGMENTS

A.K. and P.T.A. thank BASF SE for financial support.

REFERENCES

- (1) Natta, G.; Pino, P.; Corradini, P.; Danusso, F.; Mantica, E.; Mazzanti, G.; Moraglio, G. CRYSTALLINE HIGH POLYMERS OF α -OLEFINS. *J. Am. Chem. Soc.* **1955**, *77*, 1708–1710.
- (2) Brintzinger, H. H.; Fischer, D.; Mülhaupt, R.; Rieger, B.; Waymouth, R. M. Stereospecific Olefin Polymerization with Chiral Metallocene Catalysts. *Angew. Chem., Int. Ed. Engl.* **1995**, *34*, 1143–1170.
- (3) Herzog, T. A.; Zubris, D. L.; Bercaw, J. E. A New Class of Zirconocene Catalysts for the Syndiospecific Polymerization of Propylene and Its Modification for Varying Polypropylene from Isotactic to Syndiotactic. *J. Am. Chem. Soc.* **1996**, *118*, 11988–11989.
- (4) Kim, S. H.; Somorjai, G. A. Correlation between Catalyst Surface Structure and Polypropylene Tacticity in Ziegler–Natta Polymerization System†. *J. Phys. Chem. B* **2001**, *105*, 3922–3927.
- (5) Rieger, B.; Mu, X.; Mallin, D. T.; Rausch, M. D.; Chien, J. C. W. Degree of stereochemical control of racemic ethylenebis(indenyl) zirconium dichloride/methyl aluminoxane catalyst and properties of anisotactic polypropylenes. *Macromolecules* **1990**, *23*, 3559–3568.
- (6) Schöbel, A.; Herdtweck, E.; Parkinson, M.; Rieger, B. Ultra-Rigid Metallocenes for Highly Iso- and Regiospecific Polymerization of Propene: The Search for the Perfect Polypropylene Helix. *Chem. - Eur. J.* **2012**, *18*, 4174–4178.
- (7) Schöbel, A.; Lanzinger, D.; Rieger, B. Polymerization Behavior of C1-Symmetric Metallocenes (M = Zr, Hf): From Ultrahigh Molecular Weight Elastic Polypropylene to Useful Macromonomers. *Organometallics* **2013**, *32*, 427–437.
- (8) Rodriguez-Arnold, J.; Zhang, A.; Cheng, S. Z. D.; Lovinger, A. J.; Hsieh, E. T.; Chu, P.; Johnson, T. W.; Honnell, K. G.; Geerts, R. G.; Palackal, S. J.; Hawley, G. R.; Welch, M. B. Crystallization, melting and morphology of syndiotactic polypropylene fractions: 1. Thermodynamic properties, overall crystallization and melting. *Polymer* **1994**, *35*, 1884–1895.
- (9) Samuels, R. J. Quantitative structural characterization of the melting behavior of isotactic polypropylene. *J. Polym. Sci., Polym. Phys. Ed.* **1975**, *13*, 1417–1446.
- (10) Bauer, A.; Hauschild, S.; Stolzenburg, M.; Förster, S.; Mayer, C. Molecular exchange through membranes of poly(2-vinylpyridine-block-ethylene oxide) vesicles. *Chem. Phys. Lett.* **2006**, *419*, 430–433.
- (11) Bronstein, L. M.; Sidorov, S. N.; Valetsky, P. M.; Hartmann, J.; Cölfen, H.; Antonietti, M. Induced Micellization by Interaction of Poly(2-vinylpyridine)-block-poly(ethylene oxide) with Metal Compounds. Micelle Characteristics and Metal Nanoparticle Formation. *Langmuir* **1999**, *15*, 6256–6262.
- (12) Changez, M.; Kang, N.-G.; Kim, D. W.; Lee, J.-S. Hollow flower micelles from a diblock copolymer. *Nanoscale* **2013**, *5*, 11554–11560.
- (13) Changez, M.; Koh, H.-D.; Kang, N.-G.; Kim, J.-G.; Kim, Y.-J.; Samal, S.; Lee, J.-S. Molecular Level Ordering in Poly(2-vinylpyridine). *Adv. Mater.* **2012**, *24*, 3253–3257.
- (14) Chen, L.-C.; Mao, Y.-C.; Lin, S.-C.; Li, M.-C.; Ho, R.-M.; Tsai, J.-C. Induced circular dichroism of stereoregular vinyl polymers. *Chem. Commun.* **2012**, *48*, 3668–3670.
- (15) Deakin, L.; DenAuwer, C.; Revol, J.-F.; Andrews, M. P. Isotactic Poly(2-vinylpyridine), Coordination Polymers, and Magnetic Nanocomposites from Chromium Atoms. *J. Am. Chem. Soc.* **1995**, *117*, 9915–9916.
- (16) Dyakonova, M. A.; Stavrouli, N.; Popescu, M. T.; Kyriakos, K.; Grillo, I.; Philipp, M.; Jaksch, S.; Tsitsilianis, C.; Papadakis, C. M. Physical Hydrogels via Charge Driven Self-Organization of a Triblock Polyampholyte – Rheological and Structural Investigations. *Macromolecules* **2014**, *47*, 7561–7572.
- (17) Fan, Y.; Tang, S.; Thomas, E. L.; Olsen, B. D. Responsive Block Copolymer Photonics Triggered by Protein–Polyelectrolyte Coacervation. *ACS Nano* **2014**, *8*, 11467–11473.
- (18) Hameed, N.; Liu, J.; Guo, Q. Self-Assembled Complexes of Poly(4-vinylphenol) and Poly(ϵ -caprolactone)-block-poly(2-vinylpyridine) via Competitive Hydrogen Bonding. *Macromolecules* **2008**, *41*, 7596–7605.
- (19) Hayward, R. C.; Chmelka, B. F.; Kramer, E. J. Crosslinked Poly(styrene)-block-Poly(2-vinylpyridine) Thin Films as Swellable Templates for Mesostructured Silica and Titania. *Adv. Mater.* **2005**, *17*, 2591–2595.
- (20) Higashihara, T.; Ito, S.; Fukuta, S.; Koganezawa, T.; Ueda, M.; Ishizone, T.; Hirao, A. Synthesis and Characterization of ABC-Type Asymmetric Star Polymers Comprised of Poly(3-hexylthiophene), Polystyrene, and Poly(2-vinylpyridine) Segments. *Macromolecules* **2015**, *48*, 245–255.
- (21) Hückstädt, H.; Göpfert, A.; Abetz, V. Synthesis and morphology of ABC heteroarm star terpolymers of polystyrene, polybutadiene and poly(2-vinylpyridine). *Macromol. Chem. Phys.* **2000**, *201*, 296–307.
- (22) Jang, S. G.; Audus, D. J.; Klinger, D.; Krogstad, D. V.; Kim, B. J.; Cameron, A.; Kim, S.-W.; Delaney, K. T.; Hur, S.-M.; Killips, K. L.; Fredrickson, G. H.; Kramer, E. J.; Hawker, C. J. Striped, Ellipsoidal Particles by Controlled Assembly of Diblock Copolymers. *J. Am. Chem. Soc.* **2013**, *135*, 6649–6657.
- (23) Jang, S. G.; Kramer, E. J.; Hawker, C. J. Controlled Supramolecular Assembly of Micelle-Like Gold Nanoparticles in PS-*b*-P2VP Diblock Copolymers via Hydrogen Bonding. *J. Am. Chem. Soc.* **2011**, *133*, 16986–16996.
- (24) Kang, N.-G.; Cho, B.; Kang, B.-G.; Song, S.; Lee, T.; Lee, J.-S. Structural and Electrical Characterization of a Block Copolymer-Based Unipolar Nonvolatile Memory Device. *Adv. Mater.* **2012**, *24*, 385–390.
- (25) Klinger, D.; Wang, C. X.; Connal, L. A.; Audus, D. J.; Jang, S. G.; Kraemer, S.; Killips, K. L.; Fredrickson, G. H.; Kramer, E. J.; Hawker, C. J. A Facile Synthesis of Dynamic, Shape-Changing Polymer Particles. *Angew. Chem., Int. Ed.* **2014**, *53*, 7018–7022.
- (26) Kuo, S.-W.; Wu, C.-H.; Chang, F.-C. Thermal Properties, Interactions, Morphologies, and Conductivity Behavior in Blends of Poly(vinylpyridine)s and Zinc Perchlorate. *Macromolecules* **2004**, *37*, 192–200.
- (27) Mössmer, S.; Spatz, J. P.; Möller, M.; Aberle, T.; Schmidt, J.; Burchard, W. Solution Behavior of Poly(styrene)-block-poly(2-vinylpyridine) Micelles Containing Gold Nanoparticles. *Macromolecules* **2000**, *33*, 4791–4798.
- (28) Popescu, M.-T.; Korogiannaki, M.; Marikou, K.; Tsitsilianis, C. CBABC terpolymer-based nanostructured vesicles with tunable membrane permeability as potential hydrophilic drug nanocarriers. *Polymer* **2014**, *55*, 2943–2951.
- (29) Quirk, R. P.; Corona-Galvan, S. Controlled Anionic Synthesis of Polyisoprene–Poly(2-vinylpyridine) Diblock Copolymers in Hydrocarbon Solution. *Macromolecules* **2001**, *34*, 1192–1197.
- (30) Rahman, M. S.; Samal, S.; Lee, J.-S. Synthesis and Self-Assembly Studies of Amphiphilic Poly(*n*-hexyl isocyanate)-block-poly(2-vinylpyridine)-block-poly(*n*-hexyl isocyanate) Rod–Coil–Rod Triblock Copolymer. *Macromolecules* **2006**, *39*, 5009–5014.
- (31) Rahman, M. S.; Samal, S.; Lee, J.-S. Quantitative in Situ Coupling of Living Diblock Copolymers for the Preparation of Amphiphilic Coil–Rod–Coil Triblock Copolymer Poly(2-vinylpyridine)-*b*-poly(*n*-hexyl isocyanate)-*b*-poly(2-vinylpyridine). *Macromolecules* **2007**, *40*, 9279–9283.
- (32) Soller, B. S.; Salzinger, S.; Rieger, B. Rare Earth Metal-Mediated Precision Polymerization of Vinylphosphonates and Conjugated Nitrogen-Containing Vinyl Monomers. *Chem. Rev.* **2016**, *116*, 1993–2022.
- (33) Talingting, M. R.; Munk, P.; Webber, S. E.; Tuzar, Z. Onion-Type Micelles from Polystyrene-block-poly(2-vinylpyridine) and Poly(2-vinylpyridine)-block-poly(ethylene oxide). *Macromolecules* **1999**, *32*, 1593–1601.
- (34) Wen, T.; Shen, H.-Y.; Wang, H.-F.; Mao, Y.-C.; Chuang, W.-T.; Tsai, J.-C.; Ho, R.-M. Controlled Handedness of Twisted Lamellae in Banded Spherulites of Isotactic Poly(2-vinylpyridine) as Induced by Chiral Dopants. *Angew. Chem., Int. Ed.* **2015**, *54*, 14313–14316.
- (35) Natta, G.; Mazzanti, G.; Dall'Asta, G.; Longi, P. Crystalline 2-vinylpyridine polymers. *Makromol. Chem.* **1960**, *37*, 160–162.
- (36) Natta, G.; Mazzanti, G.; Longi, P.; Dall'Asta, G.; Bernardini, F. Stereospecific polymerization of 2-vinylpyridine. *J. Polym. Sci.* **1961**, *51*, 487–504.

(37) Soum, A.; Fontanille, M. Living anionic stereospecific polymerization of 2-vinylpyridine, 1. Initiation of polymerization and stereoregularity of polymers. *Makromol. Chem.* **1980**, *181*, 799–808.

(38) Soum, A.; Fontanille, M. Living anionic stereospecific polymerization of 2-vinylpyridine, 3. Structure of models of active centres and mechanism of polymerization. *Makromol. Chem.* **1982**, *183*, 1145–1159.

(39) Brigodiot, M.; Cheradame, H.; Fontanille, M.; Vairon, J. P. Microstructure of poly(2-vinylpyridine): correlation between ¹³C and ¹H n.m.r. determinations. *Polymer* **1976**, *17*, 254–256.

(40) Kaneko, H.; Nagae, H.; Tsurugi, H.; Mashima, K. End-functionalized polymerization of 2-vinylpyridine through initial C-H bond activation of N-heteroaromatics and internal alkynes by yttrium ene-diamido complexes. *J. Am. Chem. Soc.* **2011**, *133*, 19626–9.

(41) Altenbuchner, P. T.; Soller, B. S.; Kissling, S.; Bachmann, T.; Kronast, A.; Vagin, S. I.; Rieger, B. Versatile 2-Methoxyethylaminobis(phenolate)yttrium Catalysts: Catalytic Precision Polymerization of Polar Monomers via Rare Earth Metal-Mediated Group Transfer Polymerization. *Macromolecules* **2014**, *47*, 7742–7749.

(42) Zhang, N.; Salzinger, S.; Soller, B. S.; Rieger, B. Rare earth metal-mediated group-transfer polymerization: from defined polymer microstructures to high-precision nano-scaled objects. *J. Am. Chem. Soc.* **2013**, *135*, 8810–3.

(43) Yasuda, H.; Yamamoto, H.; Yokota, K.; Miyake, S.; Nakamura, A. Synthesis of monodispersed high molecular weight polymers and isolation of an organolanthanide(III) intermediate coordinated by a penultimate poly(MMA) unit. *J. Am. Chem. Soc.* **1992**, *114*, 4908–4910.

(44) Tshuva, E. Y.; Goldberg, I.; Kol, M.; Goldschmidt, Z. Zirconium Complexes of Amine–Bis(phenolate) Ligands as Catalysts for 1-Hexene Polymerization: Peripheral Structural Parameters Strongly Affect Reactivity. *Organometallics* **2001**, *20*, 3017–3028.

(45) Altenbuchner, P. T.; Adams, F.; Kronast, A.; Herdtweck, E.; Pöthig, A.; Rieger, B. Stereospecific catalytic precision polymerization of 2-vinylpyridine via rare earth metal-mediated group transfer polymerization with 2-methoxyethylamino-bis(phenolate)-yttrium complexes. *Polym. Chem.* **2015**, *6*, 6796–6801.

(46) Xu, T.-Q.; Yang, G.-W.; Lu, X.-B. Highly Isotactic and High-Molecular-Weight Poly(2-vinylpyridine) by Coordination Polymerization with Yttrium Bis(phenolate) Ether Catalysts. *ACS Catal.* **2016**, *6*, 4907–4913.

(47) Bouyahyi, M.; Ajellal, N.; Kirillov, E.; Thomas, C. M.; Carpentier, J.-F. Exploring Electronic versus Steric Effects in Stereoselective Ring-Opening Polymerization of Lactide and β -Butyrolactone with Amino-alkoxy-bis(phenolate)-Yttrium Complexes. *Chem. - Eur. J.* **2011**, *17*, 1872–1883.

(48) Dimov, D. K.; Hogen-Esch, T. E. Aromatic Quaternary Carbon Signals in the ¹³C NMR Spectrum of Poly(2-vinylpyridine) in Methanol-d₄. *Macromolecules* **1995**, *28*, 7394–7400.

(49) Hultzsich, K. C.; Voth, P.; Beckerle, K.; Spaniol, T. P.; Okuda, J. Single-Component Polymerization Catalysts for Ethylene and Styrene: Synthesis, Characterization, and Reactivity of Alkyl and Hydrido Yttrium Complexes Containing a Linked Amido–Cyclopentadienyl Ligand. *Organometallics* **2000**, *19*, 228–243.

5. Summary and Outlook

A series of electron-deficient β -diiminate-zinc(II) catalysts were synthesized and subsequently used in the catalyzed Ring-opening polymerization of the cyclic ester (*rac*)- β -butyrolactone and the cyclic diester (*rac*)-lactide. In addition to the synthesis of literature unknown preligands, zinc(II) was for the first time incorporated in this highly electron-withdrawing ligand system using zinc-ethyl as metal precursor in quantitative yields. Apart from activity enhancement stereoselective polymerization to potentially biodegradable materials was in the main focus of the project.

Single-crystal-XRD of the complexes allowed the elucidation of differences in bond-lengths and bond-angles of complexes in comparison to their less electron-deficient homologues without CF_3 -groups in the ligand backbone (**Figure 12**).

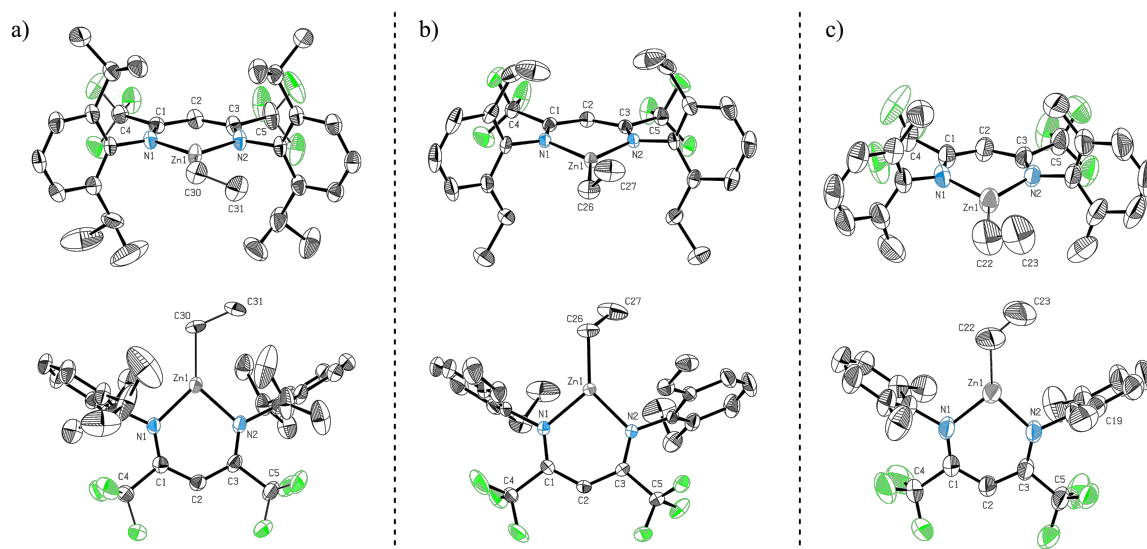
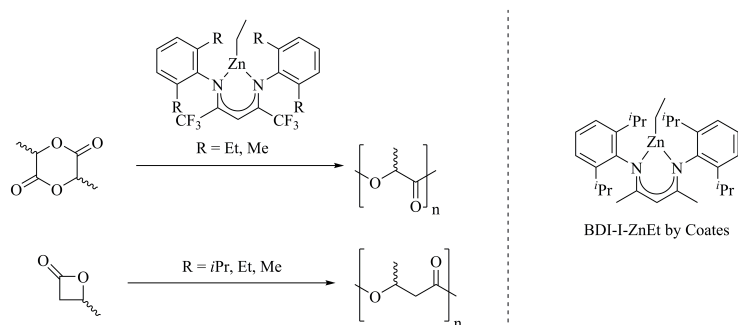


Figure 12. ORTEP style representations of $\text{BDI}^{\text{CF}_3}\text{-I-ZnEt}$ (a), $\text{BDI}^{\text{CF}_3}\text{-II-ZnEt}$ (b), and $\text{BDI}^{\text{CF}_3}\text{-III-ZnEt}$ (c) with ellipsoids drawn at the 50% probability level.

The catalysts achieved high activities in the polymerization of BL and complexes (b) and (c) in the polymerization of LA compared to a literature known BDI-I-ZnEt complex (**Scheme 9**). This improvement can be mainly attributed to the increased Lewis acidity of the zinc center resulting in a strengthened coordination of the lactone and a subsequent increased activation of the coordinated lactone.



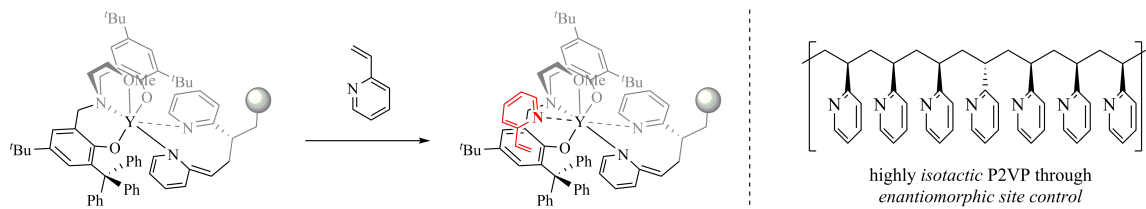
Scheme 9. Schematic Ring-opening polymerization of (*rac*)-lactide and (*rac*)- β -butyrolactone to linear aliphatic polyesters (left); literature known BDI-I-ZnEt complex (right).

The ROP of (*rac*)-LA to PLA allowed, besides increased activity, the investigation of the influence of different alkyl substituents in the *ortho* position of the aniline moieties on the polymer microstructure. The rise of steric bulk around the metal center lead, comparable to previous literature examples, to the increase of *heterotactic* proportions in the produced polymeric material. The ROP of (*rac*)-BL contrary did not show any influence of the phenyl derivatives on the obtained microstructure, which may be explained by the increased number of bridging atoms in between the stereogenic centers compared to PLA.

Alongside the synthesis of zinc catalysts also C_1 -symmetric yttrium based 2-methoxyethylamino-bis(phenolate) catalysts for the stereoselective rare earth metal-mediated group transfer polymerization of 2-vinylpyridine were developed. Previous work already introduced the basic catalyst structure in REM-GTP of *Michael*-systems and proved the major characteristics of living fashion and highly controlled, narrow weight distributions. Changes in the ligand system to increase the steric repulsion at one side of the catalyst structure enabled a new level of complexity and depth of scientific knowledge with respect to catalyst structures in isoselective REM-GTP of 2VP.

The structure-effect relationships of different ligand alterations and the ongoing polymerization mechanism was thoroughly enhanced. Improvement of microstructure control provided isotacticities over 90% and therefore opens up a completely new chapter for the adaption of polymer characteristics like crystallization and melting transitions previously unattainable *via* REM-GTP. Moreover the evaluation of the occurring mechanism *via* ^{13}C NMR allowed for the first time in P2VP chemistry a concrete assignment of four pentads in the aromatic quaternary carbon region through the

characteristics of *enantiomorphic site control* mechanism and therefore a rectification of many literature examples.



Scheme 10. Preferred orientation through steric repulsion of coordinating 2VP leading to highly isotactic P2VP.

In a summary, these two projects processed during this PhD-thesis contribute to the understanding of present and the development of future catalysts for the synthesis of new materials with unique characteristics. They address two main parts important for the creation of future polymers. On the one hand the increase of catalytic activity to allow a cost competitive production through homogenous catalysis and on the other hand the targeted control of stereoselectivity/specivity paving the way to *e.g.*, biodegradable and high melting, functional materials.

Possible points that can be addressed in future zinc based catalyst design to increase the conversion of cyclic esters in Ring-opening polymerizations can be specified using the found results. Understanding and adjusting the steric and electronic surrounding of the metal centre has the chance to pave the way to a new polymeric epoch. Beside these basic investigations especially the co-polymerization of CO₂ and epoxides, and the co-polymerization of anhydride and epoxide monomers, following recent literature examples^[95-96], offer a broad outlet for the new catalyst structures.

Insights in the mechanism and adjustment of catalyst design with a fine tuning in ligand structures in REM-GTP allow structure-effect relations and build up a basis for future research on P2VP homo and copolymers. Especially the copolymers are candidates for tremendous applications in *e.g.* electrochemical, membrane, and medical applications. The new findings represent a basis for future work introducing highly defined and *isotactic* P2VP blocks in various applications to investigate possible effects and improvements in material characteristics.

Besides the political and social challenges the world has to face right now – functional materials will play a more important role in enabling a competitive and successful future. Polymeric materials will not be the only candidates, but they will be of major interest in these discussions and revolutions.

6. Appendix

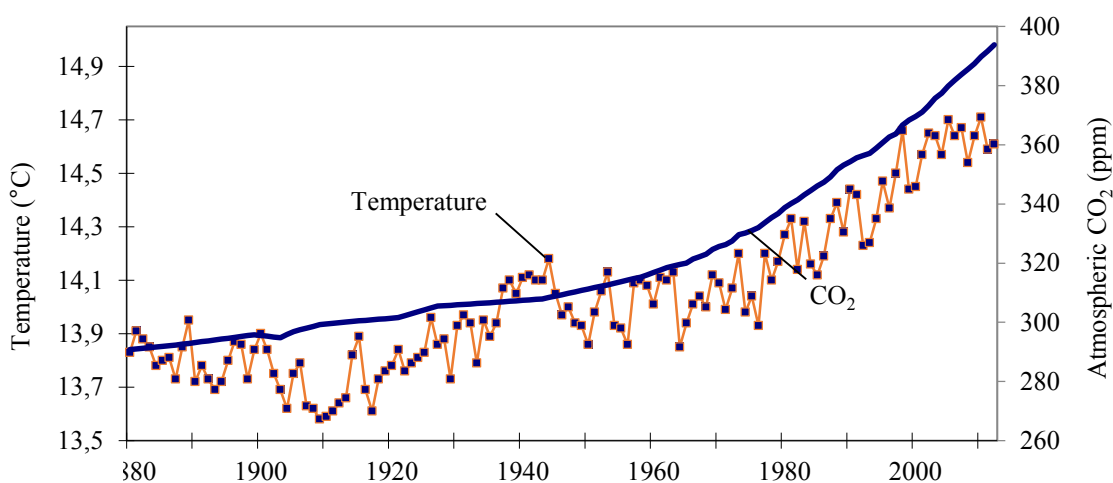
6.1 Publications beyond the Scope of this Thesis

6.1.1 Gated Channels and Selectivity Tuning of CO₂ over N₂ Sorption by Post-Synthetic Modification of a UiO-66-type MOF

Alongside polymerization catalysis a project based on post-synthetic modifications of metal-organic frameworks (MOFs), was continued during the course of this thesis due to promising preliminary results. Recent publications inside the group thereby built up the foundation for the post-functionalization of olefinic side groups inside a stable MOF (**chapter 6.1.2**). The aim was thereby to synthesize MOFs with different functionalities in the framework pores and investigate their influence on stability and guest molecule selectivity for the obtained modified MOFs.

6.1.1.1 Porous Metal-Organic Frameworks as possible CO₂ Sequestration Agents

The anthropogenic era has seen a steep rise in carbon dioxide concentration in the atmosphere due to unrestrained utilization of fossil resources in fields such as transportation, energy and chemical industry.^[97] The ramifications of this trend on our climate is still heavily debated. The abundance of carbon dioxide as a cheap C-1 building block has sparked intensive research into possible chemical utilization.^[98-99]



Source: NASA GISS; NOAA ESRL; Worldwatch

Figure 13. Increase in average global temperature and atmospheric CO₂ from 1880 to 2014 (source: earth-policy.org; accessed on April 26th, 2016).

To access the vast pool of carbon dioxide in an economical manner, techniques for post combustion flue gas separation need to be further improved. Currently employed amine scrubbing technology is wastefully ineffective, crippling the overall efficiency of power plants and hence no option for future broad application. Membranes based on structurally tailored polymer-CO₂ interactions, in comparison, are promising due to their broad window of operating conditions and applications.^[100]

The versatility of metal-organic frameworks is unrivaled which puts them into the pivotal role for further improvement of post-combustion CO₂ capture. Synthetic techniques such as post-synthetic modifications (PSMs) of MOFs allow modifications of the host-guest interactions and thereby the adjustment to certain applications.^[101-102]

The prefunctionalization and post-synthetic modification of UiO-66 results in highly stable metal-organic frameworks for the highly selective uptake of CO₂ over N₂. The frameworks resilience towards harsh reaction conditions allows the introduction of a series of new functionalities. Among others, aminoalcohol and diamine functionalities are incorporated in the network, for the first time converting an epoxy and a dibromo species in tandem PSM using anhydrous ammonia. The functionalization of the framework pores allows the installation of molecular gates with a major decrease in the uptake of nitrogen at low temperatures. Additionally, CO₂ uptake of the aminoalcohol derivative is nearly four times higher than that of the mother compound and is exceptionally high when compared with other UiO-66-MOFs in the literature.

6.1.1.2 Manuscript: Gated Channels and Selectivity Tuning of CO₂ over N₂ Sorption by Post-Synthetic Modification of a UiO-66-type MOF

Bibliographic Data

Status	Published online: August 2 nd , 2016
Journal	<i>Chemistry – A European Journal</i> Volume 22, issue 36, pages 12800–12807
Publisher	Wiley-VCH
Article type	Full Paper
DOI	10.1002/chem.201602318
Authors	<u>Alexander Kronast</u> , Sebastian Eckstein, Peter T. Altenbuchner, Konrad Hindelang, Sergei I. Vagin, and Bernhard Rieger

Abstract: The highly porous and stable metal–organic framework (MOF) UiO-66 was altered using post-synthetic modifications (PSMs). Prefunctionalization allowed the introduction of carbon double bonds into the framework through a four-step synthesis from 2-bromo-1,4-benzenedicarboxylic acid; the organic linker 2-allyl-1,4-benzenedicarboxylic acid was obtained. The corresponding functionalized MOF (UiO-66-allyl) served as a platform for further PSMs. From UiO-66-allyl, epoxy, dibromide, thioether, diamine, and amino alcohol functionalities were synthesized. The abilities of these compounds to adsorb CO₂ and N₂ were compared, which revealed the structure–selectivity correlations. All synthesized MOFs showed profound thermal stability together with an increased ability for selective CO₂ uptake and molecular gate functionalities at low temperatures.

Materials Science

Gated Channels and Selectivity Tuning of CO₂ over N₂ Sorption by Post-Synthetic Modification of a UiO-66-Type Metal–Organic Framework

 Alexander Kronast,^[a] Sebastian Eckstein,^[b] Peter T. Altenbuchner,^[a] Konrad Hindelang,^[c] Sergei I. Vagin,^[a] and Bernhard Rieger^{*[a]}

Abstract: The highly porous and stable metal–organic framework (MOF) UiO-66 was altered using post-synthetic modifications (PSMs). Prefunctionalization allowed the introduction of carbon double bonds into the framework through a four-step synthesis from 2-bromo-1,4-benzenedicarboxylic acid; the organic linker 2-allyl-1,4-benzenedicarboxylic acid was obtained. The corresponding functionalized MOF (UiO-66-allyl) served as a platform for further PSMs.

From UiO-66-allyl, epoxy, dibromide, thioether, diamine, and amino alcohol functionalities were synthesized. The abilities of these compounds to adsorb CO₂ and N₂ were compared, which revealed the structure–selectivity correlations. All synthesized MOFs showed profound thermal stability together with an increased ability for selective CO₂ uptake and molecular gate functionalities at low temperatures.

Introduction

Metal–organic frameworks (MOFs) and their underlying concept, which involves the combination of inorganic building blocks with ubiquitous organic linking units, offer numerous possibilities for modifications.^[1] In general, MOFs provide a high degree of crystallinity and high pore volumes accompanied by extraordinary internal surface areas. These unique properties make MOFs ideal candidates for gas storage and separation,^[2] catalysis,^[3] drug delivery,^[4] and chemical sensing.^[5] The host–guest interactions can be tuned by the introduction of functional groups into the framework; these groups are mainly attached to the organic-linker units. Thus, the interactions between the target molecule and the framework have been systematically tuned previously and current studies remain focused on the separation and storage of greenhouse gases.^[2d,6]

The release of CO₂ from anthropogenic sources has led to intensified concerns about the greenhouse effect and global warming and the implications for the global society.^[7] Post-

combustion capture of CO₂ is hampered by its low content (~15%) in flue gases compared to the main component (N₂) and other components present in minor quantities (H₂O, O₂, CO, NO_x, and SO_x).^[8] Solid porous materials such as zeolites, functionalized silica, activated carbon, and MOFs show distinct advantages for post-combustion CO₂ capture compared with the very energy intensive scrubbing process that uses aqueous solutions of alkanolamines, which results in substantial efficiency losses in power plants equipped with this technology.^[9] Although MOFs show lower chemical and thermal stabilities than other inorganic porous materials, the ease of modification of both the network architecture and functional groups make them promising candidates as post-combustion adsorbents. For MOFs to be an economically viable alternative in post-combustion applications, high capacities for CO₂ adsorption, high selectivity for CO₂ over N₂, and robustness against the trace amounts of water present in the flue gas are prerequisite properties that research has to tackle.^[10]

To match these requirements, convertible side chains, which do not interfere with the network synthesis, have recently been investigated. The use of these groups avoids the formation of additional crystal phases, decomposition, and other side reactions.^[11] Mainly pioneered by Wang et al. and Cohen et al., post-synthetic modifications (PSMs) have become one of the most promising and versatile routes to obtain the desired features, for example, amines or other polarized groups, on the framework surface. Recently, the concept of molecular gates has been introduced.^[12] Molecular gates enable MOFs to discriminate between different gases during adsorption and, therefore, increase the selectivity of the frameworks. Consequently, frameworks offering this feature came into focus but most lack the required stability.^[12a]

[a] A. Kronast, Dr. P. T. Altenbuchner, Dr. S. I. Vagin, Prof. Dr. B. Rieger
Wacker-Lehrstuhl für Makromolekulare Chemie
Technische Universität München, Lichtenbergstrasse 4
85747 Garching bei München (Germany)

[b] S. Eckstein
Lehrstuhl für Technische Chemie II, Technische Universität München
Lichtenbergstrasse 4, 85747 Garching bei München (Germany)

[c] Dr. K. Hindelang
Consortium für elektrochemische Industrie
Wacker Chemie AG, Zielstattstrasse 20, 81379 München (Germany)

Supporting information for this article is available on the WWW under <http://dx.doi.org/10.1002/chem.201602318>.

Chemically and thermally stable networks have recently attracted attention in the field of MOF chemistry. The UiO-66 MOF, a three-dimensional framework of Zr^{IV} -carboxylate clusters, $Zr_6(\mu_3-O)_4(\text{CO}_2)_{12}$, and linking 1,4-benzenedicarboxylate (BDC^{2-}) units, is characterized by exceptional stability, high adsorption volumes, and good functional-group tolerance during the MOF synthesis.^[6d,13] The surface area of unfunctionalized UiO-66 was determined to be greater than $1100 \text{ m}^2 \text{ g}^{-1}$. Fundamental work on the influence of functional groups on the adsorption properties of different gases in UiO-66 was performed by Cohen et al.³⁷ and Walten et al.^[13a,14] According to their results, the interaction of guest molecules like nitrogen or CO_2 rises with the polarity of the attached groups.

Herein, we report the synthesis of the highly stable MOF UiO-66-allyl and the enormous potential of PSMs for fine-tuning of the network-guest interactions. The unique network features allow the introduction of molecular gates at low temperatures, accompanied by a remarkable selectivity for adsorption of CO_2 in preference to N_2 at elevated temperatures.

Results and Discussion

We recently reported on the conversion of olefinic side chains in a Zn-based pillared MOF.^[15] As a model system, we modified a bipyridine pillar ligand connecting square paddle-wheel layers based on 9,10-triptycenedicarboxylic acid and Zn ions.^[16] As this framework did not show high tolerances to basic and acidic conditions, we decided to modify the exceptionally stable UiO-66 system by attaching an olefinic side chain to benzenedicarboxylic acid H_2 . The stability of the network is of crucial importance for the fine tuning of CO_2 adsorption through PSM.

Linker synthesis

Methyl ester protection of the commercially available 2-bromo-1,4-benzenedicarboxylic acid, followed by a Pd^0 -catalyzed Stille coupling reaction gave dimethyl 2-allylbenzene-1,4-dicarboxylate. Subsequent deprotection under basic conditions produced 2-allyl-1,4-benzenedicarboxylic acid (2-allyl-BDC) in good yield (Scheme 1 and Scheme S1 in the Supporting Information).

MOF preparation

In Zr-carboxylates, the formation of undesirable crystal phases is suppressed because of their structural homogeneity compared with other metal-linker combinations that are used in

MOF synthesis. The UiO-66 analogue was prepared by the combination of ZrCl_4 with 2-allyl-BDC in DMF. The addition of water to the reaction mixture was indispensable for the formation of the nanocrystalline powder, as a full hydrolysis of ZrCl_4 is essential.

The crystallinity of the sample was verified using powder X-ray diffraction (PXRD) and the diffraction pattern obtained was compared with literature data for the parent network. The pattern clearly confirmed the integration of the previously unknown 2-allyl-1,4-benzenedicarboxylate linker into the UiO-66 network (Scheme 2).

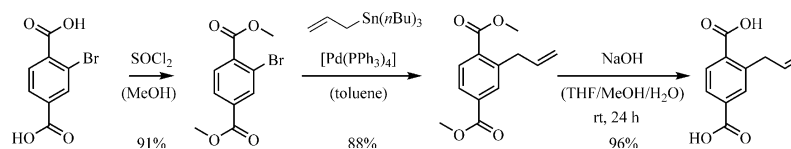
The reaction times for PSMs in MOFs fundamentally depend on the diffusion limitations within the microporous solids. Fast mass transport through the MOF cavities can be achieved by small uniform MOF-particles and a high degree of activation. The standard synthesis reported in the literature^[13b] yielded MOF samples with low Brunauer-Emmett-Teller (BET) surface areas. Behrens et al. developed a modulated MOF synthesis for Zr-carboxylate networks using monocarboxylic acids to slow down the crystallization rate and increase the accessible pore volumes through improved crystallization.^[17]

After activation, acetic acid modulation increased the accessible surface area in the unfunctionalized UiO-66 network from 711 to $1189 \text{ m}^2 \text{ g}^{-1}$ (see Scheme S2 in the Supporting Information) through slowing down the crystallization rate.^[17] The maximum surface area was obtained by using 10 vol% of acetic acid in the reaction solution; this concentration of acetic acid was also used in the synthesis of the functionalized MOF UiO-66-allyl ($736 \text{ m}^2 \text{ g}^{-1}$). The drop in the BET value for the derivative can be attributed to the increased steric demand in the pores by the attached side chains. Nevertheless, the allylic side chains could be successfully introduced while preserving both crystallinity and porosity (Figure 1).

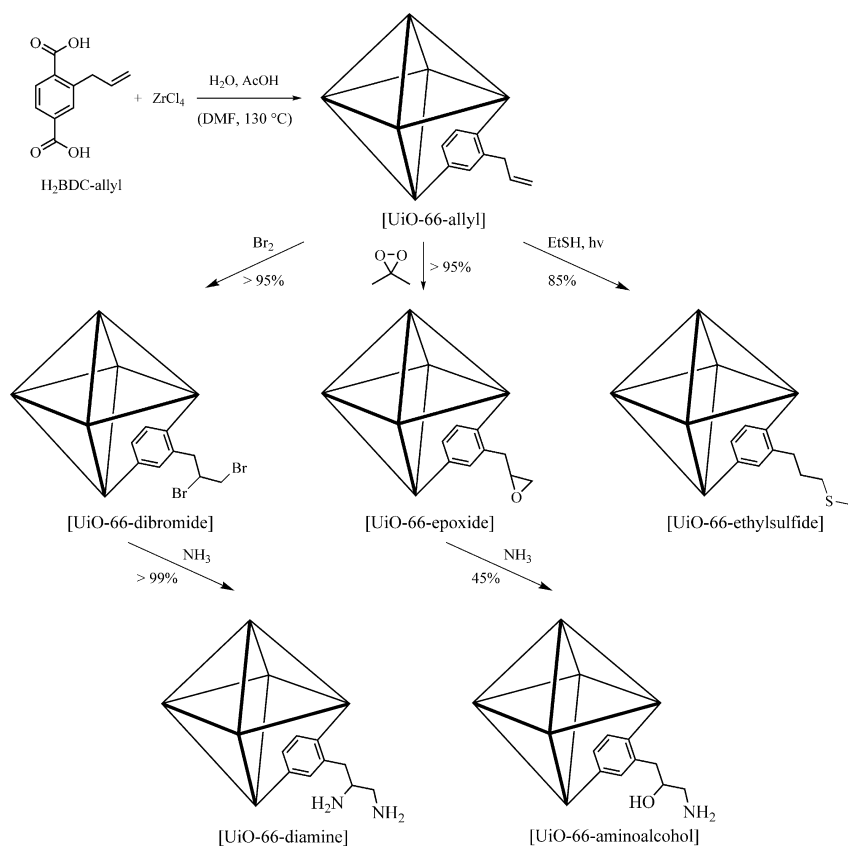
Post-synthetic modifications

The permanent porosity and stability of Zr-based MOFs make the UiO-66-allyl network a perfect substrate for PSM. The integrated $\text{C}=\text{C}$ double bond can be converted through a variety of PSMs (Scheme 2) to tune the adsorption properties for different gases like CO_2 and N_2 .

Epoxidation of the double bond was chosen as the model PSM, as it had been successfully applied in our previous work.^[15] The chemical stability of the network emerged as a challenge in the characterization of the PSM results. Besides XRD and BET measurements, solution NMR was the method of choice to quantify the degree of conversion of the allylic side chains. Cohen et al. reported the acidic disintegration of UiO-



Scheme 1. Synthesis of 2-allyl-1,4-dicarboxylic acid (L1).



Scheme 2. Synthesis of and PSMS applied to UiO-66-allyl: bromination to yield UiO-66-dibromide, epoxidation with dimethyldioxirane to yield UiO-66-epoxide, and a thiol-ene click reaction using EtSH to yield UiO-66-ethylsulfide. Tandem PSM with nucleophilic ring opening in UiO-66-epoxide to yield UiO-66-aminoalcohol, and nucleophilic substitution in UiO-66-dibromide to yield UiO-66-diamine.

66 using hydrofluoric acid.^[18] The application of this method to the UiO-66-epoxide lead to side reactions hampering further analysis. Cyclic esters and side products that were not further investigated were found (Supporting Information, Scheme S3). To avoid any further problems in product determination, we developed a new disintegration method using deuterated sodium hydroxide in D₂O. Under these conditions, the newly formed epoxide was quantitatively ring opened and converted to the glycol (Figure 2). The nearly quantitative yields achieved using the oxidizing reagent dimethyldioxirane, together with the remaining crystallinity and the high nitrogen surface area (BET = 617 m²g⁻¹), emphasize the suitability of the MOF for PSMS.

Both bromination with elemental bromine and a UV-initiated thiol-ene click reaction using ethyl mercaptane proceeded in nearly quantitative yields and good conversions of the double bond, which were comparable to the results of our previous work.^[15a] Although crystallinity was retained in both cases according to PXRD, the accessible BET surface area of the activated samples dropped to 5 and 52 m²g⁻¹, respectively. This result will be discussed in detail below in the section describ-

ing gas adsorption behavior. The basic workup of the dibromide compound led to a substitution reaction resulting in the formation of a glycol-containing product identical to the epoxidation product.

Polar functional groups, especially amine functionalities, are well known to increase the interaction and selectivity with guest molecules, such as CO₂, in porous networks.^[13a] Nevertheless, the introduction of primary amines through PSM has not been widely investigated, with the exception of the post-synthetic deprotection of *N*-Boc-tagged networks. Boc-protecting groups hamper the framework interpenetrations that occur during MOF assembly, and subsequent removal of these groups can both increase the pore volume and unmask an unprotected amine functional group. Following this route, Telfer and co-workers were able to unmask an amine functionality in IRMOF-12 as well as the secondary amine of proline in IRMOF-Pro.^[19] Although there are some examples of amine-tagged MOFs in the literature, there are, to our knowledge, no vicinal diamino- or amino alcohol-tagged frameworks known until now.^[13a,19b,20] Through the integration of these functionalities, a variety of possible applications arise, especially as chelat-

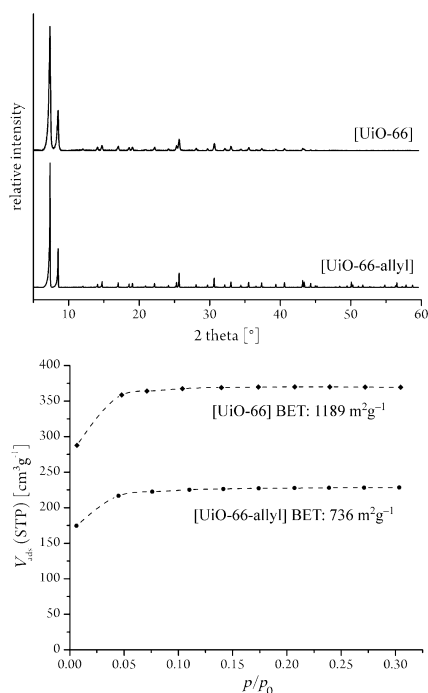


Figure 1. PXRD and BET surfaces obtained by modulated MOF synthesis using acetic acid as a modulator for UiO-66 and UiO-66-allyl.

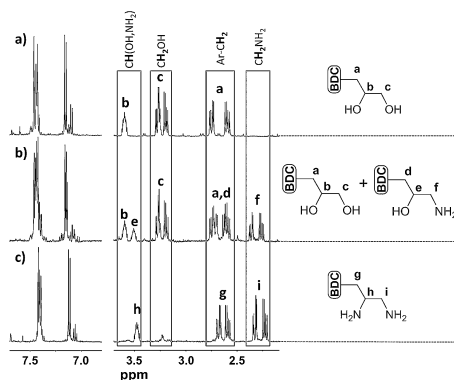


Figure 2. ^1H NMR spectra of the tandem functionalized linkers after disintegration using NaOD in D_2O : a) UiO-66-epoxide (for comparison), b) UiO-66-aminoalcohol and unreacted UiO-66-epoxide, c) UiO-66-diamine.

ing ligands for catalytic active metal ions and CO_2 -sorption substrates.

As there are different literature examples for both the nucleophilic ring-opening of epoxides and the substitution of halides using ammonia, we developed tandem PSMs for the conversion of our epoxy- and dibromide-tagged networks. On account of the fragility of the network under strongly basic conditions, it was necessary to avoid any traces of water by both activating the network before modification and working under

dry and inert atmosphere conditions. After drying the MOF powder under vacuum at 120°C for 16 h in a steel autoclave, the autoclave was pressurized with dry ammonia at room temperature and heated to 80°C overnight. After removing the gas in vacuo, the samples were characterized using standard methods (see the Supporting Information). The conversion of the dibromo-functionalized UiO-66 was quantitative, forming the diamine as proven by NMR spectroscopy.

Nevertheless, the PXRD of the functionalized network showed a decrease in reflex intensity. This can be attributed to a decrease in the crystal size, congestion of the pores by the ammonium bromide byproduct (reflexes at 22.30 and 31.70 2Θ , Figure 3), or an overall loss in crystallinity. BET measure-

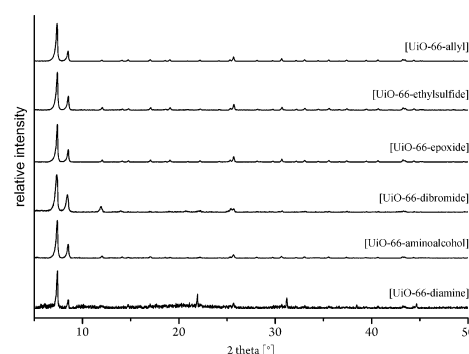


Figure 3. PXRD analysis of the different UiO-66 derivatives before (UiO-66-allyl) and after PSM (see the Supporting Information for enlarged versions of the diffractograms).

ments were conducted and revealed only a low active surface for nitrogen adsorption ($6\text{ m}^2\text{ g}^{-1}$). Although the combination of these analytics indicated framework destruction, CO_2 adsorption measurements were inconsistent with these results (Figure 5) and showed a higher CO_2 uptake than the unfunctionalized UiO-allyl-network.

As aqueous monoethanolamine is the current commercially used CO_2 -scrubbing reagent, this functional group promises a high interaction potential with CO_2 as a guest molecule. We therefore carried out the nucleophilic ring-opening of UiO-66-epoxide with the goal of preparing an amino alcohol-functionalized UiO-66 network. The nucleophilic attack of ammonia leads to the corresponding amino alcohol without the formation of any side products. The reaction product showed remaining crystallinity and a conversion of the epoxide of 45%, determined by NMR spectroscopy, which could not be accelerated by varying the reaction conditions. However, BET surface-area measurements revealed an accessible surface of only $3\text{ m}^2\text{ g}^{-1}$, which will be discussed below.

The introduction of diamino and amino alcohol functionalities offers not only a high potential for host-guest interactions but also the potential to introduce catalytically active metal ions by inclusion of donor atoms during PSM.^[11]

The wide range of PSMs that were available for the UiO-66 system is demonstrated by the multitude of different reaction

conditions applied, and the exceptional chemical stability of the system was proven by the crystallinity remaining after treatment with ammonia.

The modified MOF systems were analyzed by the common methods used for PSM experiments, including PXRD, thermogravimetric analysis, solution ^1H NMR spectroscopy, and nitrogen adsorption measurements using the BET method (see the Supporting Information). Because UiO-66-allyl was prepared as a microcrystalline powder, no single-crystal analysis was possible. To clarify the structure of this material, the crystal phase was compared to that of the original UiO-66 using PXRD.

The disintegration using NaOD offered direct access to linker solutions in deuterated water following removal of the Zr-containing salts using centrifugation. This method also revealed that the allylic side chain was preserved during the MOF synthesis, as shown in the Supporting Information. The ^1H NMR spectra of the corresponding PSM products can be attributed to either the direct reaction products or tandem products obtained as a result of the basic workup. The conversion of the C=C double bond can also be evaluated using this method.

Gas adsorption

Nitrogen adsorption isotherms revealed the influence of the newly introduced functional groups on the accessible surface area in the network. In comparison with the parent compound ($723\text{ m}^2\text{ g}^{-1}$), all PSM products showed a remarkable decrease in BET values. The smallest decrease was determined for UiO-66-epoxide, which had a pore surface area of $498\text{ m}^2\text{ g}^{-1}$. UiO-66-thioether exposes accessible pores, with the surface area reduced to $52\text{ m}^2\text{ g}^{-1}$. UiO-66-dibromide, UiO-66-diamine, and UiO-66-ethanolamine show only low or no accessible pore surface areas at 77 K in nitrogen adsorption experiments (Figure 4).

Different groups have previously reported that CO_2 adsorption depends on the interaction of the integrated side chains in UiO-66 with the corresponding gas. Polar groups were found to be more attractive for CO_2 sorption than nonpolar functionalizations.^[9,13a,14,21] However, until now, there have

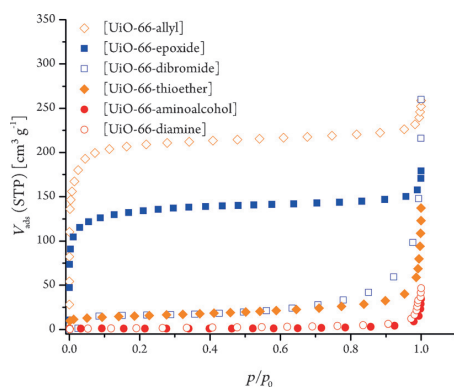


Figure 4. N_2 adsorption isotherms recorded for UiO-66-allyl and PSM derivatives at 77 K.

been no studies looking at the influence of allyl, epoxide, dibromide, ethylsulfide, diamine, or ethanolamine groups in UiO-66 MOFs on the capacity for N_2 and CO_2 sorption.

The N_2 adsorption isotherms recorded at 35°C show a strong dependence on the attached side chains in the framework cavities (Figure 5). While diamine and ethanolamine dis-

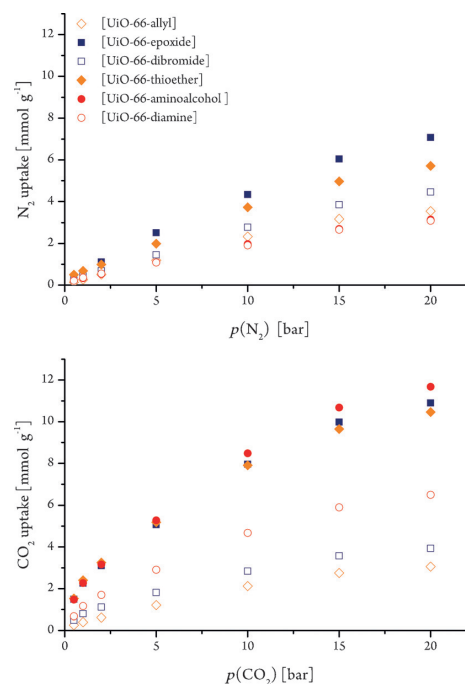


Figure 5. N_2 and CO_2 high-pressure adsorption isotherms recorded for UiO-66-allyl and PSM derivatives at 308 K.

play uptakes are comparable to the parent framework, dibromide, thioether, and epoxide show remarkably increased uptakes (up to 200% higher). As the selectivity of the substrate plays an essential role in any possible gas separation applications, the CO_2 adsorption isotherms of the PSM products and UiO-66-allyl were also recorded, and are shown in Figure 5. The isotherms clearly illustrate the influence of polar groups on the adsorption properties. Although it shows the highest BET surface value, UiO-66-allyl shows the lowest CO_2 loading of all the substrates investigated. The amino alcohol-tagged MOF (UiO-66-aminoalcohol) exhibited the highest adsorption of CO_2 combined with one of the lowest values for N_2 , followed by UiO-66-epoxide and UiO-66-thioether. The total CO_2 loading of UiO-66-aminoalcohol was about 51 wt% at 35°C and 20 bars. The comparatively low loading of UiO-66-diamine may be caused by congestion of the pore system resulting from the large amino groups, as well as the NH_4Br byproduct of the tandem PSM. As expected, the dibromo-functionalized MOF, without polar groups, displayed the lowest CO_2 loading of the PSM derivatives. Nevertheless, the CO_2 loading was still higher than that observed for the parent system. Compared to litera-

ture data, UiO-66-aminoalcohol hosts up to ten percent more CO₂ than the amino tagged UiO-66-NH₂ at 25 °C and 20 bars.^[13a]

To the best of our knowledge, this is the highest CO₂ adsorption loading of a functionalized UiO-66 MOF in the literature, and points out the importance of adjustable host–guest interactions in MOFs that are available through PSMs. Chemisorption of CO₂ was excluded for all substrates using ATR-IR measurements (see the Supporting Information, Scheme S7). Thus, UiO-66-aminoalcohol represents a promising candidate for possible CO₂–N₂ gas separation.

The astonishing differences in the adsorption properties of the frameworks at different temperatures point to a gated-pore effect in the MOFs similar to that found by Fischer et al.^[12a] This group described a honeycomb-like zinc-dicarboxylate-bipyridine network with flexible ether side chains. The effect was attributed to the low thermal energy of the ether substituents and subsequent congestion of the pore windows, which prevented N₂ diffusion at low temperatures. Nevertheless, these examples did not employ covalent PSM for the introduction of the molecular gates.

The tandem PSMs performed by epoxidation and nucleophilic ring-opening impressively demonstrate the versatility and viability of PSM to precisely adjust adsorption properties in MOFs. UiO-66-allyl showed only a low capacity for CO₂ adsorption, at about 13 wt% at 35 °C and 20 bars. The oxidized UiO-66-epoxide exhibited an increased CO₂ adsorption of 48 wt% with a preserved BET surface of 498 m²g⁻¹. The final product, UiO-66-aminoalcohol, displayed the highest CO₂ loading of 51 wt% in combination with a closed-gate effect for nitrogen diffusion at 77 K and the lowest N₂ loading at 35 °C.

Conclusion

We have successfully used PSMs to introduce molecular gates into the MOF UiO-66-allyl. The obtained functionalities enable a powerful tuning for the adsorption of CO₂ over N₂.

The functionalization of the linking 1,4-benzenedicarboxylate ligand, as well as the optimization of the MOF synthesis using acetic acid as a modulator, was intensively investigated to optimize both crystallinity and pore accessibility. The known bromination (UiO-66-dibromide), epoxidation (UiO-66-epoxide), and thiol-ene click reaction (UiO-66-ethylsulfide) PSMs were applied to UiO-66-allyl and resulted in the formation of the desired products in good to quantitative yields. Furthermore, we have, for the first time, introduced a vicinal 1,2-diamino functionality into UiO-66 using a tandem PSM by the reaction of the dibromide with dry ammonia at elevated temperatures (UiO-66-diamine). In another tandem PSM, we successfully ring-opened the epoxide with ammonia to give the corresponding vicinal amino alcohol functionalized compound (UiO-66-aminoalcohol). These tandem PSM steps illustrate the exceptional stability of the UiO-66 system.

All the products resulting from PSM displayed increased CO₂ adsorptions, and, with the exception of UiO-66-epoxide, displayed gated pores with a major decrease in the uptake of nitrogen gas at 77 K in comparison with the mother compound

UiO-66-allyl. The CO₂ adsorption of UiO-66-aminoalcohol was nearly four times higher than that of the mother compound, and was exceptionally high when compared with other compounds reported in the literature.

The PSMs developed herein illustrate the importance of reactive side groups, introduced in pre-synthetic modifications, which do not hinder the MOF crystallization process, but may be converted in high yields to functionalities that are not accessible through pre-synthetic functionalization. Moreover, our work highlights the possibilities of tailoring host–guest interactions through PSMs and, therefore, enabling applications in gas sorption and separation.

Experimental Section

General

All reactions containing air- and/or moisture-sensitive compounds were performed under dry argon using standard Schlenk or glove-box techniques. All chemicals were purchased from Aldrich, ABCR or Acros. Solvents were obtained from an MBraun MB-SPS solvent purification system.

UV irradiation for the photoinduced thiol–ene click reaction was executed with a MAX-302 ASAHI SECTRA. NMR spectra were recorded on a Bruker Avance 500 UltraShield (500 MHz) and a Bruker Avance 300 (300 MHz). They were recorded in ppm and the solvents residual proton signal and carbon signal were used as the internal standard. X-ray powder diffraction was measured on a STOE STADI P system with a DECTRIS MYTHEN 1 K detector. TGA was carried out on a Texas Instruments TGA-Q500 with a heating rate of 10 Kmin⁻¹. Brunauer-Emmett-Teller (BET) adsorption measurements were obtained by using a Quantachrome Nova 4000e sorption apparatus and a PMI automatic Sorptometer. The samples were activated in vacuum at 135 °C for 2 h before measurement. Apparent surface area was calculated by applying the BET theory. CO₂ and N₂ isotherms were obtained at 35 °C in a range of 0.5–20 bar using a Rubotherm magnetic suspension balance. Approximately 300 mg of the sorbent was placed in a steel crucible and dried at 135 °C for 8 h under vacuum prior to adsorption. To correct for buoyancy, reference adsorption isotherms of nonadsorbing glass spheres (300 mg, particle size: 425–600 μm) were determined and subtracted from the isotherms. Elemental analyses were measured at the Laboratory for Microanalytics at the Institute of Inorganic Chemistry at the Technische Universität München. ESI-MS analytical measurements were performed with acetonitrile, THF, isopropanol, or toluene solutions on a Varian 500-MS spectrometer. IR spectra were recorded with a liquid nitrogen cooled Bruker Vertex 70 FTIR-spectrometer with an attenuated total reflectance unit Platinum ATR of Bruker using 32 scans in a region of 4500 to 600 cm⁻¹.

Linker synthesis

2-Bromoterephthalic acid dimethylester: To a stirred suspension of 2-bromoterephthalic acid (6.2 g, 25.3 mmol, 1.0 equiv) in dry methanol (100 mL), thionylchloride (7.3 mL, 101 mmol, 4.0 equiv) was added dropwise at room temperature. The reaction mixture was heated to reflux for 16 h and excess of thionylchloride and the solvent were evaporated in vacuo. To the residue, 50 mL of a saturated sodiumbicarbonate solution was added and extracted with ethyl acetate (50 mL) three times. The organic extracts were combined, dried over sodium sulfate, and evaporated in vacuo to give 6.26 g 2-bromoterephthalic acid (22.9 mmol; 92%) as a colorless

solid. ^1H NMR (300 MHz; CDCl_3): $\delta = 3.94$ (s, 3H, $-\text{CH}_3$), 3.95 (s, 3H, $-\text{CH}_3$), 7.80 (m, 1H, H_{arom}), 8.01 (dd, 1H, $^3J = 8.1$ Hz, 1.7 Hz, H_{arom}), 8.31 ppm (d, 1H, $^3J = 1.7$ Hz, H_{arom}); ^{13}C NMR (75.5 MHz; CDCl_3): $\delta = 52.81$, 52.91, 121.57, 128.22, 131.14, 133.83, 135.32, 136.25, 165.12, 166.26 ppm.

2-Allylterephthalic acid dimethylester: 2-Bromoterephthalic acid dimethylester (12.0 g, 43.9 mmol, 1.0 equiv) and 1.0 g tetrakis-(triphenylphosphine)palladium(0) [$\text{Pd}(\text{PPh}_3)_4$] (0.88 mmol; 0.02 equiv) were dissolved in 200 mL of degassed toluene under an argon atmosphere. 15.0 mL allyltri(*n*-butyl)tin were added and the reaction solution was heated to reflux for 5 days. The reaction mixture was quenched using 100 mL of a 4% cesium fluoride solution and extracted with ethyl acetate. After drying over sodium sulfate, the raw product was purified using flash chromatography (silica gel, hexane/ethyl acetate 95:5) to give 9.07 g 2-allylterephthalic acid dimethylester (38.7 mmol, 88%) as a colorless oil. TLC: $R_f = 0.16$ (hexane/ethyl acetate = 95:5) [UV]; ^1H NMR (300 MHz; CDCl_3): $\delta = 3.77$ (d, 1H, $^3J = 6.4$ Hz, $-\text{CH}_2-$), 3.90 (s, 3H, $-\text{OCH}_3$), 3.93 (s, 3H, $-\text{OCH}_3$), 5.01–5.05 (m, 2H, $-\text{CH}=\text{CH}_2$), 5.99 (ddt, 1H, $^3J = 16.7$, 10.1, 6.4 Hz, $-\text{CH}=\text{CH}_2$), 7.90–7.94 ppm (m, 3H, H_{arom}); ^{13}C NMR (75.5 MHz; CDCl_3): $\delta = 38.33$, 52.39, 52.51, 116.35, 127.32, 130.64, 132.05, 133.05, 133.88, 136.77, 141.69, 166.44, 167.57 ppm; elemental analysis calcd (%) for $\text{C}_{13}\text{H}_{14}\text{O}_4$: C 66.66, H 6.02, O 27.32; found: C 66.57, H 6.09; IR (ATR): $\nu = 3080$ –2840 (w, multiple weak maxima, Ar–H, C–H), 1718 (vs, C=O), 1638 (w, C=C str), 1571 (w), 1492 (w), 1434 (m), 1405 (w), 1257 (s, C–O), 1194 (m), 1111 (s), 1072 (m), 992 (m, $\text{CH}=\text{CH}_2$ twist), 963 (w), 915 (s, $\text{CH}=\text{CH}_2$ wag), 883 (w), 857 (w), 815 (m), 750 (s), 717 (m), 654 cm^{-1} (w).

2-Allylterephthalic acid (L1): 2-Allylterephthalic acid dimethyl ester (6.28 g, 26.8 mmol, 1.0 equiv) were dissolved in 100 mL of a 1:1 mixture of THF and methanol. After the addition of sodium hydroxide solution (65 mL, 1 M, 65.0 mmol, 2.4 equiv) the mixture was stirred for 24 h at room temperature. The organic solvents were removed in vacuo and the residue was dissolved in 50 mL of water. The aqueous solution was neutralized using concentrated hydrochloric acid and the formed precipitate was isolated by filtration. The white powder was repeatedly washed with water and dried in vacuo to obtain 5.30 g 2-allylterephthalic acid (25.7 mmol, 96%) as a colorless solid. ^1H NMR (300 MHz; $[\text{D}_6]\text{DMSO}$): $\delta = 3.74$ (d, 1H, $^3J = 6.6$ Hz, $-\text{CH}_2-$), 5.03 (m, 2H, $-\text{CH}=\text{CH}_2$), 5.95 (m, 1H, $-\text{CH}=\text{CH}_2$), 7.82–7.86 (m, 3H, H_{arom}), 13.26 ppm (s, 2H, $-\text{COOH}$); ^{13}C NMR (75.5 MHz; $[\text{D}_6]\text{DMSO}$): $\delta = 37.39$, 116.19, 127.10, 130.27, 131.35, 134.70, 137.18, 140.58, 166.67, 168.31 ppm; elemental analysis calcd (%) for $\text{C}_{11}\text{H}_{10}\text{O}_4$: C 64.07, H 4.89, O 31.04; found: C 63.93, H 4.79; IR (ATR): $\nu = 3200$ –2500 (s, broad signal with multiple maxima, O–H, Ar–H, C–H), 1681 (s, C=O), 1634 (w, C=C str), 1568 (w), 1495 (w), 1414 (m), 1284 (s, C–O), 1206 (w), 1193 (w), 1134 (w), 1105 (w), 1070 (w), 993 (m, $\text{CH}=\text{CH}_2$ twist), 914 (s, $\text{CH}=\text{CH}_2$ wag), 860 (w), 784 (m), 748 (m), 706 (w), 678 (w), 654 cm^{-1} (w).

MOF-synthesis

UiO-66-allyl: A solution of 1.50 g 2-allyl benzene-1,4-dicarboxylic acid (7.27 mmol, 1.00 equiv) in 160 mL DMF was added in one portion to a solution of 1.61 g ZrCl_4 (6.91 mmol, 0.95 equiv) in a mixture of 164 mL DMF, 36 mL acetic acid, and 393 μL water. The mixture was placed in a glass autoclave and heated under static conditions to 130 °C for 20 h. After cooling down the microcrystalline powder was isolated using centrifugation and repeatedly washed with DMF, methanol, and DCM. Every washing step included the treatment in an ultrasonic bath for 5 min prior to drying in vacuo at 120 °C. Elemental analysis: calcd (%) for $[\text{Zr}_6\text{O}_4(\text{OH})_4(\text{C}_{11}\text{H}_8\text{O}_4)_6]_n$: C 41.62, H 2.75, O 26.88, Zr 27.74; found: C 40.92, H 2.28.

Postsynthetic modifications

UiO-66-epoxide: Activated UiO-66-allyl (300 mg, 0.95 mmol) was treated with a solution of dimethyl-dioxirane (DMDO) (0.05 M, 40 mL, 2.0 mmol) in acetone for 72 h at 4 °C. At the end of the reaction time, the solution was removed using centrifugation and the MOF powder was washed three times with 10 mL of fresh acetone. Afterwards, the product was dried in vacuo. Conversion (^1H NMR): 95%.

Proton NMR shows signals for the corresponding glycol through nucleophilic ring-opening of the epoxide.

^1H NMR (500 MHz, Deuterium Oxide): $\delta = 2.56$ –2.82 (m, 2H), 3.15–3.35 (m, 2H), 3.60 (td, $^3J = 9.4$, 7.8, 4.5, 1H), 7.16 (d, $^3J = 7.8$, 1H), 7.41–7.51 (m, 2H); elemental analysis calcd (%) for $[\text{Zr}_6\text{O}_4(\text{OH})_4(\text{C}_{11}\text{H}_8\text{O}_5)_6]_{0.95}[\text{Zr}_6\text{O}_4(\text{OH})_4(\text{C}_{11}\text{H}_8\text{O}_4)_6]_{0.05}$: C 39.72, H 2.63, O 30.22, Zr 27.43; found: C 41.02, H 2.89.

UiO-66-dibromide: Activated UiO-66-allyl (300 mg, 0.95 mmol) was placed in a Schlenk flask, suspended in 5 mL of fresh trichloromethane and cooled to 0 °C. 0.2 mL bromine (4.12 mmol) was added dropwise to the MOF and the reaction mixture was stirred at room temperature for 16 h. The solvent was removed using centrifugation and decantation. The MOF powder was washed several times using trichloromethane and dichloromethane and dried under vacuo. Conversion (^1H NMR): 100%.

Proton NMR shows signals for the corresponding glycol through nucleophilic substitution of bromide by hydroxide.

^1H NMR (500 MHz, Deuterium Oxide): $\delta = 2.79$ –2.53 (m, 2H), 3.34–3.14 (m, 3H), 3.63–3.52 (m, 1H), 7.15 (d, $^3J = 7.9$, 1H), 7.48–7.40 (m, 3H); elemental analysis calcd (%) for $[\text{Zr}_6\text{O}_4(\text{OH})_4(\text{C}_{11}\text{H}_8\text{Br}_2\text{O}_4)_6]_n$: C 27.69, H 1.83, Br 33.49, O 17.88, Zr 19.12; found: C 26.25, H 2.15.

UiO-66-ethylsulfide: Activated UiO-66-allyl (250 mg, 0.79 mmol) was placed in a quartz Schlenk tube to ensure UV light transparency. Degassed ethylmercaptane (3.5 mL, 47 mmol) was added at room temperature and the mixture was allowed to stay in the dark for 2 h impregnating the pores with the reactant. Subsequently, the reaction mixture was irradiated with UV light for 8 h under moderate stirring. After the reaction, the MOF powder was washed three times using THF (5 mL) and dried in vacuo. Conversion (^1H NMR): 80%. ^1H NMR (500 MHz, Deuterium Oxide): $\delta = 0.81$ –0.93 (m, 3H), 1.48–1.68 (m, 2H), 2.19–2.33 (m, 4H), 2.56 (t, $^3J = 7.6$, 2H), 7.07 (dd, $^3J = 12.8$, 7.8, 1H), 7.36–7.44 ppm (m, 2H); elemental analysis calcd for $[\text{Zr}_6\text{O}_4(\text{OH})_4(\text{C}_{13}\text{H}_{14}\text{O}_4\text{S})_6]_{0.80}[\text{Zr}_6\text{O}_4(\text{OH})_4(\text{C}_{11}\text{H}_8\text{O}_4)_6]_{0.20}$: C 41.22, H 3.70, O 23.24; S 6.99, Zr 24.85; found: C 39.13, H 3.68, S 5.65.

UiO-66-aminoalcohol: Activated UiO-66-epoxide (300 mg, 0.90 mmol) was placed in a 25 mL steel autoclave and pressurized with ammonia (8 bar). The autoclave was heated to 80 °C for 72 h and the ammonia was released followed by sequential washing with methanol (3 \times 5 mL) and drying in vacuo. Conversion (^1H NMR): 45%. ^1H NMR (500 MHz, Deuterium Oxide): $\delta = 2.21$ –2.42 (m, 2H), 2.62–2.76 (m, 2H), 3.49–3.53 (m, 1H), 7.14 (d, $^3J = 3.3$, 1H), 7.44–7.47 ppm (m, 2H); elemental analysis calcd (%) for $[\text{Zr}_6\text{O}_4(\text{OH})_4(\text{C}_{11}\text{H}_{11}\text{NO}_5)_6]_{0.43}[\text{Zr}_6\text{O}_4(\text{OH})_4(\text{C}_{11}\text{H}_8\text{O}_5)_6]_{0.52}[\text{Zr}_6\text{O}_4(\text{OH})_4(\text{C}_{11}\text{H}_8\text{O}_4)_6]_{0.05}$: C 38.87, H 2.95, N 1.77, O 29.57, Zr 26.84; found: C 36.12, H 3.13, N 1.97.

UiO-66-diamine: Activated UiO-66-dibromide (300 mg, 0.63 mmol) was placed in a 25 mL steel autoclave and pressurized with ammonia (8 bar). The autoclave was heated to 80 °C for 16 h and the ammonia was released followed by sequential washing with methanol (3 \times 5 mL) and drying in vacuo. Conversion (^1H NMR): 100%. ^1H NMR (500 MHz, Deuterium Oxide): $\delta = 2.15$ –2.39 (m, 2H), 2.54–2.76 (m, 2H), 3.43–3.55 (m, 1H), 7.12 (d, $^3J = 7.9$, 1H), 7.38–7.43 (m,

2H); elemental analysis calcd (%) for $[\text{Zr}_6\text{O}_4(\text{OH})_4(\text{C}_{11}\text{H}_{12}\text{N}_2\text{O}_4)_6(\text{HBr})_3]$: C 33.88, H 3.40, Br 10.25, N 7.18, O 21.88, Zr: 23.40; found: C 31.23, H 3.15, N 6.88; EDX: Zr: 24.53; Br: 12.14.

Acknowledgements

K.H. acknowledges financial support by the TUM International Graduate School of Science and Engineering (IGSSE) at the TU München. The authors gratefully thank Christina Schwarzenböck and Rike Adams for proofreading the manuscript.

Keywords: carbon dioxide sorption · gate effects · metal-organic frameworks · post-synthetic modification · UiO-66

- [1] a) H. Li, M. Eddaoudi, T. L. Groy, O. M. Yaghi, *J. Am. Chem. Soc.* **1998**, *120*, 8571–8572; b) H. Li, M. Eddaoudi, M. O’Keeffe, O. M. Yaghi, *Nature* **1999**, *402*, 276–279; c) O. M. Yaghi, G. Li, H. Li, *Nature* **1995**, *378*, 703–706.
- [2] a) A. R. Millward, O. M. Yaghi, *J. Am. Chem. Soc.* **2005**, *127*, 17998–17999; b) H. Furukawa, O. M. Yaghi, *J. Am. Chem. Soc.* **2009**, *131*, 8875–8883; c) P. V. Dau, S. M. Cohen, *CrystEngComm* **2013**, *15*, 9304–9307; d) P. V. Dau, S. M. Cohen, *Chem. Commun.* **2014**, *50*, 12154–12157.
- [3] a) H. Fei, S. M. Cohen, *Chem. Commun.* **2014**, *50*, 4810–4812; b) Y. Luan, N. Zheng, Y. Qi, J. Yu, G. Wang, *Eur. J. Inorg. Chem.* **2014**, *2014*, 4268–4272; c) H. Fei, M. D. Sampson, Y. Lee, C. P. Kubiak, S. M. Cohen, *Inorg. Chem.* **2015**, *54*, 6821–6828; d) I. Luz, C. Rösler, K. Epp, F. X. Llabrés i Xamena, R. A. Fischer, *Eur. J. Inorg. Chem.* **2015**, *2015*, 3904–3912.
- [4] a) H. Oh, T. Li, J. An, *Chem. Eur. J.* **2015**, *21*, 17010–17015; b) P. Horcajada, T. Chalati, C. Serre, B. Gillet, C. Sebrie, T. Baati, J. F. Eubank, D. Heurtaux, P. Clayette, C. Kreuz, J.-S. Chang, Y. K. Hwang, V. Marsaud, P.-N. Bories, L. Cynober, S. Gil, G. Ferey, P. Couvreur, R. Gref, *Nat. Mater.* **2010**, *9*, 172–178; c) K. M. L. Taylor-Pashow, J. D. Rocca, Z. Xie, S. Tran, W. Lin, *J. Am. Chem. Soc.* **2009**, *131*, 14261–14263.
- [5] a) J. Aguilera-Sigalat, D. Bradshaw, *Chem. Commun.* **2014**, *50*, 4711–4713; b) L. Heinke, M. Tu, S. Wannapaiboon, R. A. Fischer, C. Wöll, *Microporous Mesoporous Mater.* **2015**, *216*, 200–215; c) S. S. Nagarkar, A. V. Desai, S. K. Ghosh, *Chem. Eur. J.* **2015**, *21*, 9994–9997; d) M. Tu, S. Wannapaiboon, K. Khaletskaia, R. A. Fischer, *Adv. Funct. Mater.* **2015**, *25*, 4470–4479.
- [6] a) B. Arstad, H. Fjellvåg, K. Kongshaug, O. Swang, R. Blom, *Adsorption* **2008**, *14*, 755–762; b) J. H. Cavka, C. A. Grande, G. Mondino, R. Blom, *Ind. Eng. Chem. Res.* **2014**, *53*, 15500–15507; c) F. Ragon, B. Campo, Q. Yang, C. Martineau, A. D. Wiersum, A. Lago, V. Guillermin, C. Hemsley, J. F. Eubank, M. Vishnuvarthan, F. Taulelle, P. Horcajada, A. Vimont, P. L. Llewellyn, M. Daturi, S. Devautour-Vinot, G. Maurin, C. Serre, T. Devic, G. Clet, *J. Mater. Chem. A* **2015**, *3*, 3294–3309; d) J. Ethiraj, E. Albanese, B. Civalieri, J. G. Vitillo, F. Bonino, S. Chavan, G. C. Shearer, K. P. Lillerud, S. Bordiga, *ChemSusChem* **2014**, *7*, 3382–3388; e) M. Hammann, D. Castillo, C. Anger, B. Rieger, *J. Mater. Chem. A* **2014**, *2*, 16389–16396.
- [7] K. Sumida, D. L. Rogow, J. A. Mason, T. M. McDonald, E. D. Bloch, Z. R. Herm, T. H. Bae, J. R. Long, *Chem. Rev.* **2012**, *112*, 724–781.
- [8] a) A. Demessence, D. M. D’Alessandro, M. L. Foo, J. R. Long, *J. Am. Chem. Soc.* **2009**, *131*, 8784–8786; b) E. J. Granite, H. W. Pennline, *Ind. Eng. Chem. Res.* **2002**, *41*, 5470–5476.
- [9] M. W. Hahn, M. Steib, A. Jentys, J. A. Lercher, *J. Mater. Chem. A* **2014**, *2*, 13624–13634.
- [10] a) R. Sabouni, H. Kazemian, S. Rohani, *Environ. Sci. Pollut. Res. Int.* **2014**, *21*, 5427–5449; b) Z. Zhang, Z.-Z. Yao, S. Xiang, B. Chen, *Energy Environ. Sci.* **2014**, *7*, 2868–2899; c) J.-R. Li, Y. Ma, M. C. McCarthy, J. Sculley, J. Yu, H.-K. Jeong, P. B. Balbuena, H.-C. Zhou, *Coord. Chem. Rev.* **2011**, *255*, 1791–1823.
- [11] S. M. Cohen, *Chem. Rev.* **2012**, *112*, 970–1000.
- [12] a) S. Henke, R. A. Fischer, *J. Am. Chem. Soc.* **2011**, *133*, 2064–2067; b) S. Mondal, A. Bhunia, I. A. Baburin, C. Jager, A. Kelling, U. Schilde, G. Seifert, C. Janiak, H.-J. Holdt, *Chem. Commun.* **2013**, *49*, 7599–7601; c) S. Yang, G. S. B. Martin, J. J. Titman, A. J. Blake, D. R. Allan, N. R. Champness, M. Schröder, *Inorg. Chem.* **2011**, *50*, 9374–9384; d) S. Yang, S. K. Callear, A. J. Ramirez-Cuesta, W. I. F. David, J. Sun, A. J. Blake, N. R. Champness, M. Schröder, *Faraday Discuss.* **2011**, *151*, 19–36; e) Y. Cheng, H. Kajiro, H. Noguchi, A. Kondo, T. Ohba, Y. Hattori, K. Kaneko, H. Kanoh, *Langmuir* **2011**, *27*, 6905–6909; f) A. Banerjee, S. Nandi, P. Nasa, R. Vaidhyanathan, *Chem. Commun.* **2016**, *52*, 1851–1854; g) M. E. Casco, Y. Q. Cheng, L. L. Daemen, D. Fairen-Jimenez, E. V. Ramos-Fernandez, A. J. Ramirez-Cuesta, J. Silvestre-Albero, *Chem. Commun.* **2016**.
- [13] a) G. E. Cmarik, M. Kim, S. M. Cohen, K. S. Walton, *Langmuir* **2012**, *28*, 15606–15613; b) J. H. Cavka, S. Jakobsen, U. Olsbye, N. Guillou, C. Lamberti, S. Bordiga, K. P. Lillerud, *J. Am. Chem. Soc.* **2008**, *130*, 13850–13851.
- [14] H. Jasuja, K. S. Walton, *J. Phys. Chem. C* **2013**, *117*, 7062–7068.
- [15] a) K. Hindelang, A. Kronast, S. I. Vagin, B. Rieger, *Chem. Eur. J.* **2013**, *19*, 8244–8252; b) K. Hindelang, S. I. Vagin, C. Anger, B. Rieger, *Chem. Commun.* **2012**, *48*, 2888.
- [16] a) S. Vagin, A. Ott, H.-C. Weiss, A. Karbach, D. Volkmer, B. Rieger, *Eur. J. Inorg. Chem.* **2008**, *2008*, 2601–2609; b) S. I. Vagin, A. K. Ott, S. D. Hoffmann, D. Lanzinger, B. Rieger, *Chem. Eur. J.* **2009**, *15*, 5845–5853.
- [17] A. Schaate, P. Roy, A. Godt, J. Lippke, F. Waltz, M. Wiebcke, P. Behrens, *Chem. Eur. J.* **2011**, *17*, 6643–6651.
- [18] S. J. Garibay, S. M. Cohen, *Chem. Commun.* **2010**, *46*, 7700–7702.
- [19] a) R. K. Deshpande, J. L. Minnaar, S. G. Telfer, *Angew. Chem. Int. Ed.* **2010**, *49*, 4598–4602; *Angew. Chem.* **2010**, *122*, 4702–4706; b) D. J. Lun, G. I. N. Waterhouse, S. G. Telfer, *J. Am. Chem. Soc.* **2011**, *133*, 5806–5809.
- [20] A. M. Fracaroli, H. Furukawa, M. Suzuki, M. Dodd, S. Okajima, F. Gándara, J. A. Reimer, O. M. Yaghi, *J. Am. Chem. Soc.* **2014**, *136*, 8863–8866.
- [21] a) S. Biswas, P. Van Der Voort, *Eur. J. Inorg. Chem.* **2013**, *2013*, 2154–2160; b) S. Biswas, J. Zhang, Z. Li, Y. Y. Liu, M. Grzywa, L. Sun, D. Volkmer, P. Van Der Voort, *Dalton Trans.* **2013**, *42*, 4730–4737; c) N. C. Burtch, H. Jasuja, K. S. Walton, *Chem. Rev.* **2014**, *114*, 10575–10612; d) M. W. Hahn, J. Jelic, E. Berger, K. Reuter, A. Jentys, J. A. Lercher, *J. Phys. Chem. B* **2015**; e) Z. Qiao, N. Wang, J. Jiang, J. Zhou, *Chem. Commun.* **2016**, *52*, 974–977.

Received: May 16, 2016

Published online on August 2, 2016

6.1.2 Functionalization of Metal–Organic Frameworks through the Postsynthetic Transformation of Olefin Side Groups

Bibliographic Data

Status	Published online: May 2 nd , 2013
Journal	<i>Chemistry – A European Journal</i> Volume 19, issue 25, pages 8244–8252
Publisher	Wiley-VCH
Article type	Full Paper
DOI	10.1002/chem.201300477
Authors	Konrad Hindelang, <u>Alexander Kronast</u> , Sergei I. Vagin, and Bernhard Rieger

Abstract: For the first time, the adaptability of the C=C double bond as a versatile precursor for the postsynthetic modification (PSM) of microporous materials was extensively investigated and evaluated. Therefore, an olefin-tagged 4,4'-bipyridine linker was synthesized and successfully introduced as pillar linker within a 9,10-triptycenedicarboxylate (TDC) zinc paddle-wheel metal–organic framework (MOF) through microwave-assisted synthesis. Different reactions, predominately used in organic chemistry, were tested, leading to the development of new postsynthetic reactions for the functionalization of solid materials. The postsynthetic oxidation of the olefin side groups applying osmium tetroxide (OsO₄) as a catalyst led to the formation of a microporous material with free vicinal diol functionalities. The epoxidation with dimethyldioxirane (DMDO) enabled the synthesis of epoxy-functionalized MOFs. In addition to that, reaction procedures for a postsynthetic hydroboration with borane dimethyl sulfide as well as a photoinduced thiol–ene click reaction with ethyl mercaptan were developed. For all of these PSMs, yields of more than 90 % were obtained, entirely maintaining the crystallinity of the MOFs. Since the direct introduction of the corresponding groups by means of pre-

synthetic approaches is hardly possible, these new PSMs are useful tools for the functionalization of porous solids towards applications such as selective adsorption, separation, and catalysis.

6.1.3 Mechanistic Investigations of the Stereoselective Rare Earth Metal-Mediated Ring-Opening Polymerization of β -Butyrolactone

Bibliographic Data

Status	Published online: August 11 th , 2015
Journal	<i>Chemistry – A European Journal</i> Volume 21, issue 39, pages 13609–13617
Publisher	Wiley-VCH
Article type	Full Paper
DOI	10.1002/chem.201501156
Authors	Peter T. Altenbuchner, <u>Alexander Kronast</u> , Stefan Kissling, Sergei I. Vagin, Eberhardt Herdtwack, Alexander Pöthig, Peter Deglmann, Robert Loos, and Bernhard Rieger

Abstract: Poly(3-hydroxybutyrate) (PHB) is produced by numerous bacteria as carbon and energy reserve storage material. Whereas nature only produces PHB in its strictly *isotactic* (*R*) form, homogeneous catalysis, when starting from *racemic* (*rac*) β -butyrolactone (BL) as monomer, can in fact produce a wide variety of tacticities. The variation of the metal center and the surrounding ligand structure enable activity as well as tacticity tuning. However, no homogeneous catalyst exists to date that is easy to modify, highly active, and able to produce PHB with high *isotacticities* from *rac*- β -BL. Therefore, in this work, the reaction kinetics of various 2-methoxyethylamino-bis(phenolate) lanthanide (Ln = Sm, Tb, Y, Lu) catalysts are examined in detail. The order in monomer and catalyst are determined to elucidate the reaction mechanism and the results are correlated with DFT calculations of the catalytic cycle. Furthermore, the enthalpies and entropies of the rate-determining steps are determined through temperature-dependent in situ IR measurements. Experimental and computational results converge in one specific

mechanism for the Ring-opening polymerization of BL and even allow us to rationalize the preference for *syndiotactic* PHB.

6.1.4 In Situ Generated ABA Block Copolymers from CO₂, Cyclohexene Oxide, and Poly(dimethylsiloxane)s

Bibliographic Data

Status	Published online: March 7 th , 2016
Journal	<i>ACS Macro Letters</i> Volume 5, issue 3, pages 419–423
Publisher	American Chemical Society
Article type	Communication
DOI	10.1021/acsmacrolett.6b00133
Authors	Marina Reiter, <u>Alexander Kronast</u> , Stefan Kissling, and Bernhard Rieger

Abstract: Chain-transfer polymerization reactions with siloxanes, CO₂, and cyclohexene oxide have been conducted, utilizing two β -diiminate (BDI) zinc-based catalysts, BDI^{CF₃}(**1**)-ZnEt and BDI^{CF₃}(**2**)-ZnEt ((BDI^{CF₃}(**1**))H = [CH(CCF₃NC₆H₄-2,6-C₂H₅)₂] and (BDI^{CF₃}(**2**))H = [CH(CCF₃NC₆H₄-2,6-CH(CH₃)₂)₂]). The correlation between equivalents of siloxane and the corresponding molecular masses and glass transition temperatures is exhibited. Furthermore, the in situ preparation of ABA block copolymers from carbon dioxide, cyclohexene oxide, and α,ω -bis(hydroxymethyl)poly-(dimethylsiloxane)s is presented. This reaction was found to strongly relate to a robust Lewis acid catalyst like the outlined complexes. The polymer properties can be tuned by varying the amount of chain-transfer agent or changing the catalyst. The resulting polymer structures and incorporation of siloxanes were revealed by ²⁹Si NMR spectroscopy, ¹H NMR spectroscopy, ESI-MS, GPC, and DSC.

6.1.5 Template mediated and solvent-free route to a variety of UiO-66 metal-organic frameworks

Bibliographic Data

Status	Published online: October 25 th , 2016
Journal	<i>RSC Advances</i> . Volume XX, issue XX, pages XX
Publisher	Royal Society of Chemistry
Article type	Communication
DOI	10.1039/C6RA23947A
Authors	Chao Zou, Sergei I. Vagin, <u>Alexander Kronast</u> , and Bernhard Rieger

Abstract: A facile and efficient solvent-free, template oriented route has been applied for the synthesis of UiO-66 and UiO-66 analogue metal–organic frameworks (MOFs). The crystal growth was observed via time dependent powder X-ray diffraction (PXRD) and the obtained product was fully characterized by PXRD and ATR-IR. Different substances were screened as possible templates and the water content was found to be of vital importance for morphology control.

6.1.6 Stereospecific catalytic precision polymerization of 2-vinylpyridine via rare earth metal-mediated group transfer polymerization with 2-methoxyethylamino-bis(phenolate)-yttrium complexes

Bibliographic Data

Status	Published online: August 13 th , 2015
Journal	<i>Polymer Chemistry</i> Volume 6, issue 38, pages 6796-6801
Publisher	Royal Society of Chemistry
Article type	Communication
DOI	10.1039/C5PY01146A
Authors	Peter T. Altenbuchner, Friederike Adams, <u>Alexander Kronast</u> , Eberhardt Herdtweck, Alexander Pöthig, and Bernhard Rieger

Abstract: 2-Methoxyethylamino-bis(phenolate)-yttrium complexes were employed in the catalytic precision polymerization of 2-vinylpyridine (2VP). The C₁-symmetric catalyst systems are able to isospecifically polymerize prochiral 2-vinylpyridine with moderate to high activities. Tacticities ranging from atactic to *isotactic* can be achieved ($P_m = 0.54$ – 0.74). Mechanistic studies through ¹³C NMR microstructure analysis of the resulting *isotactic* P2VP show an *enantiomorphic site control* mechanism.

6.1.7 New Insights into the Ring-opening Polymerization of β -Butyrolactone Catalyzed by Chromium(III) Salphen Complexes

Bibliographic Data

Status	Published online: September 23 rd , 2015
Journal	<i>ChemCatChem</i> Volume 7, issue 23, pages 3963-3971
Publisher	Wiley-VCH
Article type	Full Paper
DOI	10.1002/cctc.201500717
Authors	Sergei I. Vagin, Malte Winnacker, <u>Alexander Kronast</u> , Peter T. Altenbuchner, Peter Deglmann, Carsten Sinkel, Robert Loos, and Bernhard Rieger

Abstract: The heterogeneous nature of β -butyrolactone (BL) polymerization towards tactic poly(3-hydroxybutyrate) (PHB) in the presence of chromium(III) salphen (salphen=*N,N'*-disalicylidene-*o*-phenylenediamine) complexes is supported by a number of experimental observations. Depending on the substitution pattern, initially soluble chromium(III) salphen chloride complexes can generate microcrystalline agglomerates under the polymerization conditions, driven by formation of μ -OH bridges between metal centers. Coordinated water molecules are suggested to be the source of such bridging ligands. The formation of these/this heterogeneous species is a prerequisite for the stereocontrolled Ring-opening polymerization (ROP) of BL, whereas both *iso*- and *syndioselective* enchainment occurs simultaneously. According to the analysis of the ^{13}C NMR spectra of the polymers, the ratio of the corresponding triads depends on a number of parameters in a not yet understood manner. Besides dual stereoselectivity, the heterogeneous chromium(III) salphen species feature catalytic sites with different activities, which is reflected in the very broad molecular mass distribution of the produced PHB. Highly active catalytic sites cause the formation of

polymer chains with a high molecular mass at the beginning of polymerization. The described behavior is not inherent to truly homogeneous chromium salphen complexes and is more in line with a bimetallic ROP mechanism proposed earlier, which requires a particular mutual spatial orientation of two salphen complexes for the efficient catalysis of BL polymerization.

6.1.8 Dinuclear zinc catalysts with unprecedented activities for the copolymerization of cyclohexene oxide and CO₂

Bibliographic Data

Status	Published online: February 10 th , 2015
Journal	<i>Chemical Communications</i> Volume 51, issue 22, pages 4579-4582
Publisher	Royal Society of Chemistry
Article type	Communication
DOI	10.1039/C5CC00784D
Authors	Stefan Kissling, Maximilian W. Lehenmeier, Peter T. Altenbuchner, <u>Alexander Kronast</u> , Marina Reiter, Peter Deglmann, Uwe B. Seemann, and Bernhard Rieger

Abstract: A variety of new dinuclear zinc catalysts was developed and tested for the copolymerization of cyclohexene oxide and carbon dioxide. Electron-withdrawing groups thereby led to unprecedented activities with turnover frequencies up to 155 000 h⁻¹. These are by far the highest polymerization rates ever reported for the copolymerization of cyclohexene oxide and CO₂.

6.1.9 Versatile 2-Methoxyethylaminobis(phenolate)yttrium Catalysts: Catalytic Precision Polymerization of Polar Monomers via Rare Earth Metal-Mediated Group Transfer Polymerization

Bibliographic Data

Status	Published online: November 10 th , 2014
Journal	<i>Macromolecules</i>
	Volume 47, issue 22, pages 7742–7749
Publisher	American Chemical Society
Article type	Full Paper
DOI	10.1021/ma501754u
Authors	Peter T. Altenbuchner, Benedikt S. Soller, Stefan Kissling, Thomas Bachmann, <u>Alexander Kronast</u> , Sergei I. Vagin, and Bernhard Rieger

Abstract: The present study is one of the first examples for rare earth metal-mediated group transfer polymerization (REM-GTP) with non-metallocene catalyst systems. 2-Methoxyethylaminobis(phenolate)yttrium trimethylsilylmethyl complexes were synthesized and showed moderate to high activities in the rare earth metal-mediated group transfer polymerizations of 2-vinylpyridine, 2-isopropenyl-2-oxazoline, diethyl vinylphosphonate, diisopropyl vinylphosphonate, and *N,N*-dimethyl acrylamide as well as in the Ring-opening polymerization of β -butyrolactone. Reaction orders in catalyst and monomer were determined for the REM-GTP of 2-vinylpyridine. The mechanistic studies revealed that the catalyst systems follow a living monometallic group transfer polymerization mechanism allowing a precise molecular-weight control of the homopolymers and the block copolymers with very narrow molecular weight distributions. Temperature-dependent reaction kinetics were conducted and allowed conclusions about

the influence of the bulky substituents around the metal center on the polymerization activity. Additional polymerization experiments concerning the combination of REM-GTP and ROP to obtain block copolymers were performed.

6.1.10 Next Generation Multiresponsive Nanocarriers for Targeted Drug Delivery to Cancer Cells

Bibliographic Data

Status	Published online: August 19 th , 2016
Journal	<i>Chemistry – A European Journal</i> Volume 22, issue 41, pages 14576-14584
Publisher	Wiley-VCH
Article type	Full Paper
DOI	10.1002/chem.201601822
Authors	Peter T. Altenbuchner, Patrick D.L. Werz, Patricia Schöppner, Friederike Adams, <u>Alexander Kronast</u> , Christina Schwarzenböck, Alexander Pöthig, Christian Jandl, Martin Haslbeck, and Bernhard Rieger

Abstract: C–H bond activation of 2-methoxyethylamino-bis(phenolate)-yttrium catalysts allowed the synthesis of BAB block copolymers comprised of 2-vinylpyridine (2VP; monomer A) and diethylvinylphosphonate (DEVP; monomer B) as the A and B blocks, respectively, by rare-earth-metal-mediated group-transfer polymerization (REM-GTP). The inherent multi-stimuli-responsive character and drug-loading and -release capabilities were observed to be dependent on the chain length and monomer ratios. Cytotoxicity assays revealed the biocompatibility and nontoxic nature of the obtained micelles toward ovarian cancer (HeLa) cells. The BAB block copolymers effectively encapsulated, transported, and released doxorubicin (DOX) within HeLa cells. REM-GTP enables access to previously unattainable vinylphosphonate copolymer structures, and thereby unlocks their full potential as nanocarriers for stimuli-responsive drug delivery in

HeLa cells. The self-evident consequence is the application of these new micelles as potent drug-delivery vehicles with reduced side effects in future cancer therapies.

6.2 Extended Synthetic Procedures and Analytical Data – Supplementary Informations

6.2.1 Electron-Deficient β -Diiminato-Zinc-Ethyl Complexes: Synthesis, Structure, and Reactivity in Ring-Opening Polymerization of Lactones

Electron-Deficient β -Diiminato-Zinc-Ethyl Complexes: Synthesis, Structure and Reactivity in Ring-Opening Polymerization of Lactones

Alexander Kronast^{†,‡}, Marina Reiter^{†,‡}, Peter T. Altenbuchner[†], Christian Jandl[‡], Alexander Pöthig[‡], and Bernhard Rieger^{†*}.

[†]WACKER-Lehrstuhl für Makromolekulare Chemie, Technische Universität München, Lichtenbergstraße 4, 85747 Garching bei München, Germany

[‡]Zentralinstitut für Katalyseforschung, Technische Universität München, Ernst-Otto-Fischer Straße 1, 85747 Garching bei München, Germany

Supporting Information

1. Experimental procedures.....	2
Methods and materials.....	2
2. In situ ATR-IR-Autoclave Data.....	3
3. Kinetic Investigations.....	4
4. GPC Results	5
5. Microstructure determination via NMR Spectroscopy.....	9
6. Single Crystal XRD (SC-XRD) data.....	10

1. EXPERIMENTAL PROCEDURES

METHODS AND MATERIALS

Unless otherwise stated, all manipulations were performed under an argon atmosphere using standard Schlenk techniques or an MBraun glovebox. Chemicals were purchased from Sigma-Aldrich or ABCR GmbH&Co KG and used without further treatment if not otherwise stated. All glassware was heat-dried under vacuum prior to use. Toluene, dichloromethane, diethylether, pentane and tetrahydrofuran were dried applying an MBraun SPS-800 and used as received. Monomers were dried over calcium hydride and distilled prior to polymerization. NMR spectra were recorded on a Bruker AVIII-300 and AVIII-500 Cryo spectrometer. ^1H NMR spectroscopic chemical shifts δ are reported in ppm relative to tetramethylsilane and calibrated to the residual proton signal of the deuterated solvent. Deuterated solvents were obtained from Sigma Aldrich and dried over 3 Å molecular sieves. ESI-MS analytical measurements were performed in acetonitrile solutions on a Varian 500 MS spectrometer. *In-situ* IR measurements were carried out under an argon atmosphere using an ATR-IR Mettler Toledo system. IR spectra were performed on a Bruker Vertex 70 spectrometer with a Bruker Platinum ATR setup and the integrated MCT detector. Gel permeation chromatography (GPC) analysis was performed on a Varian PL-GPC 50. As eluent, chloroform (HPLC grade) with 1.5 g L^{-1} tetrabutylammonium tetrafluoroborate was used. Polystyrene standards were used for calibration.

2. IN SITU ATR-IR-AUTOCCLAVE DATA

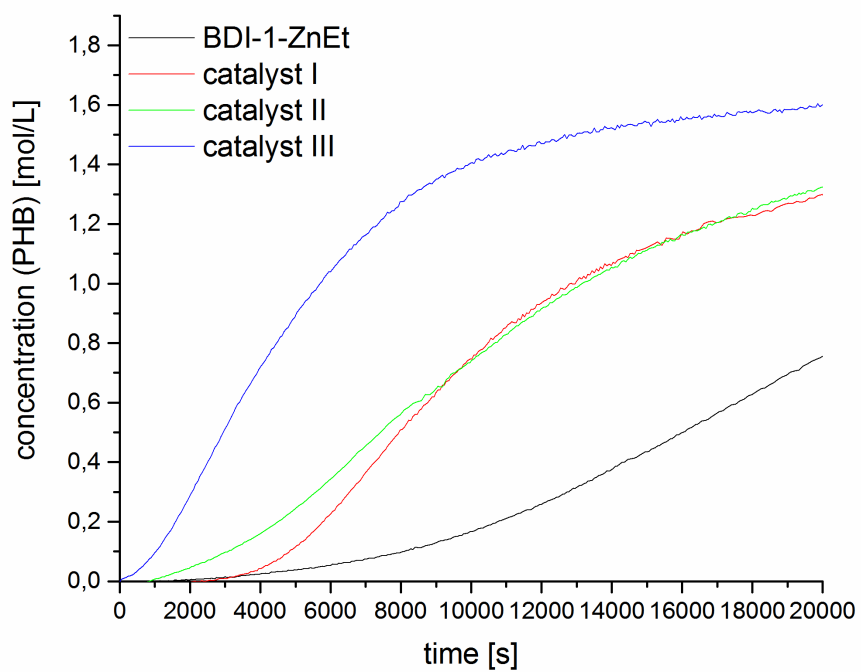


Figure S1. *In situ* IR data for the ROP of *rac*-BL with literature known catalyst BDI-1-ZnEt and complexes I-III during the first 5.5 h.

3. KINETIC INVESTIGATIONS

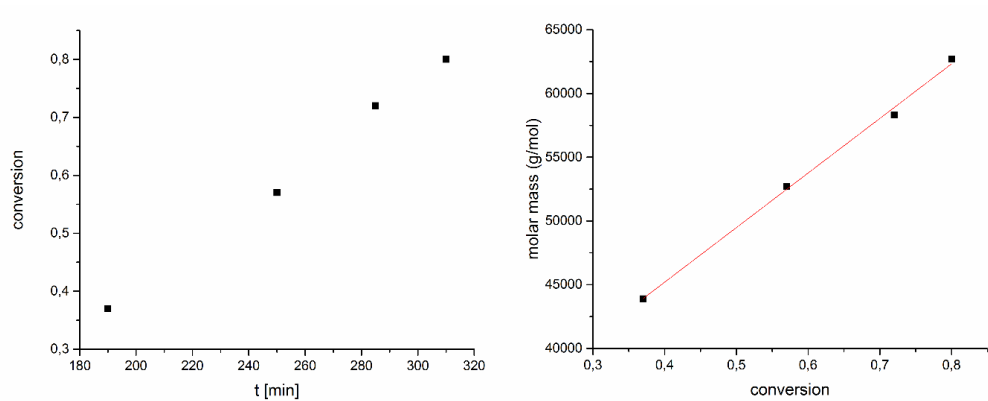
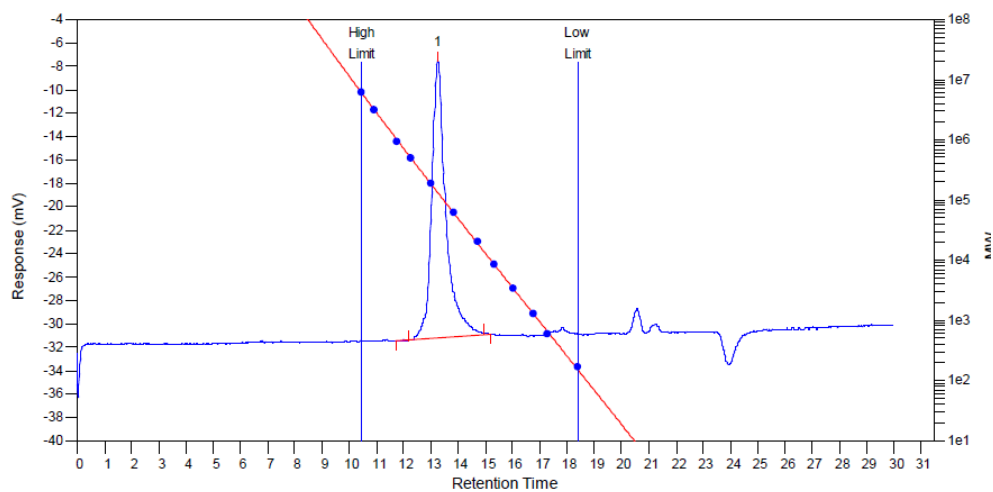


Figure S2. Catalytic activity of III for the ROP of *rac*-BL (left) and linear growth of M_n as a function of monomer conversion (determined by ^1H NMR) (right).

4. GPC RESULTS

a) Polyhydroxybutyrate:

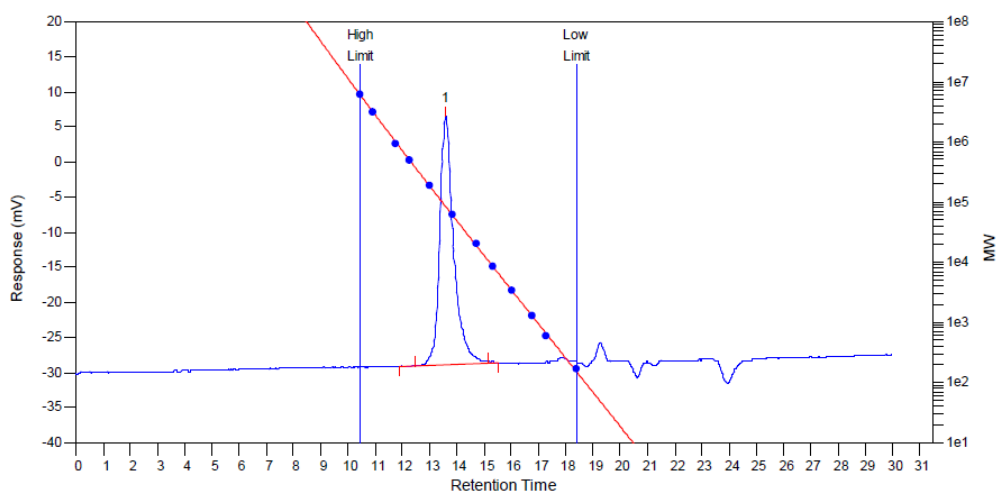
BDI-1-ZnEt



MW Averages

Peak No	Mp	Mn	Mw	Mz	Mz+1	Mv	PD
1	130967	99335	124644	145798	167933	121430	1.25478

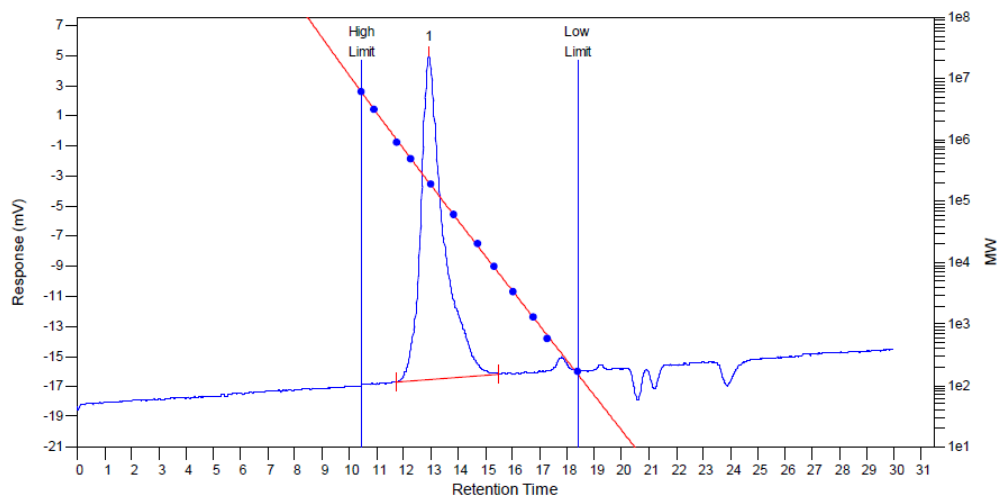
Catalyst I



MW Averages

Peak No	Mp	Mn	Mw	Mz	Mz+1	Mv	PD
1	83861	66613	79436	90772	102784	77732	1.1925

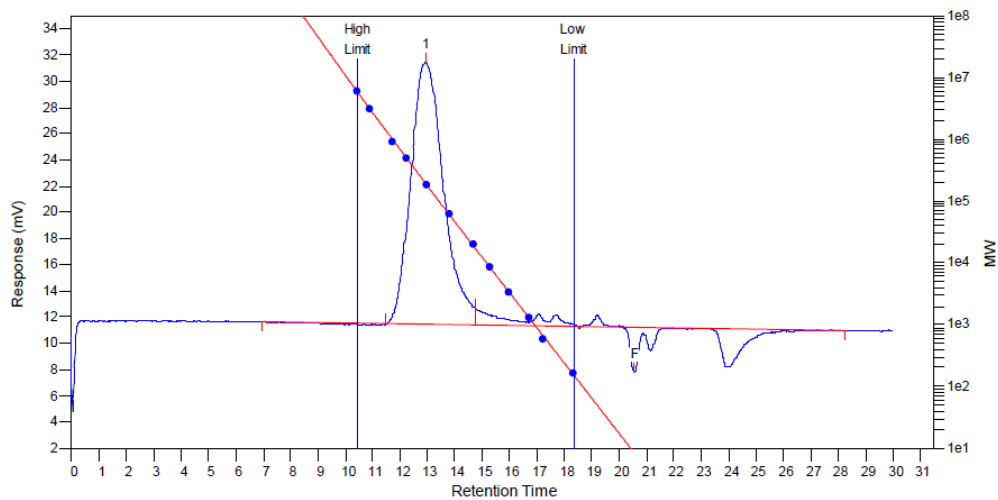
Catalyst II



MW Averages

Peak No	Mp	Mn	Mw	Mz	Mz+1	Mv	PD
1	204878	107302	178810	245353	313646	169127	1.66642

Catalyst III

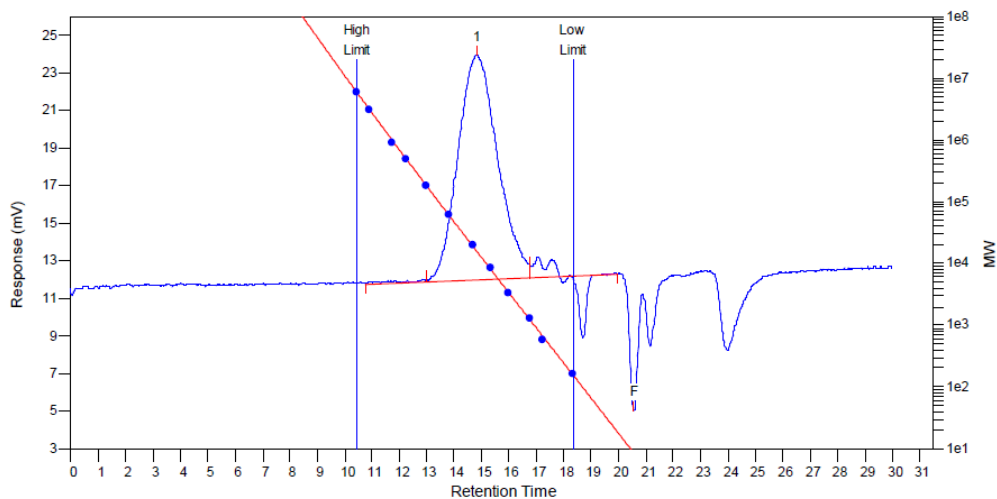


MW Averages

Peak No	Mp	Mn	Mw	Mz	Mz+1	Mv	PD
1	196402	120787	214077	331085	456979	198757	1.77235
2	0	0	0	0	0	0	0

b) Polylactide

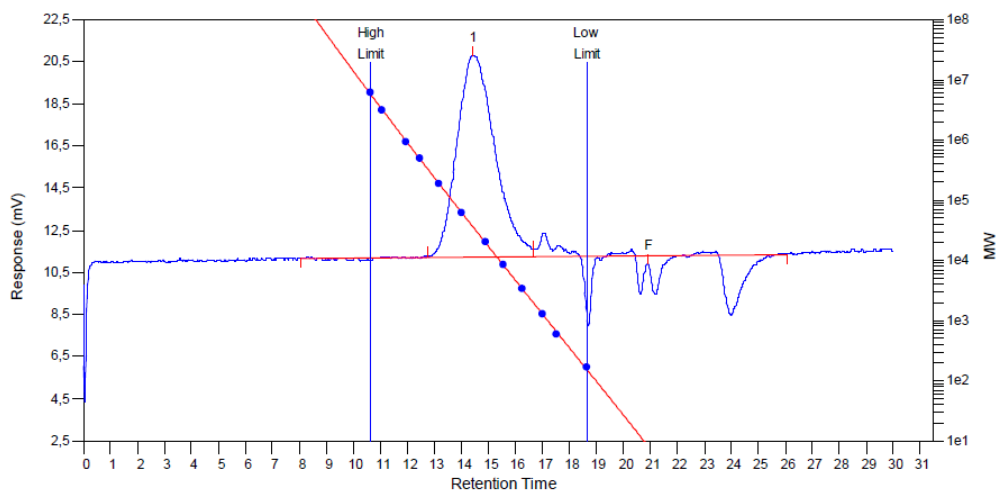
BDI-1-ZnEt



MW Averages

Peak No	Mp	Mn	Mw	Mz	Mz+1	Mv	PD
1	15812	9344	20041	36990	58197	18074	2.1448
2	0	0	0	0	0	0	0

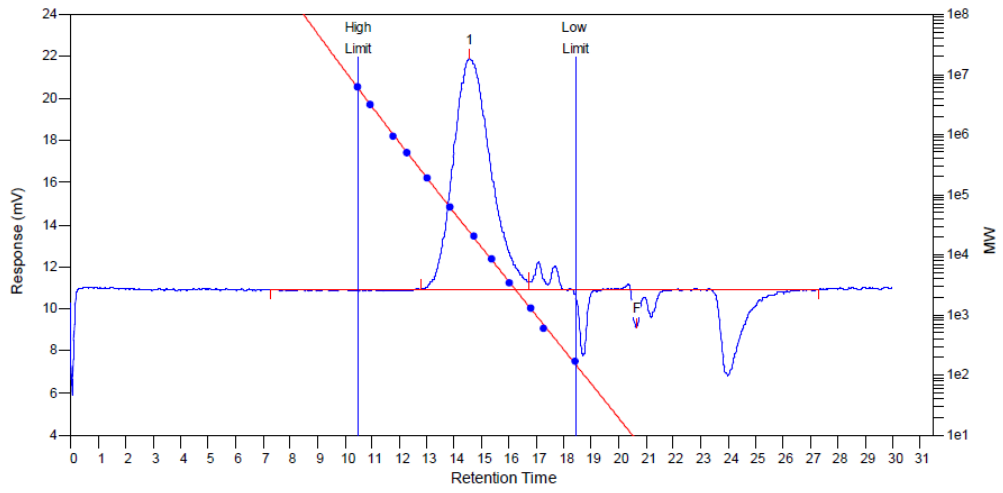
Catalyst II



MW Averages

Peak No	Mp	Mn	Mw	Mz	Mz+1	Mv	PD
1	34884	18764	39500	67902	100507	35980	2.10509
2	0	0	0	0	0	0	0

Catalyst III



MW Averages

Peak No	Mp	Mn	Mw	Mz	Mz+1	Mv	PD
1	23949	13050	27249	48025	74372	24775	2.08805
2	0	0	0	0	0	0	0

5. MICROSTRUCTURE DETERMINATION VIA NMR SPECTROSCOPY

Polyhydroxybutyrate

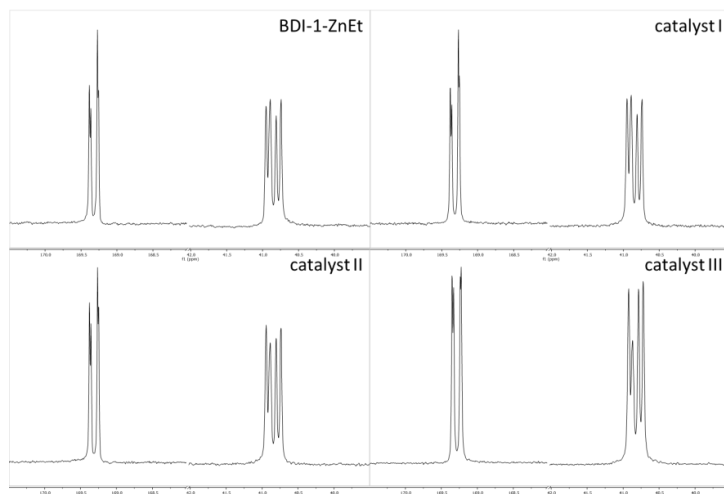


Figure S3. ^{13}C spectra applied in the microstructure analysis for polyhydroxybutyrates obtained with BDI-1-ZnEt and catalysts I-III (methylene (40.8 ppm) and carbonyl regions (169.3 ppm)).

Poly lactide

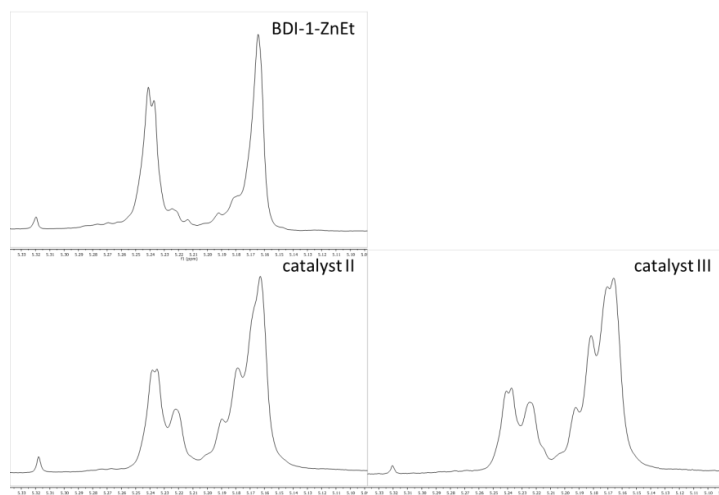


Figure S4. Homodecoupled ^1H -NMR spectra applied in the microstructure analysis for poly lactides obtained with BDI-1-ZnEt and catalysts II-III (methine region).

6. Single Crystal XRD (SC-XRD) data

General:

Data were collected on an X-ray single crystal diffractometer equipped with a CCD detector (APEX II, CCD), a rotating anode FR591 and a Montel mirror optic (Compound I) or a fine-focus sealed tube and a Triumph optic (Compound II, III) by using the SMART software package.⁽¹⁾ The measurements were performed on single crystals coated with perfluorinated ether. The crystals were fixed on the top of a glass fiber and transferred to the diffractometer. Crystals were cooled under a stream of cold nitrogen. A matrix scan was used to determine the initial lattice parameters. Reflections were merged and corrected for Lorentz and polarization effects, scan speed, and background using SAINT.⁽²⁾ Absorption corrections, including odd and even ordered spherical harmonics were performed using SADABS.⁽²⁾ Space group assignments were based upon systematic absences, *E* statistics, and successful refinement of the structures. Structures were solved by direct methods with the aid of successive difference Fourier maps,⁽³⁾ and were refined against all data using the APEX 2 software⁽¹⁾ in conjunction with SHELXL-97 or SHELXL-2014⁽⁴⁾ and SHELXLE⁽⁵⁾. Methyl hydrogen atoms were refined as part of rigid rotating groups, with a C–H distance of 0.98 Å and $U_{\text{iso(H)}} = 1.5 \cdot U_{\text{eq(C)}}$. Other H atoms were placed in calculated positions and refined using a riding model, with methylene and aromatic C–H distances of 0.99 and 0.95 Å, respectively, and $U_{\text{iso(H)}} = 1.2 \cdot U_{\text{eq(C)}}$. Non-hydrogen atoms were refined with anisotropic displacement parameters. Full-matrix least-squares refinements were carried out by minimizing $\sum w(F_o^2 - F_c^2)^2$ with SHELXL-97⁽⁴⁾ weighting scheme. Neutral atom scattering factors for all atoms and anomalous dispersion corrections for the non-hydrogen atoms were taken from *International Tables for Crystallography*.⁽⁶⁾ Images of the molecular structure in the single crystal were generated with PLATON.⁽⁷⁾ For compound I a superstructure with a tripled b axis was identified but the data quality did not allow a proper refinement so the smaller higher symmetric cell was used.

References:

- (1) APEX suite of crystallographic software. APEX 2 Version 2013.4. Bruker AXS Inc., Madison, Wisconsin, USA (2013).
- (2) SAINT, Version 8.27b and SADABS Version 2012/1. Bruker AXS Inc., Madison, Wisconsin, USA (2012).
- (3) Sheldrick, G. M. "SHELXS-97", Program for Crystal Structure Solution, Göttingen, (1997).
- (4) Sheldrick, G. M. "SHELXL-97", University of Göttingen, Göttingen, Germany, (1998). or Sheldrick, G. M. "SHELXL-2014", University of Göttingen, Göttingen, Germany, (2014).
- (5) Huebschle, C. B., Sheldrick, G. M. & Dittrich, B. "SHELXLE", *J. Appl. Cryst.* **2011**, *44*, 1281-1284.
- (6) International Tables for Crystallography, Vol. C, Tables 6.1.1.4 (pp. 500-502), 4.2.6.8 (pp. 219-222), and 4.2.4.2 (pp. 193-199), Wilson, A. J. C., Ed., Kluwer Academic Publishers, Dordrecht, The Netherlands, 1992.
- (7) Spek, A. L. "PLATON", A Multipurpose Crystallographic Tool, Utrecht University, Utrecht, The Netherlands, (2011).

Compound I (CCDC 1439897)

Diffractometer operator C. Jandl
 scanspeed 5 s per frame
 dx 70 mm
 5762 frames measured in 15 data sets
 phi-scans with delta_phi = 0.5
 omega-scans with delta_omega = 0.5

Crystal data

$C_{31}H_{40}F_6N_2Zn$	
$M_r = 620.04$	$D_x = 1.325 \text{ Mg m}^{-3}$
Monoclinic, $C2/c$	Melting point: ? K
Hall symbol: -C 2yc	Mo $K\alpha$ radiation, $\lambda = 0.71073 \text{ \AA}$
$a = 35.2290 (11) \text{ \AA}$	Cell parameters from 9001 reflections
$b = 11.4852 (3) \text{ \AA}$	$\theta = 2.4\text{--}28.1^\circ$
$c = 16.5381 (5) \text{ \AA}$	$\mu = 0.85 \text{ mm}^{-1}$
$\beta = 111.691 (1)^\circ$	$T = 123 \text{ K}$
$V = 6217.7 (3) \text{ \AA}^3$	Fragment, yellow
$Z = 8$	$0.53 \times 0.32 \times 0.24 \text{ mm}$
$F(000) = 2592$	

Data collection

Bruker APEX-II CCD diffractometer	5686 independent reflections
Radiation source: rotating anode FR591	5156 reflections with $i > 2\sigma(i)$
MONTEL optic monochromator	$R_{\text{int}} = 0.041$
Detector resolution: $16 \text{ pixels mm}^{-1}$	$\theta_{\text{max}} = 25.4^\circ$, $\theta_{\text{min}} = 1.9^\circ$
phi- and ω -rotation scans	$h = -42 \text{--} 42$
Absorption correction: multi-scan SADABS, Bruker, 2008b	$k = -13 \text{--} 13$
$T_{\text{min}} = 0.602$, $T_{\text{max}} = 0.746$	$l = -19 \text{--} 19$

77572 measured reflections

Refinement

Refinement on F^2	Secondary atom site location: <u>difference Fourier map</u>
Least-squares matrix: full	Hydrogen site location: inferred from neighbouring sites
$R[F^2 > 2\sigma(F^2)] = 0.039$	H-atom parameters constrained
$wR(F^2) = 0.097$	$W = 1/[\Sigma^2(FO^2) + (0.0399P)^2 + 14.6952P]$ WHERE $P = (FO^2 + 2FC^2)/3$
$S = 1.03$	$(\Delta/\sigma)_{\max} = 0.001$
5686 reflections	$\Delta\rho_{\max} = 0.81 \text{ e } \text{\AA}^{-3}$
446 parameters	$\Delta\rho_{\min} = -0.63 \text{ e } \text{\AA}^{-3}$
41 restraints	Extinction correction: none
- constraints	Extinction coefficient: -
Primary atom site location: <u>structure-invariant direct methods</u>	

Compound II (CCDC 1439898)

Diffractometer operator C. Jandl
 scanspeed 1 s per frame
 dx 40 mm
 3804 frames measured in 10 data sets
 phi-scans with delta_phi = 0.5
 omega-scans with delta_omega = 0.5

Crystal data

$C_{27}H_{32}F_6N_2Zn$	
$M_r = 563.94$	$D_x = 1.395 \text{ Mg m}^{-3}$
Monoclinic, $P2_1/n$	Melting point: ? K
Hall symbol: -P 2yn	Mo $K\alpha$ radiation, $\lambda = 0.71073 \text{ \AA}$
$a = 12.4913 (7) \text{ \AA}$	Cell parameters from 9804 reflections
$b = 10.7240 (6) \text{ \AA}$	$\theta = 2.5\text{--}26.3^\circ$
$c = 20.1647 (11) \text{ \AA}$	$\mu = 0.97 \text{ mm}^{-1}$
$\beta = 96.137 (3)^\circ$	$T = 150 \text{ K}$
$V = 2685.7 (3) \text{ \AA}^3$	Fragment, yellow
$Z = 4$	$0.53 \times 0.44 \times 0.34 \text{ mm}$
$F(000) = 1168$	

Data collection

Bruker APEX-II CCD diffractometer	5299 independent reflections
Radiation source: fine-focus sealed tube	4766 reflections with $i > 2\sigma(i)$
Triumph optic monochromator	$R_{\text{int}} = 0.023$
Detector resolution: 16 pixels mm^{-1}	$\theta_{\text{max}} = 26.0^\circ$, $\theta_{\text{min}} = 1.8^\circ$
phi- and ω -rotation scans	$h = -15 \text{--} 15$
Absorption correction: multi-scan SADABS, Bruker, 2008b	$k = -13 \text{--} 13$
$T_{\text{min}} = 0.685$, $T_{\text{max}} = 0.745$	$l = -24 \text{--} 24$

78871 measured reflections

Refinement

Refinement on F^2	Secondary atom site location: <u>difference Fourier map</u>
Least-squares matrix: full	Hydrogen site location: inferred from neighbouring sites
$R[F^2 > 2\sigma(F^2)] = 0.028$	H-atom parameters constrained
$wR(F^2) = 0.077$	$W = 1/[\Sigma^2(FO^2) + (0.0398P)^2 + 1.6972P]$ WHERE $P = (FO^2 + 2FC^2)/3$
$S = 1.06$	$(\Delta/\sigma)_{\max} = 0.001$
5299 reflections	$\Delta\rho_{\max} = 0.61 \text{ e } \text{\AA}^{-3}$
330 parameters	$\Delta\rho_{\min} = -0.36 \text{ e } \text{\AA}^{-3}$
0 restraints	Extinction correction: none
- constraints	Extinction coefficient: -
Primary atom site location: <u>structure-invariant direct methods</u>	

Compound III (CCDC 1439899)

Diffractometer operator C. Jandl
 scanspeed 30 s (scan 1-4) and 5 s (scan 5) per frame
 dx 40 mm
 2747 frames measured in 5 data sets
 phi-scans with delta_phi = 0.5
 omega-scans with delta_omega = 0.5

Crystal data

$C_{23}H_{23}F_6N_2Zn$	
$M_r = 506.82$	$D_x = 1.435 \text{ Mg m}^{-3}$
Monoclinic, $P2_1/n$	Melting point: ? K
Hall symbol: -P 2yn	Mo $K\alpha$ radiation, $\lambda = 0.71073 \text{ \AA}$
$a = 12.3089 (3) \text{ \AA}$	Cell parameters from 9961 reflections
$b = 9.6492 (3) \text{ \AA}$	$\theta = 2.4\text{--}26.4^\circ$
$c = 19.8991 (5) \text{ \AA}$	$\mu = 1.11 \text{ mm}^{-1}$
$\beta = 96.953 (1)^\circ$	$T = 200 \text{ K}$
$V = 2346.06 (11) \text{ \AA}^3$	Fragment, yellow
$Z = 4$	$0.33 \times 0.33 \times 0.27 \text{ mm}$
$F(000) = 1036$	

Data collection

Bruker APEX-II CCD diffractometer	4814 independent reflections
Radiation source: fine-focus sealed tube	4108 reflections with $i > 2\sigma(i)$
Triumph optic monochromator	$R_{\text{int}} = 0.018$
Detector resolution: 16 pixels mm^{-1}	$\theta_{\text{max}} = 26.4^\circ$, $\theta_{\text{min}} = 2.1^\circ$
phi- and ω -rotation scans	$h = -15 \text{--} 15$
Absorption correction: multi-scan SADABS, Bruker, 2008b	$k = -12 \text{--} 11$
$T_{\text{min}} = 0.677$, $T_{\text{max}} = 0.745$	$l = -24 \text{--} 24$

46707 measured reflections

Refinement

Refinement on F^2	Secondary atom site location: <u>difference Fourier map</u>
Least-squares matrix: full	Hydrogen site location: inferred from neighbouring sites
$R[F^2 > 2\sigma(F^2)] = 0.046$	H-atom parameters constrained
$wR(F^2) = 0.129$	$W = 1/[\Sigma^2(FO^2) + (0.0563P)^2 + 2.3228P]$ WHERE $P = (FO^2 + 2FC^2)/3$
$S = 1.03$	$(\Delta/\sigma)_{\max} = 0.001$
4814 reflections	$\Delta\rho_{\max} = 0.61 \text{ e } \text{\AA}^{-3}$
312 parameters	$\Delta\rho_{\min} = -0.67 \text{ e } \text{\AA}^{-3}$
39 restraints	Extinction correction: none
- constraints	Extinction coefficient: -
Primary atom site location: <u>structure-invariant direct methods</u>	

6.2.2 2-Methoxyethylamino-bis(phenolate) yttrium catalysts for the synthesis of highly isotactic poly(2-vinylpyridine) by rare-earth metal-mediated group transfer polymerization

- Supporting Information -

2-Methoxyethylamino-bis(phenolate)yttrium Catalysts for the Synthesis of Highly Isotactic Poly(2-vinylpyridine) by Rare-Earth Metal-Mediated Group Transfer Polymerization

Alexander Kronast,[‡] Dominik Reiter,[‡] Peter T. Altenbuchner, Sergei I. Vagin, and Bernhard Rieger*

WACKER-Lehrstuhl für Makromolekulare Chemie, Technische Universität München, Lichtenbergstraße 4, 85748 Garching b. München, Germany.

*B. Rieger: E-Mail: rieger@tum.de; <http://www.makro.ch.tum.de>; Fax: +49-89-289-13562; Tel: +49-89-289-13570.

1. Experimental	1
1.1 General	1
1.2 Proligand Precursor Synthesis	2
2. Kinetic Investigations	6
3. Microstructure Analysis	7
3.1 ¹³ C NMR spectra	7
3.2 Theoretical Investigations	10
4. Thermoanalysis	11
4.1 DSC	11
4.2 TGA	12
5. Literature	13

1. Experimental

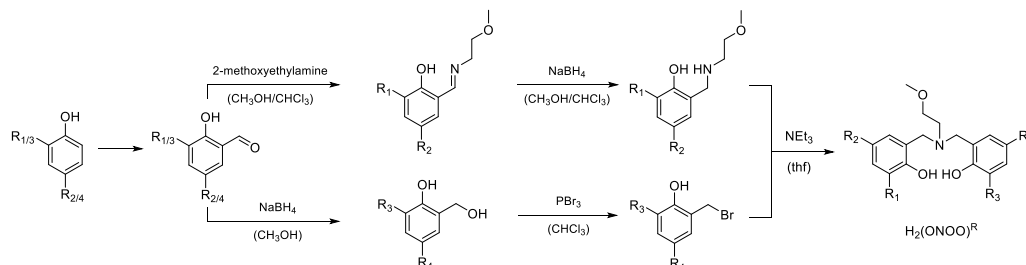
1.1 General

All air and moisture sensitive reactions were carried out under an argon atmosphere using standard Schlenk or glovebox techniques. All glassware was heat dried under vacuum prior to use. Unless otherwise stated, all chemicals were purchased from Acros Organics, Sigma-Aldrich, or ABCR and used as received. Dichloromethane, pentane, THF and toluene were dried using an MBraun SPS-800 solvent purification system. The precursor complex $[Y(CH_2SiMe_3)_3(THF)_2]$ was prepared following literature procedures.^[1] Triethylamine and 2-vinylpyridine were dried over calcium hydride and distilled prior to use. 2-(((2-methoxyethyl)amino)methyl)-4,6-dimethylphenol and 2,4-di-*tert*-butyl-6-(((2-methoxyethyl)amino)methyl)phenol were synthesized according to literature procedures.^[2] NMR Spectra were recorded on Bruker AVIII-300 and AVIII-500C spectrometers. ¹H NMR spectroscopic chemical shifts δ are reported in ppm relative to the residual proton signals of deuterated solvents. Unless otherwise stated ¹³C NMR spectroscopic chemical shifts δ are referenced to the carbon atoms of the solvent. Coupling constants J are given in Hertz (Hz) as averaged values and refer to couplings between protons. The following abbreviations are used to describe signal multiplicities: s (singlet), d (doublet), t (triplet), m (multiplet), dd (doublet of doublets), dt (doublet of triplets), br (broad signal). Deuterated solvents were obtained from Sigma-Aldrich and dried over 3 Å molecular sieves.

Quantitative elemental analyses (EA) were measured at the Laboratory for Microanalysis at the Institute of Inorganic Chemistry at the Technische Universität München. Low resolution mass spectrometry (LRMS) analytical measurements were obtained by electrospray ionization (ESI) with acetonitrile and toluene solutions on a Varian LC/MS 500-MS spectrometer. X-Ray Powder Diffraction was measured on a PANalytical Empyrean system. DSC was carried out on a Texas Instruments DSC Q2000 with a heating rate of 5 K min⁻¹. TGA was carried out on a Texas Instruments TGA Q5000 with a heating rate of 10 K min⁻¹. Gel permeation chromatography (GPC) measurements were carried out on a Varian 920-LC HPLC equipped with two PL Polargel columns.

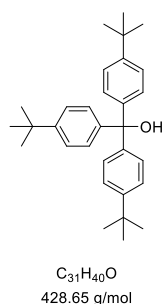
Initiator efficiency ($I^* = M_{n,calc}/M_{n,exp}$) is determined by taking aliquots during and at the end of the polymerization. I^*_t is determined for polymerization kinetics as the average initiator efficiency I^* at the maximum rate of the reaction (maximum slope of the conversion-reaction time plot).

1.2 Proligand Precursor Synthesis



Scheme S1. Proligand synthesis starting from phenols **3** and **10** for Ligands **L1-L4**.

Tris(4-*tert*-butylphenyl)methanol (**1**)

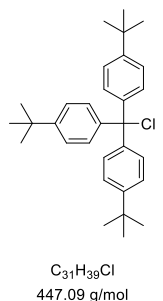


A solution of 1-bromo-4-*tert*-butylbenzene (24.4 mL, 30.0 g, 141 mmol, 3.0 eq) in dry THF (20 mL) was added dropwise to a stirred suspension of magnesium turnings (3.76 g, 155 mmol, 3.3 eq) in dry THF (200 mL). The reaction mixture was heated to initiate the reaction and stirred until the reaction subsided. A solution of diethyl carbonate (5.69 mL, 5.54 g, 46.9 mmol, 1.0 eq) in dry THF (100 mL) was added dropwise to the *Grignard* reagent and stirred for 3 h at room temperature. Ice-cold 2 M HCl (100 mL) was then poured into the reaction mixture and the organic phase was separated and washed with 2 M HCl (50 mL) and brine (50 mL). The organic phase was dried over $MgSO_4$, filtered and the solution concentrated *in vacuo*. Addition of *n*-hexane led to precipitation of **1** as colorless crystals (12.4 g, 29.0 mmol, 62%).

1H NMR (300 MHz, $CDCl_3$, 300 K): δ [ppm] = 1.31 (s, 27H, $C(CH_3)_3$), 7.19 (d, $^3J = 8.5$ Hz, 6H, Ar-H), 7.31 (d, $^3J = 8.5$ Hz, 6H, Ar-H).

^{13}C NMR (75 MHz, $CDCl_3$, 300 K): δ [ppm] = 31.5, 34.6, 81.7, 124.8, 127.7, 144.3, 149.9.

Tris(4-*tert*-butylphenyl)methyl chloride (**2**)

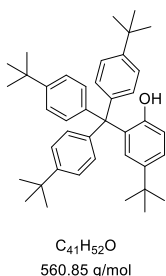


To a vigorously stirred solution of **1** (12.4 g, 29.0 mmol, 1.0 eq) in dry toluene (30 mL) was added freshly distilled acetyl chloride (5.18 mL, 5.69 g, 72.6 mmol, 2.5 eq). The reaction mixture was heated under reflux for 30 min. After the solution was allowed to cool down to ambient temperature, *n*-hexane (40 mL) was added and the flask was left at 4 °C overnight. The resulting precipitate was filtered and dried under vacuum to afford **2** as a beige powder (10.0 g, 22.4 mmol, 77%).

1H NMR (300 MHz, $CDCl_3$, 300 K): δ [ppm] = 1.33 (s, 27H, $C(CH_3)_3$), 7.16 (d, $^3J = 8.6$ Hz, 6H, Ar-H), 7.31 (d, $^3J = 8.6$ Hz, 6H, Ar-H).

^{13}C NMR (75 MHz, $CDCl_3$, 300 K): δ [ppm] = 31.5, 34.7, 81.8, 124.6, 129.5, 142.7, 150.6.

4-*tert*-Butyl-2-(tris(4-*tert*-butylphenyl)methyl)phenol (**3**)



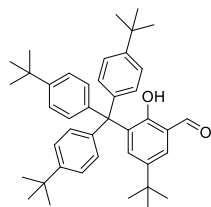
To molten 4-*tert*-butylphenol (33.7 g, 224 mmol, 10.0 eq) was added sodium metal (722 mg, 31.4 mmol, 1.4 eq) at 110 °C with vigorous stirring. **2** (10.0 g, 22.4 mmol, 1.0 eq) was added to the melt of phenolate and the resulting mixture was heated to 145 °C for 3 h. The reaction mixture was treated with 7% aqueous NaOH (67 mL) and Et_2O (77 mL) after cooling down to 80 °C. The organic layer was separated and the aqueous phase extracted with Et_2O (3 × 34 mL). The combined organic phases were washed with 7% aqueous NaOH (3 × 34 mL), distilled water (34 mL) and brine (34 mL). After drying over anhydrous $MgSO_4$ and filtration, the solvent of the amber solution was removed *in vacuo*. Recrystallization of the crude product from ethanol yielded **3** as colorless crystals (9.99 g, 17.8 mmol, 79%).

1H NMR (500 MHz, $CDCl_3$, 300 K): δ [ppm] = 1.12 (s, 9H, $C(CH_3)_3$), 1.32 (s, 27H, $C(CH_3)_3$), 4.41 (s, 1H, Ar-OH), 6.78 (d, $^3J = 8.3$ Hz, 1H, Ar-H), 6.86 (d, $^4J = 2.5$ Hz, 1H, Ar-H), 7.13 (d, $^3J = 8.5$ Hz, 6H, Trit-H), 7.22 (dd, $^4J = 2.4$ Hz, $^3J = 8.3$ Hz, 1H, Ar-H), 7.31 (d, $^3J = 8.5$ Hz, 6H, Trit-H).

^{13}C NMR (126 MHz, $CDCl_3$, 300 K): δ [ppm] = 31.5, 31.5, 34.3, 34.5, 61.8, 117.0, 124.7, 125.3, 128.1, 130.8, 133.0, 141.3, 142.5, 149.5, 152.2.

LRMS (ESI, MeCN): $m/z = 584.2$ [$M+Na$] $^+$.

EA [%]: calculated: C 87.80 H 9.35; found: C 87.94 H 9.43

5-tert-Butyl-2-hydroxy-3-(tris(4-tert-butylphenyl)methyl)-benzaldehyde (4)

$C_{42}H_{52}O_2$
588.86 g/mol

A mixture of **3** (9.96 g, 17.8 mmol, 1.0 eq), hexamethylenetetramine (2.74 g, 19.5 mmol, 1.1 eq) and trifluoroacetic acid (100 mL) was heated at 110 °C under reflux for 40 h. Subsequently the warm reaction mixture was poured into vigorously stirred 2 M HCl (250 mL). The cold mixture was extracted with chloroform (3 × 125 mL) and the combined organic layers were washed with 2 M HCl (3 × 75 mL), distilled water (175 mL) and brine (100 mL). After drying over $MgSO_4$ and filtration, the solvent was removed under reduced pressure. Silica gel column chromatography (*n*-hexane:EtOAc = 30:1) was utilized to purify the residue and afford **4** as a white powder (6.65 g, 11.3 mmol, 64%).

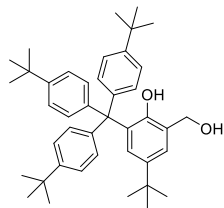
TLC: R_f = 0.19 (silica gel, *n*-hexane:EtOAc = 30:1, [UV]).

1H NMR (500 MHz, $CDCl_3$, 300 K): δ [ppm] = 1.16 (s, 9H, $C(CH_3)_3$), 1.31 (s, 27H, $C(CH_3)_3$), 7.09 (d, 3J = 8.6 Hz, 6H, Trit-H), 7.25 (d, 3J = 8.5 Hz, 6H, Trit-H), 7.33 (d, 4J = 2.5 Hz, 1H, Ar-H), 7.43 (d, 4J = 2.5 Hz, 1H, Ar-H), 9.86 (s, 1H, CHO), 11.13 (s, 1H, Ar-OH).

^{13}C NMR (126 MHz, $CDCl_3$, 300 K): δ [ppm] = 31.2, 31.5, 34.3, 34.4, 62.1, 120.2, 124.1, 128.8, 130.6, 136.0, 136.7, 141.4, 142.1, 148.5, 158.8, 197.0.

LRMS (ESI, MeCN): m/z = 612.2 [$(M+Na)^+$].

EA [%]: calculated: C 85.67, H 8.90; found: C 85.59, H 9.05.

4-tert-Butyl-2-hydroxymethyl-6-(tris(4-tert-butylphenyl)methyl)phenol (5)

$C_{42}H_{54}O_2$
590.88 g/mol

To a suspension of **4** (3.10 g, 5.26 mmol, 1.0 eq) in methanol (100 mL) was added sodium borohydride (398 mg, 10.5 mmol, 2.0 eq) in small portions. After the reaction mixture was stirred at room temperature for 1 h, the solvent was removed under reduced pressure. The residue was redissolved in distilled water (150 mL) and neutralized with glacial acetic acid. The aqueous phase was extracted with chloroform (3 × 100 mL) and the combined organic layers were dried over anhydrous $MgSO_4$. After filtration, the solvent was removed *in vacuo* to yield **6** as a white powder (3.09 g, 5.23 mmol, 99%). The product was utilized in the next step without further purification.

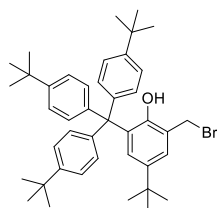
1H NMR (500 MHz, $CDCl_3$, 300 K): δ [ppm] = 1.11 (s, 9H, $C(CH_3)_3$), 1.31 (s, 27H, $C(CH_3)_3$), 2.45 (br s, 1H, CH_2OH), 4.64 (s, 2H, CH_2), 4.86 (s, 1H, Ar-OH), 6.84 (d, 4J = 2.4 Hz, 1H, Ar-H), 7.11 (d, 3J = 8.5 Hz, 6H, Trit-H), 7.19 (d, 4J = 2.4 Hz, 1H, Ar-H),

7.30 (d, 3J = 8.5 Hz, 6H, Trit-H).

^{13}C NMR (126 MHz, $CDCl_3$, 300 K): δ [ppm] = 31.5, 31.5, 34.3, 34.5, 61.8, 63.5, 124.7, 125.0, 127.8, 127.9, 130.7, 133.2, 141.3, 142.2, 149.5, 150.6.

LRMS (ESI, MeCN): m/z = 614.2 [$(M+Na)^+$].

EA [%]: calculated: C 85.37, H 9.21; found: C 79.31, H 8.63.

2-Bromomethyl-4-tert-butyl-6-(tris(4-tert-butylphenyl)methyl)phenol (6)

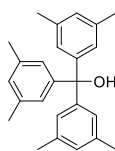
$C_{42}H_{53}BrO$
653.77 g/mol

To a solution of **5** (3.06 g, 5.18 mmol, 1.0 eq) in chloroform (100 mL) was added phosphorus tribromide (0.25 mL, 701 mg, 2.59 mmol, 0.5 eq). After the reaction mixture was stirred at room temperature for 1 h, iced water (40 mL) was added over 5 min. The resulting phases were separated and the aqueous phase was extracted with chloroform (3 × 25 mL). The combined organic layers were dried over anhydrous $MgSO_4$, filtered and the solvent removed *in vacuo* to afford **7** as a white powder (3.39 g, 5.18 mmol, quantitative yield).

1H NMR (500 MHz, $CDCl_3$, 300 K): δ [ppm] = 1.11 (s, 9H, $C(CH_3)_3$), 1.31 (s, 27H, $C(CH_3)_3$), 4.53 (s, 2H, CH_2), 4.77 (s, 1H, Ar-OH), 6.87 (d, 4J = 2.4 Hz, 1H, Ar-H), 7.10 (d, 3J = 8.6 Hz, 6H, Trit-H), 7.25 (d, 4J = 3.0 Hz, 1H, Ar-H), 7.30 (d, 3J = 8.6 Hz, 6H, Trit-H).

^{13}C NMR (126 MHz, $CDCl_3$, 300 K): δ [ppm] = 31.1, 31.4, 31.5, 34.3, 34.5, 61.9, 124.3, 124.8, 126.6, 129.2, 130.7, 133.7, 141.0, 142.4, 149.7, 150.7.

LRMS (ESI, MeCN): m/z = 677.1 [$(M+Na)^+$].

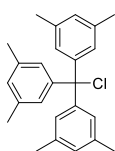
Tris(3,5-dimethylphenyl)methanol (7)

$C_{25}H_{26}O$
344.49 g/mol

A solution of 1-bromo-3,5-dimethylbenzene (18.4 mL, 25.0 g, 135 mmol, 3.0 eq) in dry THF (20 mL) was added dropwise to a stirred suspension of magnesium turnings (3.61 g, 149 mmol, 3.3 eq) in dry THF (200 mL). The reaction mixture was heated to initiate the reaction and stirred until the reaction subsided. A solution of diethyl carbonate (5.46 mL, 5.32 g, 45.0 mmol, 1.0 eq) in dry THF (100 mL) was added dropwise to the *Grignard* reagent and stirred for 3 h at room temperature. Ice-cold 2 M HCl (100 mL) was then poured into the reaction mixture and the organic phase was separated and washed with 2 M HCl (50 mL) and brine (50 mL). The organic phase was dried over $MgSO_4$, filtered and the solution concentrated *in vacuo*. Addition of *n*-hexane led to precipitation of **7** as colorless crystals (7.96 g, 23.1 mmol, 51%).

1H NMR (300 MHz, $CDCl_3$, 300 K): δ [ppm] = 2.27 (s, 18H, CH_3), 2.68 (s, 1H, OH), 6.88 (s, 6H, Ar-H), 6.91 (s, 3H, Ar-H).

^{13}C NMR (75 MHz, $CDCl_3$, 300 K): δ [ppm] = 21.7, 83.2, 126.7, 128.6, 136.5, 143.7.

Tris(3,5-dimethylphenyl)methyl chloride (8)

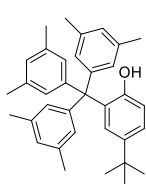
$C_{25}H_{27}Cl$
362.93 g/mol

To a vigorously stirred solution of **7** (7.96 g, 23.1 mmol, 1.0 eq) in dry toluene (25 mL) was added freshly distilled acetyl chloride (4.12 mL, 4.54 g, 57.8 mmol, 2.5 eq). The reaction mixture was heated under reflux for 30 min. After the solution was allowed to cool down to ambient temperature, *n*-hexane (35 mL) was added and the flask was left at 4 °C overnight. The resulting precipitate was filtered and dried under vacuum to furnish **8** as colorless crystals (6.44 g, 17.7 mmol, 77%).

1H NMR (500 MHz, $CDCl_3$, 300 K): δ [ppm] = 2.29 (s, 18H, CH_3), 6.88 (s, 6H, Ar-H), 6.95 (s, 3H, Ar-H).

^{13}C NMR (126 MHz, $CDCl_3$, 300 K): δ [ppm] = 21.6, 82.2, 127.7, 129.5, 137.1, 145.6.

EA [%]: calculated: C 82.73, H 7.50, Cl 9.77; found: C 82.23, H 7.45, Cl 9.30

4-tert-Butyl-2-(tris(3,5-dimethylphenyl)methyl)phenol (9)

$C_{35}H_{40}O$
476.69 g/mol

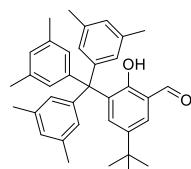
To molten 4-*tert*-butylphenol (25.7 g, 171 mmol, 10.0 eq) was added sodium metal (550 mg, 23.9 mmol, 1.4 eq) at 110 °C with vigorous stirring. **8** (6.20 g, 17.1 mmol, 1.0 eq) was added to the formed phenolate and the resulting mixture was heated at 145 °C under reflux for 3 h. The reaction mixture was treated with 7% aqueous NaOH (52 mL) and Et_2O (60 mL) after cooling down to about 80 °C. The organic layer was separated and the aqueous phase extracted with Et_2O (3 × 26 mL). The combined organic phases were washed with 7% aqueous NaOH (3 × 26 mL), distilled water (26 mL) and brine (26 mL). After drying over anhydrous $MgSO_4$ and filtration, the solvent of the amber solution was removed *in vacuo*. Recrystallization of the crude product from ethanol yielded **9** as colorless crystals (5.72 g, 12.0 mmol, 70%).

1H NMR (500 MHz, $CDCl_3$, 300 K): δ [ppm] = 1.18 (s, 9H, $C(CH_3)_3$), 2.24 (s, 18H, CH_3), 4.52 (s, 1H, Ar-OH), 6.73 (d, $^3J = 8.2$ Hz, 1H, Ar-H), 6.81 (s, 6H, Trit-H), 6.86 (s, 3H, Trit-H), 7.16 (d, $^4J = 2.4$ Hz, 1H, Ar-H), 7.20 (dd, $^4J = 2.4$ Hz, $^3J = 8.3$ Hz, 1H, Ar-H).

^{13}C NMR (126 MHz, $CDCl_3$, 300 K): δ [ppm] = 21.8, 31.6, 34.3, 62.7, 117.1, 125.0, 128.3, 128.3, 128.9, 132.6, 137.0, 142.2, 144.6, 152.4.

LRMS (ESI, MeCN): $m/z = 500.2$ [$(M+Na)^+$].

EA [%]: calculated: C 88.19, H 8.46; found: C 88.09, H 8.57.

5-tert-Butyl-2-hydroxy-3-(tris(3,5-dimethylphenyl)methyl)benzaldehyde (10)

$C_{36}H_{40}O_2$
504.70 g/mol

To a suspension of **9** (6.00 g, 12.6 mmol, 1.0 eq), anhydrous magnesium chloride (2.64 g, 27.7 mmol, 2.2 eq) and paraformaldehyde (831 mg, 27.7 mmol, 2.2 eq) in dry THF (70 mL) was added dropwise freshly distilled triethylamine (1.76 mL, 1.27 g, 12.6 mmol, 1.0 eq). The resulting reaction mixture was heated under reflux for 3 d. Subsequently the mixture was allowed to cool down to room temperature and diluted with distilled water (30 mL). The aqueous layer was extracted with CH_2Cl_2 (3×50 mL) and the combined organic phases were washed with distilled water (75 mL) and brine (2×75 mL). After drying over anhydrous $MgSO_4$ and filtration, the solvent was removed *in vacuo*. Silica gel column chromatography (*n*-pentane/ Et_2O = 40/1) and subsequent recrystallization from ethanol were utilized to purify the residue and afford **11** as colorless crystals (3.67 g, 7.27 mmol, 58%).

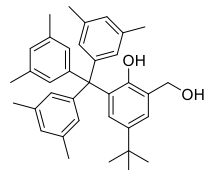
TLC: R_f = 0.23 (silica gel, *n*-pentane: Et_2O = 40:1, [UV]).

1H NMR (500 MHz, $CDCl_3$, 300 K): δ [ppm] = 1.26 (s, 9H, $C(CH_3)_3$), 2.23 (s, 18H, CH_3), 6.80 (s, 3H, Trit-H), 6.89 (s, 6H, Trit-H), 7.41 (d, 4J = 2.4 Hz, 1H, Ar-H), 7.77 (d, 4J = 2.4 Hz, 1H, Ar-H), 9.83 (s, 1H, CHO), 11.22 (s, 1H, Ar-OH).

^{13}C NMR (126 MHz, $CDCl_3$, 300 K): δ [ppm] = 21.8, 31.2, 34.3, 63.0, 120.2, 127.3, 128.5, 128.7, 135.4, 136.3, 137.1, 141.3, 145.2, 158.8, 196.9.

LRMS (ESI, MeCN): m/z = 527.4 [(M+Na) $^+$].

EA [%]: calculated: C 85.67, H 7.99; found: C 85.73, H 8.17.

4-tert-Butyl-2-hydroxymethyl-6-(tris(3,5-dimethylphenyl)methyl)phenol (11)

$C_{36}H_{42}O_2$
506.72 g/mol

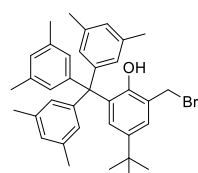
To a suspension of **10** (2.60 g, 5.15 mmol, 1.0 eq) in methanol (100 mL) was added sodium borohydride (390 mg, 10.3 mmol, 2.0 eq) in small portions. After the reaction mixture was stirred at room temperature for 2 h, the solvent was removed under reduced pressure. The residue was redissolved in water (125 mL) and neutralized with glacial acetic acid. The aqueous phase was extracted with chloroform (3×75 mL) and the combined organic layers were dried over anhydrous $MgSO_4$. After filtration, the solvent was removed *in vacuo* to yield **12** as a white powder (2.58 g, 5.09 mmol, 99%). The product was utilized in the next step without further purification.

1H NMR (500 MHz, $CDCl_3$, 300 K): δ [ppm] = 1.19 (s, 9H, $C(CH_3)_3$), 2.24 (s, 18H, CH_3), 4.63 (s, 2H, CH_2), 6.80 (s, 6H, Trit-H), 6.87 (s, 3H, Trit-H), 7.15 (d, 4J = 2.5 Hz, 1H, Ar-H), 7.18 (d, 4J = 2.5 Hz, 1H, Ar-H).

^{13}C NMR (126 MHz, $CDCl_3$, 300 K): δ [ppm] = 21.8, 31.6, 34.4, 62.7, 63.6, 124.7, 128.3, 128.9, 132.9, 136.3, 137.0, 142.0, 144.5, 145.2, 150.8.

LRMS (ESI, MeCN): m/z = 529.4 [(M+Na) $^+$].

EA [%]: calculated: C 85.33, H 8.35; found: C 85.04, H 8.99.

2-Bromomethyl-4-tert-butyl-6-(tris(3,5-dimethylphenyl)methyl)phenol (12)

$C_{36}H_{41}BrO$
569.91 g/mol

To a solution of **11** (2.58 g, 5.09 mmol, 1.0 equiv.) in chloroform (100 mL) was added phosphorus tribromide (0.24 mL, 689 mg, 2.55 mmol, 0.5 eq). After the reaction mixture was stirred at room temperature for 1 h, iced water (40 mL) was added over 5 min. The resulting phases were separated and the aqueous phase was extracted with chloroform (3×25 mL). The combined organic layers were dried over anhydrous $MgSO_4$, filtered and the solvent removed under reduced pressure. The residue was recrystallized from acetonitrile to afford **13** as colorless crystals (2.60 g, 4.56 mmol, 90%).

1H NMR (500 MHz, $CDCl_3$, 300 K): δ [ppm] = 1.18 (s, 9H, $C(CH_3)_3$), 2.24 (s, 18H, CH_3), 4.52 (s, 2H, CH_2), 6.78 (s, 6H, Trit-H), 6.88 (s, 3H, Trit-H), 7.14 (d, 4J = 2.4 Hz, 1H, Ar-H), 7.23 (d, 4J = 2.5 Hz, 1H, Ar-H).

^{13}C NMR (126 MHz, $CDCl_3$, 300 K): δ [ppm] = 21.8, 31.5, 31.5, 34.3, 62.8, 125.1, 126.2, 128.4, 129.0, 129.4, 133.4, 137.1, 142.1, 144.1, 151.0.

LRMS (ESI, MeCN): m/z = 593.2 [(M+Na) $^+$].

EA [%]: calculated: C 75.91, H 7.26; found: C 76.08, H 7.28.

2. Kinetic Investigations

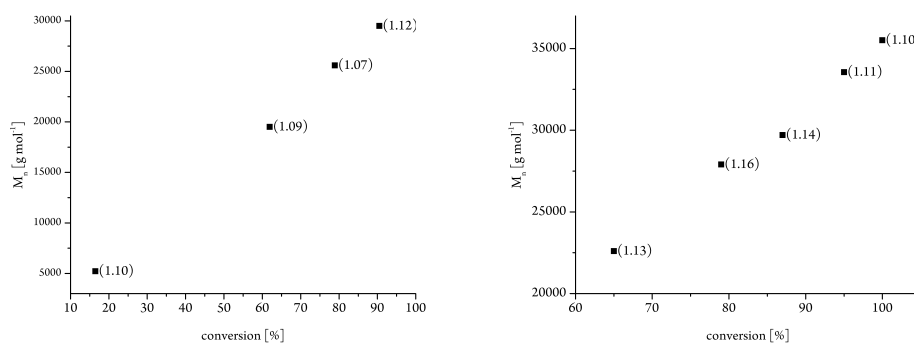


Figure S1. Linear growth of the absolute molecular weight (M_n) as a function of monomer conversion (determined gravimetrically) and the corresponding PDIs. Left: catalyst **1**, right: catalyst **2**.

3. Microstructure Analysis

3.1 ^{13}C NMR spectra

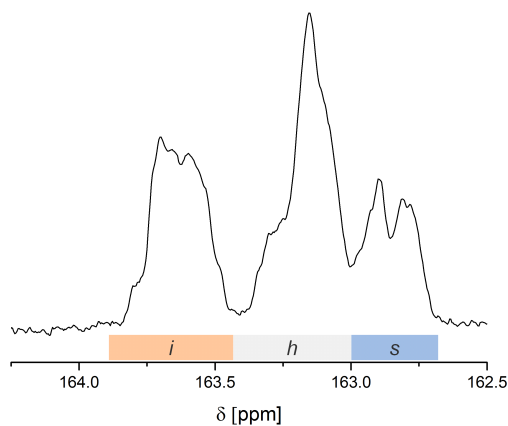


Figure S2. Aromatic quaternary ^{13}C NMR resonances (i , h , s proportions for *isotactic*, *heterotactic*, and *syndiotactic* triads) of poly(2-vinylpyridine) (30 mg of P2VP in 0.6 mL of CD_3OD for catalyst **5**. ([2VP]:[Cat.] = 200:1, [M] = 2.7 mmol, 2 mL of toluene, 25 °C)).

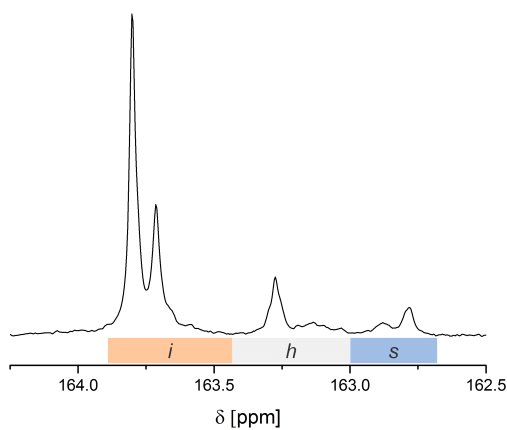


Figure S3. Aromatic quaternary ^{13}C NMR resonances (i , h , s proportions for *isotactic*, *heterotactic*, and *syndiotactic* triads) of poly(2-vinylpyridine) (30 mg of P2VP in 0.6 mL of CD_3OD for catalyst **1**. ([2VP]:[Cat.] = 200:1, [M] = 2.7 mmol, 2 mL of toluene, 25 °C)).

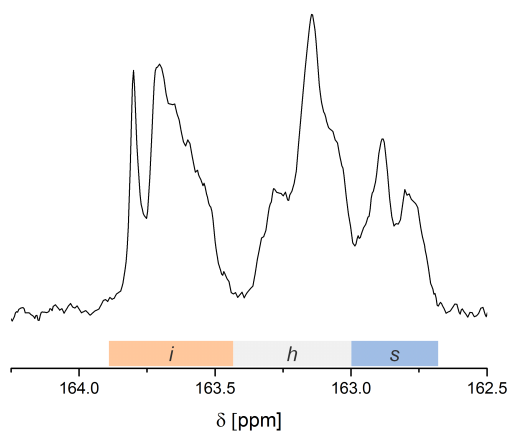


Figure S4. Aromatic quaternary ¹³C NMR resonances (*i*, *h*, *s* proportions for *isotactic*, *heterotactic*, and *syndiotactic* triads) of poly(2-vinylpyridine) (30 mg of P2VP in 0.6 mL of CD₃OD for catalyst **2**. ([2VP]:[Cat.] = 200:1, [M] = 2.7 mmol, 2 mL of toluene, 25 °C)).

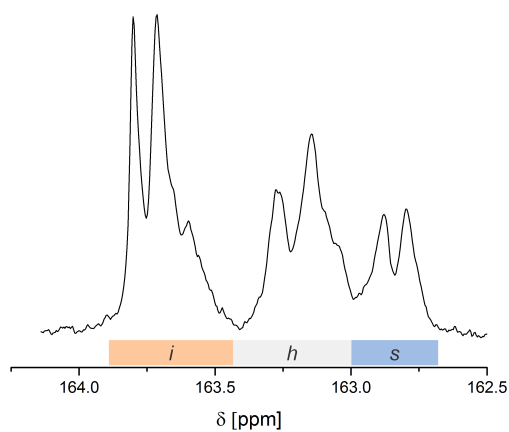


Figure S5. Aromatic quaternary ¹³C NMR resonances (*i*, *h*, *s* proportions for *isotactic*, *heterotactic*, and *syndiotactic* triads) of poly(2-vinylpyridine) (30 mg of P2VP in 0.6 mL of CD₃OD for catalyst **3**. ([2VP]:[Cat.] = 200:1, [M] = 2.7 mmol, 2 mL of toluene, 25 °C)).

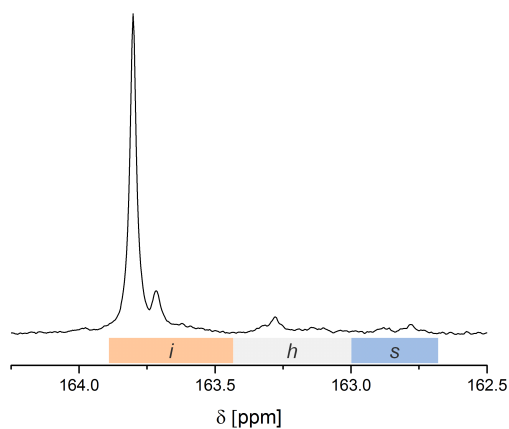


Figure S6. Aromatic quaternary ¹³C NMR resonances (*i*, *h*, *s* proportions for *isotactic*, *heterotactic*, and *syndiotactic* triads) of poly(2-vinylpyridine) (30 mg of P2VP in 0.6 mL of CD₃OD for catalyst **4**. ([2VP]:[Cat.] = 200:1, [M] = 2.7 mmol, 2 mL of toluene, 25 °C)).

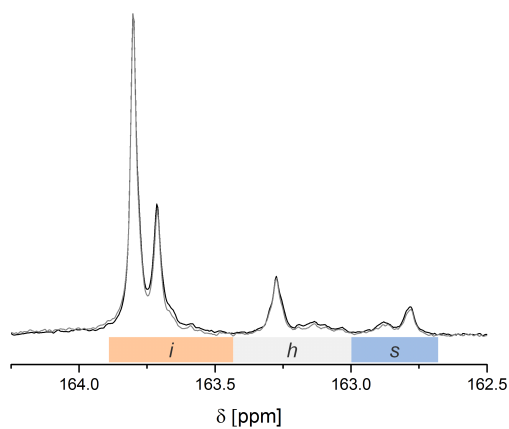


Figure S7. Aromatic quaternary ¹³C NMR resonances (*i*, *h*, *s* proportions for *isotactic*, *heterotactic*, and *syndiotactic* triads) of poly(2-vinylpyridine) (30 mg P2VP in 0.6 mL of CD₃OD for catalysts **1**. ([2VP]:[Cat.] = 200:1, [M] = 2.7 mmol, 2 mL of toluene, 25 °C: black, 50 °C: grey)).

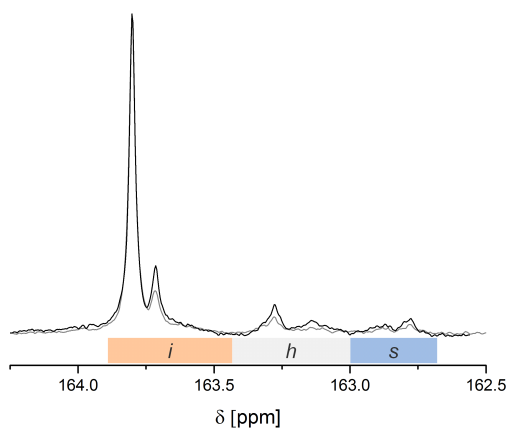


Figure S8. Aromatic quaternary ^{13}C NMR resonances (i , h , s proportions for *isotactic*, *heterotactic*, and *syndiotactic* triads) of poly(2-vinylpyridine) (30 mg P2VP in 0.6 mL of CD_3OD for catalysts **4**. ($[\text{2VP}]:[\text{Cat.}] = 200:1$, $[\text{M}] = 2.7$ mmol, 2 mL of toluene, 25 °C: black, 50 °C: grey)).

3.2 Theoretical Investigations

- P_m is the probability of meso linkages between monomer units and is determined by ^{13}C NMR spectroscopy.
- Theoretical triad distributions are calculated using the following correlations:

Probability of prochiral monomer addition via *re* or *si* side of the catalyst, where $P_m = m = \sigma + (1 - \sigma)^2$ and $P_r = 1 - P_m$

$$mm = P_m^2$$

$$mr = P_m P_r$$

$$rr = P_r^2$$

4. Thermoanalysis

4.1 DSC

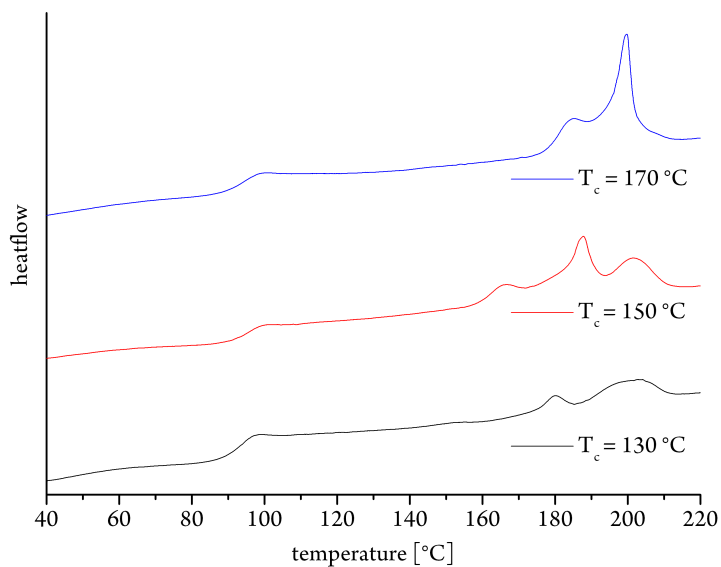


Figure S9. DSC curves of crystallized P2VP samples at different crystallization temperatures T_c for 150 min (catalyst **4**, [2VP]:[Cat.] = 200:1, [M] = 2.7 mmol, 2 mL toluene, 25 °C).

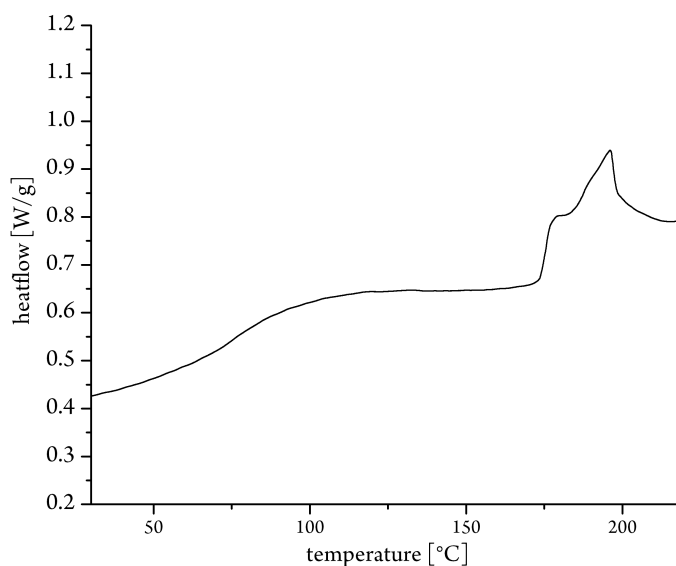


Figure S10. DSC curves of crystallized P2VP samples at a $T_c = 130^\circ\text{C}$ for 16 h (catalyst **1**, [2VP]:[Cat.] = 200:1, [M] = 2.7 mmol, 2 mL of toluene, 25 °C).

4.2 TGA

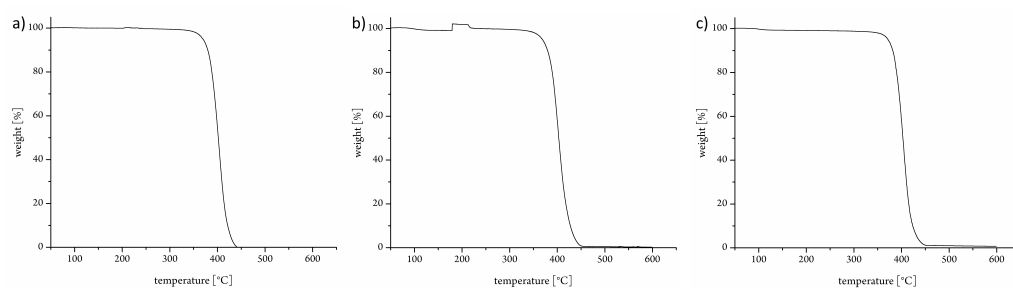


Figure S11. TGA curves of atactic (a), highly *isotactic* amorphous ($P_m = 0.92$, b), and highly *isotactic* crystallized P2VP ($P_m = 0.92$, $T_c = 170$ °C, crystallization time 150 min, c).

5. Literature

- [1] K. C. Hultsch, P. Voth, K. Beckerle, T. P. Spaniol, J. Okuda, *Organometallics* **2000**, *19*, 228-243.
- [2] P. T. Altenbuchner, F. Adams, A. Kronast, E. Herdtweck, A. Pöthig, B. Rieger, *Polym. Chem.* **2015**, *6*, 6796-6801.

6.2.3 Gated Channels and Selectivity Tuning of CO₂ over N₂ Sorption by Post-Synthetic Modification of a UiO-66-type MOF

CHEMISTRY
A European Journal

Supporting Information

Gated Channels and Selectivity Tuning of CO₂ over N₂ Sorption by Post-Synthetic Modification of a UiO-66-Type Metal–Organic Framework

Alexander Kronast,^[a] Sebastian Eckstein,^[b] Peter T. Altenbuchner,^[a] Konrad Hindelang,^[c] Sergei I. Vagin,^[a] and Bernhard Rieger^{*[a]}

chem_201602318_sm_miscellaneous_information.pdf

Table of Contents

1. Additional experimental Information	2
Linker and MOF Synthesis	3
2. MOF Analysis.....	4
Proton NMRs of extracted linkers.....	4
Thermogravimetric Analysis.....	8
Brunauer-Emmet-Teller Surface areas (BET).....	9
ATR-IR	11
Powder Xray Diffraction (P-XRD)	13
High pressure N ₂ and CO ₂ adsorption.....	14

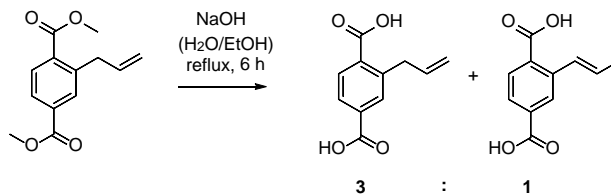
1. Additional experimental Information

All reactions containing air- and/or moisture sensitive compounds were performed under dry argon using standard Schlenk or glovebox techniques. All chemicals were purchased from Aldrich, ABCR or Acros. Solvents were obtained from an MBraun MB-SPS solvent purification system.

UV irradiation for the photo-induced thiol-ene click reaction was executed with a MAX-302 ASAHI SECTRA. NMR spectra were recorded on a Bruker Avance 500 UltraShield (500 MHz) and a Bruker Avance 300 (300 MHz). They were recorded in ppm and the solvents residual proton signal and carbon signal were used as internal standard. X-Ray Powder Diffraction was measured on a STOE STADI P system with a DECTRIS MYTHEN 1K detector. TGA was carried out on a Texas Instruments TGA-Q500 with a heating rate of 10 K min⁻¹. Brunauer-Emmett-Teller (BET) adsorption measurements were obtained by using a Quantachrome Nova 4000e sorption apparatus and a PMI automatic Sorptometer. The samples were activated in vacuum at 135 °C for 2 h before measurement. Apparent surface area was calculated by applying the Brunauer-Emmett-Teller (BET) theory. CO₂ and N₂ isotherms were obtained at 35 °C in a range of 0.5 – 20 bar using a Rubotherm magnetic suspension balance. Approximately 300 mg of the sorbent was placed in a steel crucible and dried at 135 °C for 8 hours under vacuum prior to adsorption. In order to correct for buoyancy, reference adsorption isotherms of non-adsorbing glass spheres (300 mg, particle size 425 – 600 µm) were determined and subtracted from the isotherms. Elemental analyses were measured at the Laboratory for Microanalytics at the Institute of Inorganic Chemistry at the Technische Universität München. ESI-MS analytical measurements were performed with acetonitrile, THF, isopropanol or toluene solutions on a Varian 500-MS spectrometer. IR spectra were recorded with a liquid nitrogen cooled Bruker Vertex 70 FTIR-spectrometer with a attenuated total reflectance unit Platinum ATR of Bruker using 32 scans in a region of 4500 cm⁻¹ to 600 cm⁻¹.

Linker and MOF Synthesis

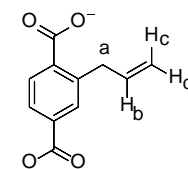
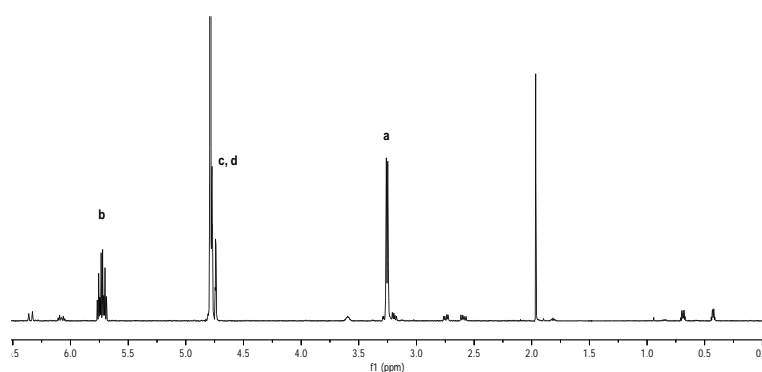
Linker Synthesis



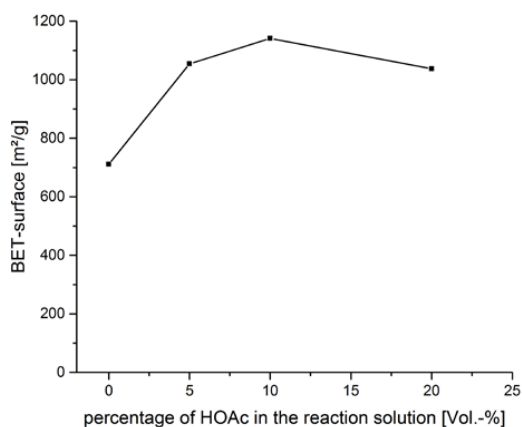
S1. Side reaction occurring through harsh reaction conditions while saponification giving isomers 2-allylterephthalic acid and (*E*)-2-(prop-1-en-1-yl)terephthalic acid.

MOF Synthesis

UiO-66-allyl: 2-allyl-terephthalate



$^1\text{H NMR}$ (500 MHz, Deuterium Oxide) δ 7.45 – 7.40 (m, 2H), 7.09 (d, J = 7.8 Hz, 1H), 5.73 (ddt, J = 16.8, 10.2, 6.5 Hz, 1H), 4.76 (dq, J = 17.1, 1.8 Hz, 2H), 3.26 (dt, J = 6.5, 1.6 Hz, 2H).

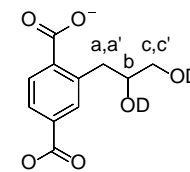
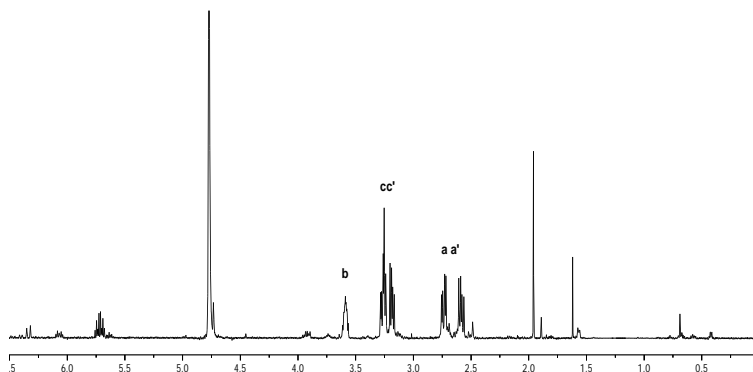


S2. Influence of concentration of modulating agent acetic acid during UiO-66 synthesis on pore surface areas determined by BET.

2. MOF Analysis

Proton NMRs of extracted linkers

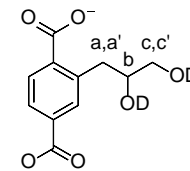
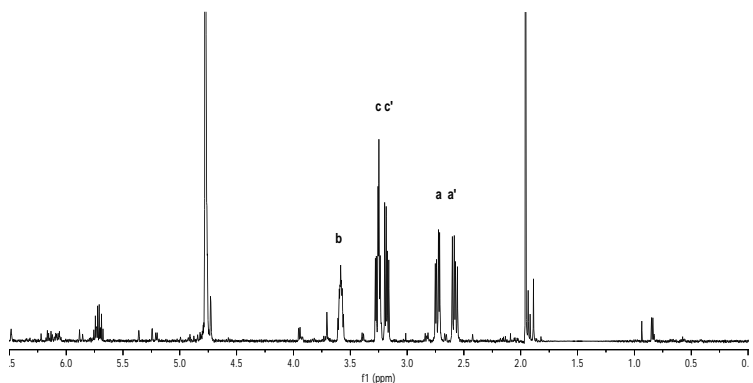
UiO-66-epoxide: 2-(oxiran-2-ylmethyl)terephthalate



Proton NMR shows signals for the ring opened oxirane:

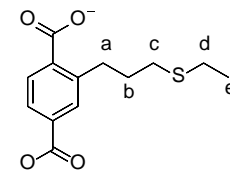
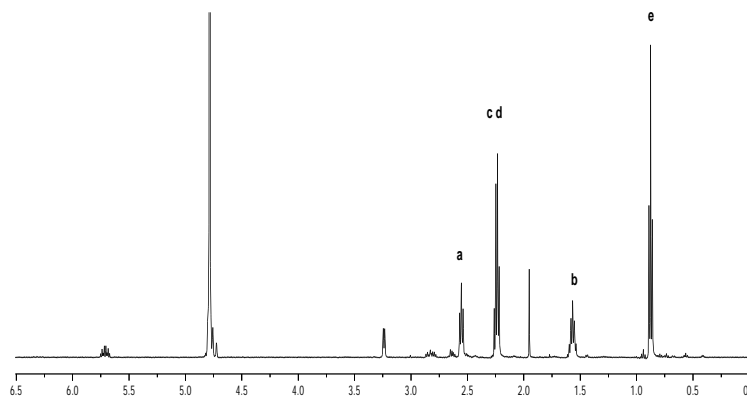
$^1\text{H NMR}$ (500 MHz, Deuterium Oxide) $\delta = 7.51 - 7.41$ (m, 2H), 7.16 (d, $J=7.8$, 1H), 3.60 (td, $J=9.4, 7.8, 4.5$, 1H), 3.35 - 3.15 (m, 2H), 2.82 - 2.56 (m, 2H).

UiO-66-dibromide: 2-(2,3-dibromopropyl)terephthalate

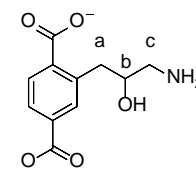
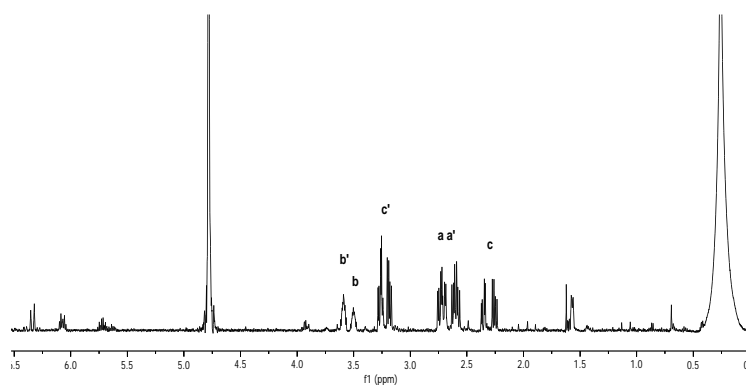


Proton NMR shows signals for the corresponding glycole through nucleophilic substitution of Br^- by HO^- .

$^1\text{H NMR}$ (500 MHz, Deuterium Oxide) $\delta = 7.48 - 7.40$ (m, 3H), 7.15 (d, $J=7.9$, 1H), 3.63 - 3.52 (m, 1H), 3.34 - 3.14 (m, 3H), 2.79 - 2.53 (m, 2H).

UiO-66-ethylsulfide: 2-(3-(ethylthio)propyl)terephthalate

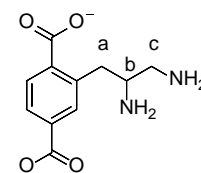
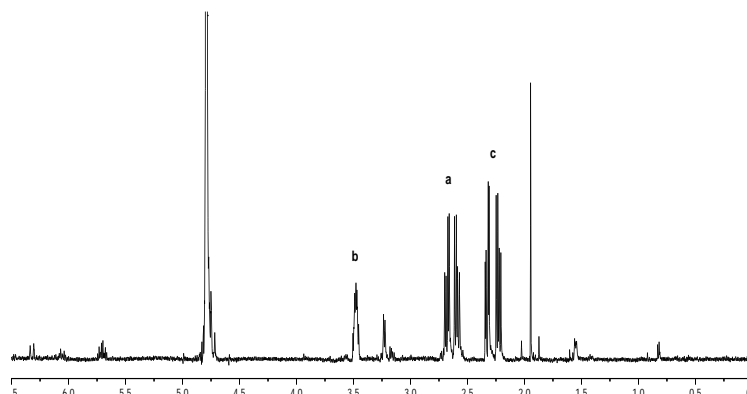
$^1\text{H NMR}$ (500 MHz, Deuterium Oxide) δ = 7.44 – 7.36 (m, 2H), 7.07 (dd, J =12.8, 7.8, 1H), 2.56 (t, J =7.6, 2H), 2.33 – 2.19 (m, 4H), 1.68 – 1.48 (m, 2H), 0.93 – 0.81 (m, 3H).

UiO-66-aminoalcohol: 2-(3-amino-2-hydroxypropyl)terephthalate

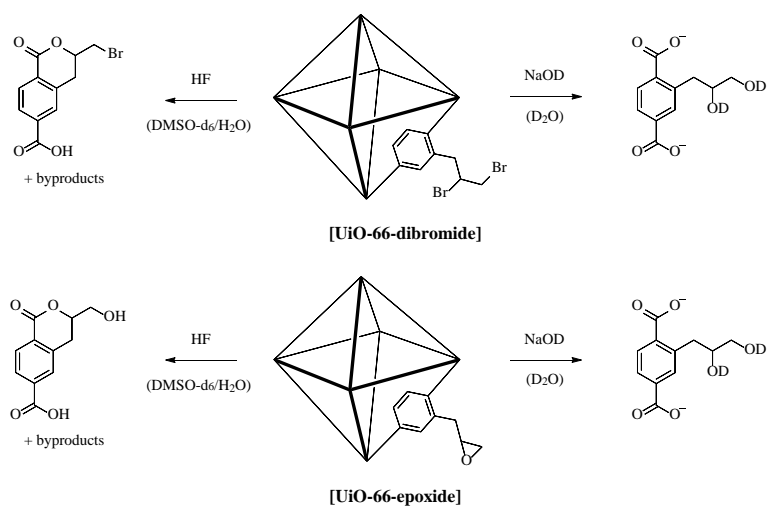
Proton NMR shows beside the product signals a set for the ring opened products of not converted epoxide (a', b', c').

$^1\text{H NMR}$ (500 MHz, Deuterium Oxide) δ = 7.47 – 7.44 (m, 2H), 7.14 (d, J =3.3, 1H), 3.51 (m, 1H), 2.76 – 2.62 (m, 2H), 2.42 – 2.21 (m, 2H).

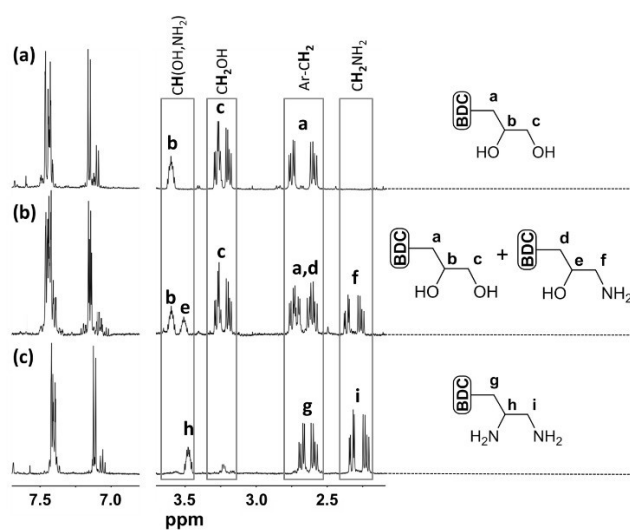
UiO-66-diamine: 2-(2,3-diaminopropyl)terephthalate



^1H NMR (500 MHz, Deuterium Oxide) δ = 7.43 – 7.38 (m, 2H), 7.12 (d, J =7.9, 1H), 3.55 – 3.43 (m, 1H), 2.76 – 2.54 (m, 2H), 2.39 – 2.15 (m, 2H).

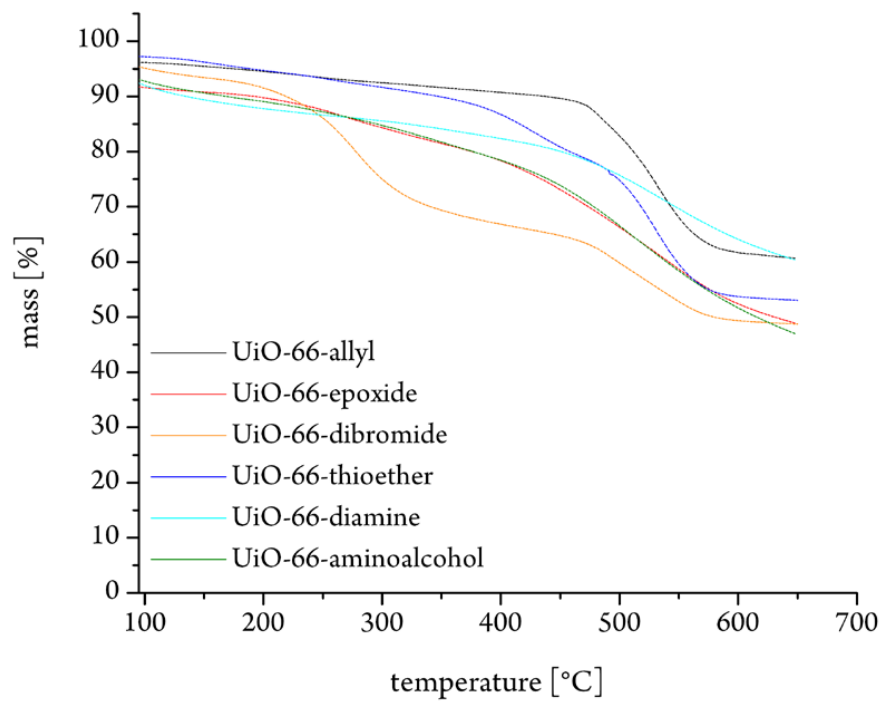


S3: Difference of acidic and basic workup on reaction products dibromide and epoxide.



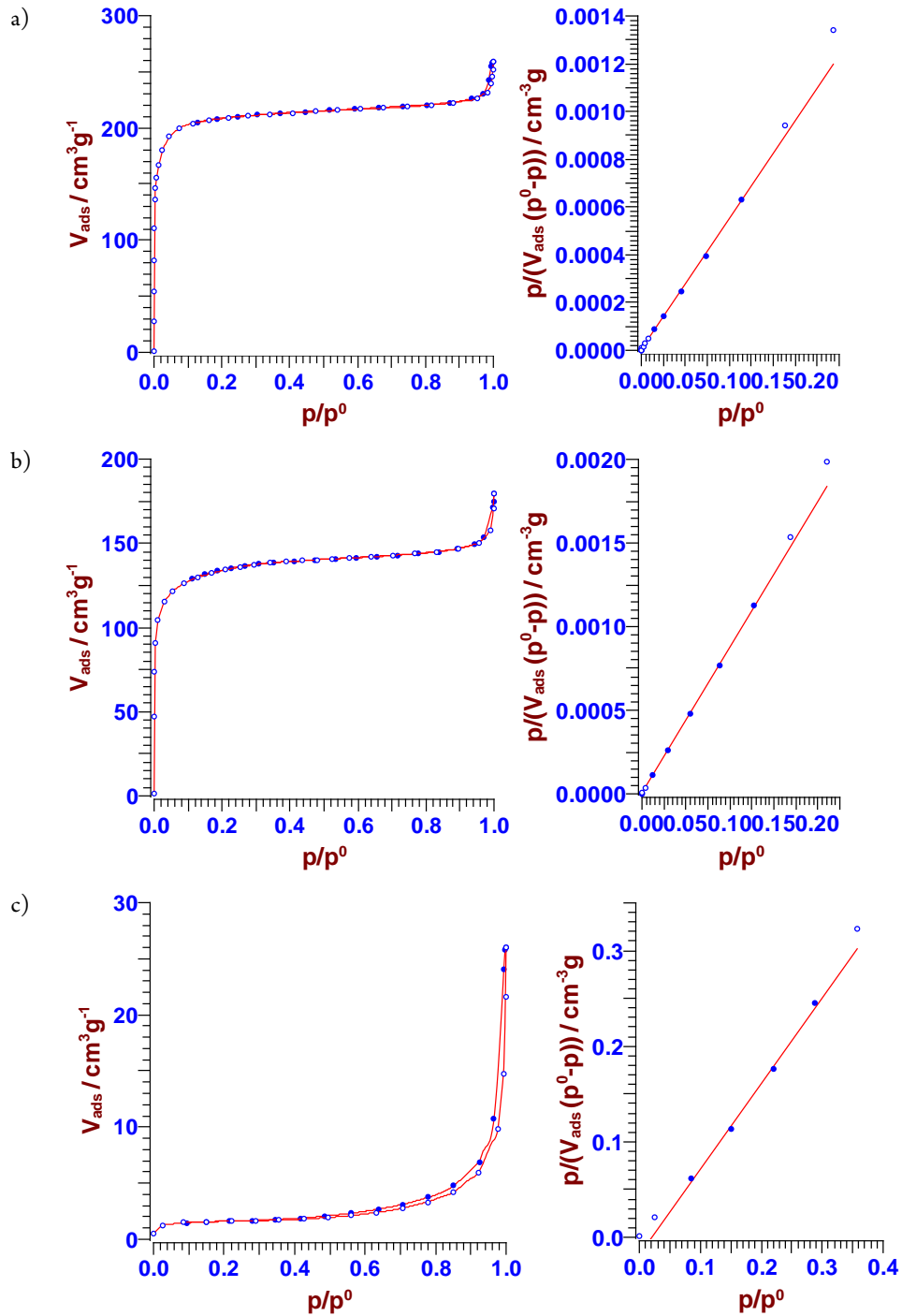
S4. ^1H NMR spectra of the tandem functionalized linkers after disintegration using NaOD in D_2O : (a) UiO-66-epoxide (for comparison), (b) UiO-66-aminoalcohol and unreacted UiO-66-epoxide, (c) UiO-66-diamine.

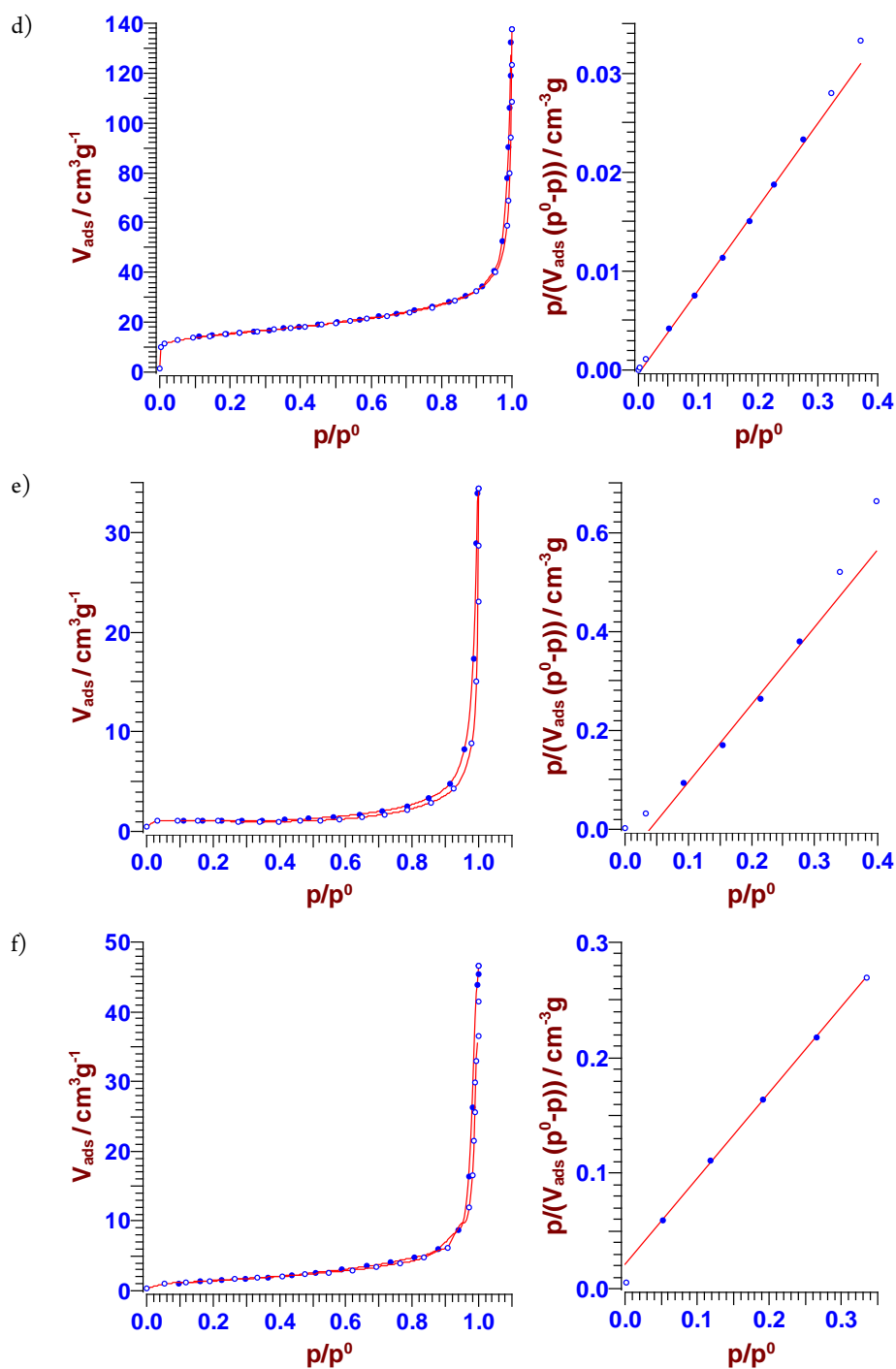
Thermogravimetric Analysis



S5: TGA data of UiO-66-allyl and the corresponding PSM products.

Brunauer-Emmet-Teller Surface areas (BET)

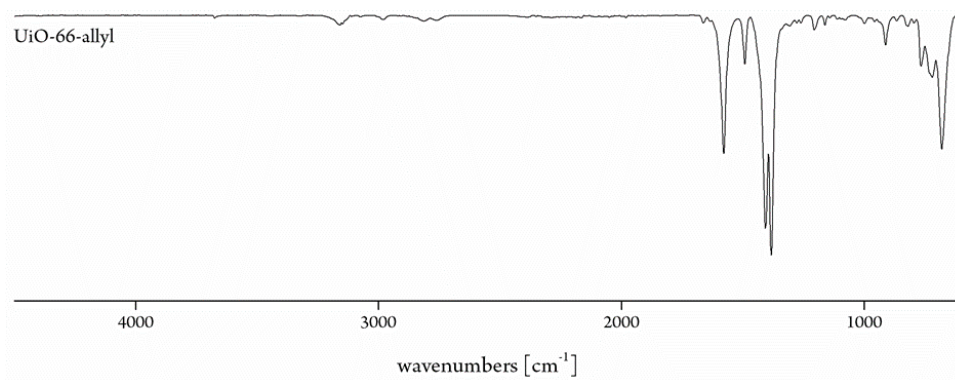




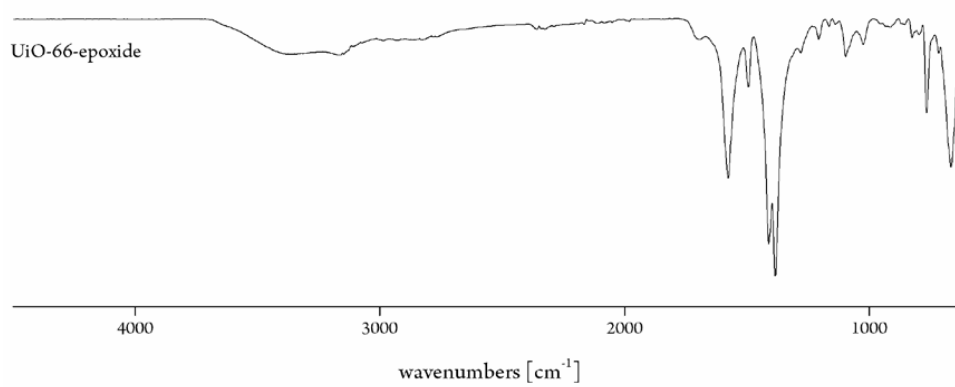
S6: N₂ isotherms recorded at 77 K and BET plots for a) UiO-66-allyl: 798 m²g⁻¹; b) UiO-66-epoxide: 498 m²g⁻¹; c) UiO-66-dibromide: 5 m²g⁻¹; d) UiO-66-ethylsulfide: 52 m²g⁻¹; e) UiO-66-aminoalcohol: 3 m²g⁻¹; f) UiO-66-diamine: 6 m²g⁻¹.

ATR-IR

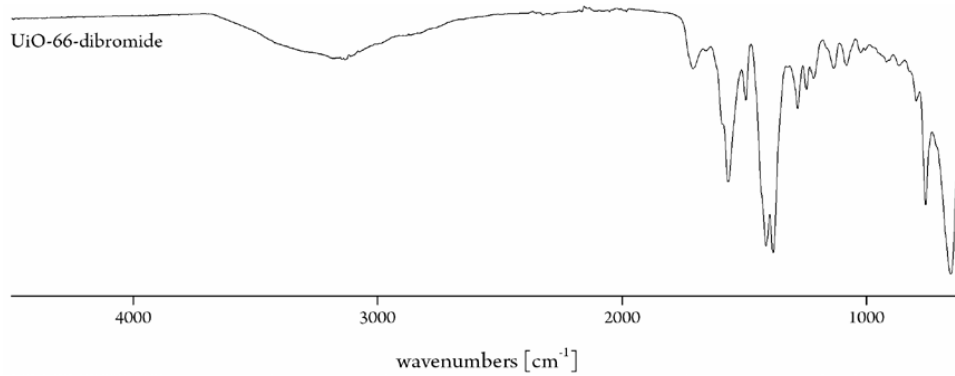
a)

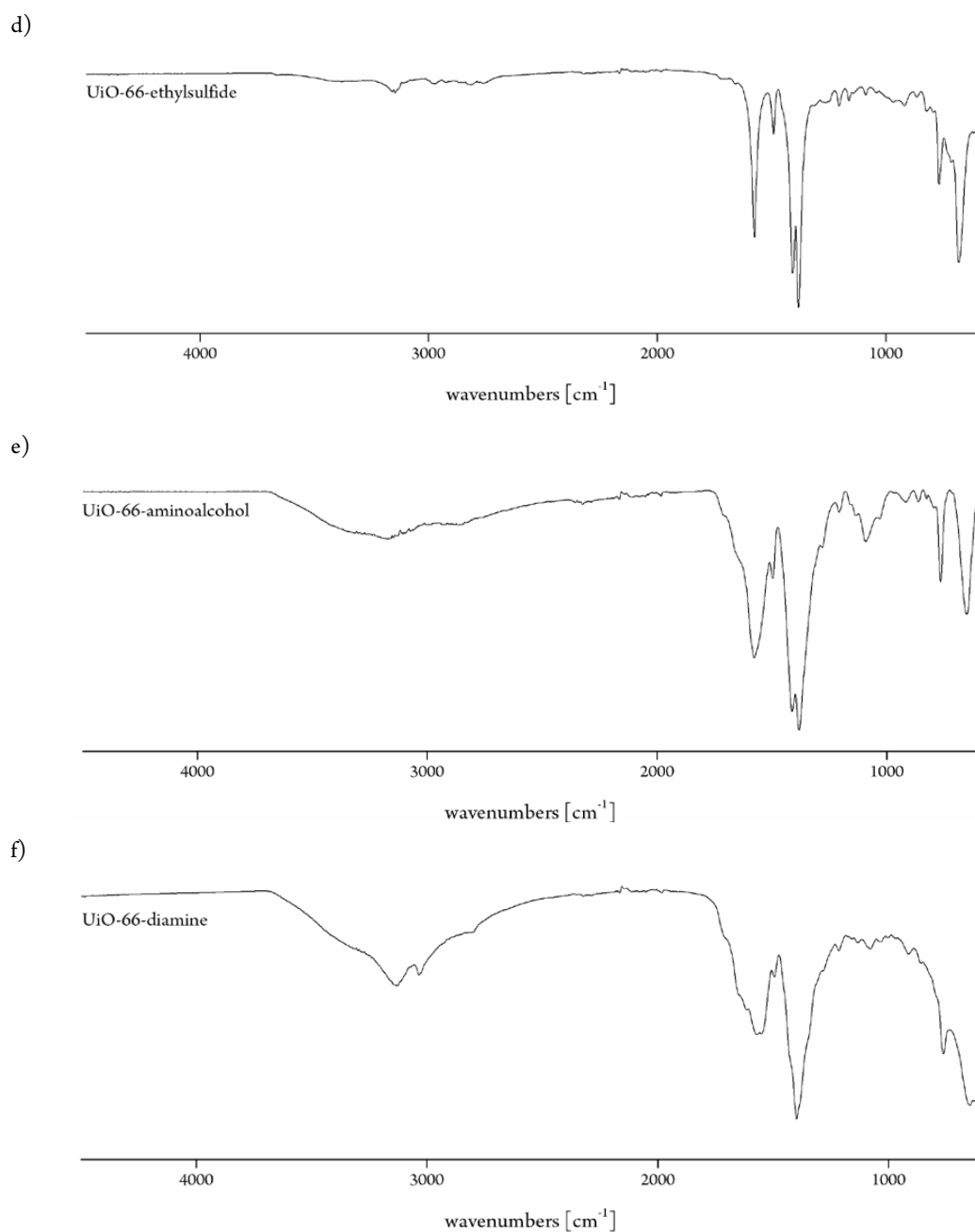


b)



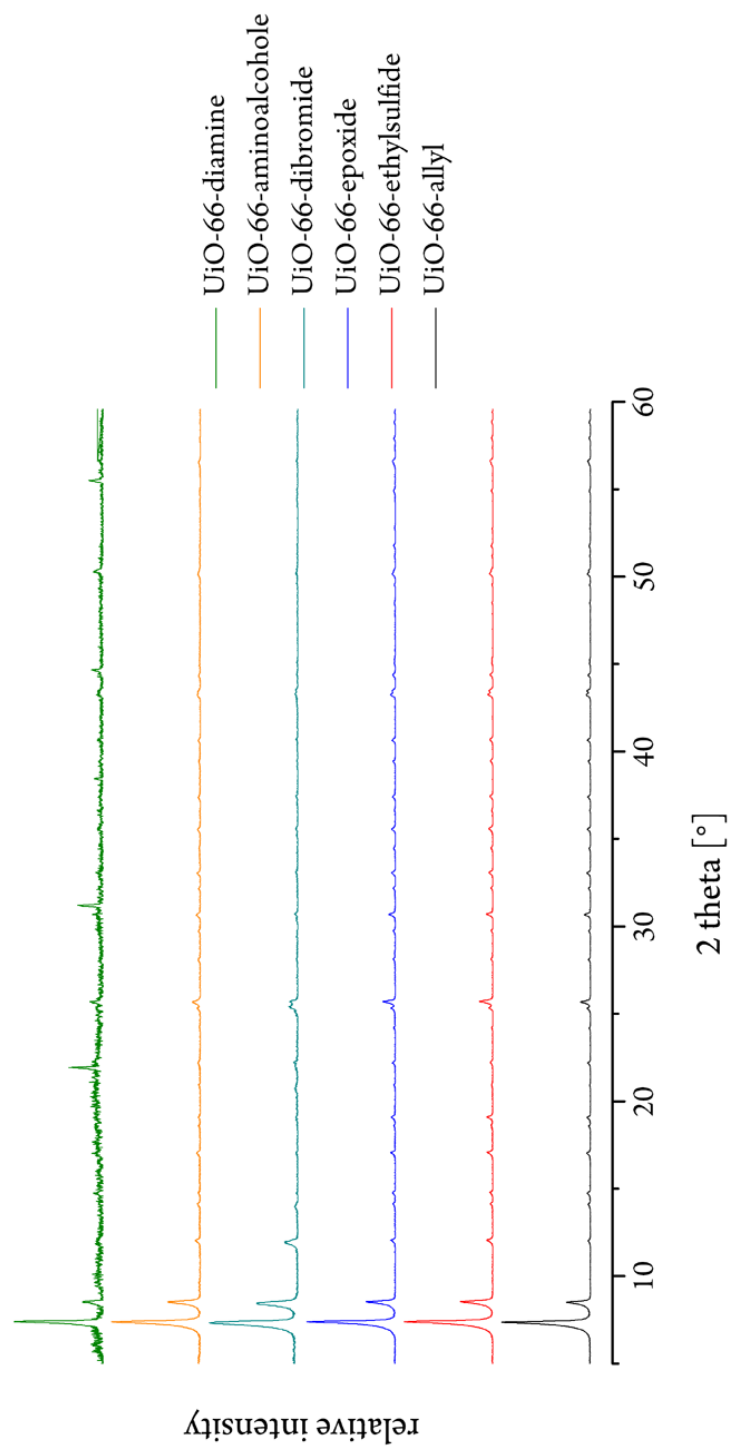
c)





S7: ATR-IR spectra of a) UiO-66-allyl; b) UiO-66-epoxide; c) UiO-66-dibromide; d) UiO-66-ethylsulfide; e) UiO-66-aminoalcohol; f) UiO-66-diamine.

Powder X-ray Diffraction (P-XRD)



S8: ATR-IR spectra of UiO-66-allyl; UiO-66-ethylsulfide; UiO-66-epoxide; UiO-66-dibromide; UiO-66-aminoalcohol; UiO-66-diamine.

High pressure N₂ and CO₂ adsorptionST1: N₂ and CO₂ high pressure adsorption data for UiO-66-allyl and the corresponding PSM products.

pressure [bar]	N ₂ uptake [mmol g ⁻¹]					
	UiO-66-allyl	UiO-66-epoxide	UiO-66-dibromide	UiO-66-ethylsulfide	UiO-66-aminoalcohol	UiO-66-diamine
0.5	0.13364	0.29615	0.25663	0.49689	0.21834	0.20362
1	0.26410	0.59231	0.42772	0.68323	0.32751	0.35366
2	0.51304	1.11058	0.68435	0.99379	0.53130	0.54657
5	1.19510	2.51731	1.45423	1.98758	1.09171	1.08241
10	2.32823	4.33865	2.78015	3.72671	1.96508	1.90762
15	3.16929	6.04154	3.84944	4.96894	2.69289	2.65781
20	3.53721	7.07807	4.45680	5.71429	3.12958	3.08649

pressure [bar]	CO ₂ uptake [mmol g ⁻¹]					
	UiO-66-allyl	UiO-66-epoxide	UiO-66-dibromide	UiO-66-ethylsulfide	UiO-66-aminoalcohol	UiO-66-diamine
0.5	0.25287	1.49433	0.49414	1.52630	1.47172	0.66957
1	0.39741	2.25865	0.79988	2.40441	2.26632	1.16233
2	0.61715	3.10243	1.11269	3.25354	3.15487	1.69956
5	1.20718	5.07044	1.81305	5.18837	5.27881	2.90818
10	2.12148	7.96305	2.83571	7.90307	8.47795	4.67625
15	2.75454	9.97849	3.57401	9.65203	10.67939	5.90154
20	3.05640	10.90207	3.92953	10.45937	11.67338	6.50299

6.3 Reprint Permissions

6.3.1 Electron-Deficient β -Diiminato-Zinc-Ethyl Complexes: Synthesis, Structure, and Reactivity in Ring-Opening Polymerization of Lactones




Title: Electron-Deficient β -Diiminato-Zinc-Ethyl Complexes: Synthesis, Structure, and Reactivity in Ring-Opening Polymerization of Lactones

Author: Alexander Kronast, Marina Reiter, Peter T. Altenbuchner, et al

Publication: Organometallics

Publisher: American Chemical Society

Date: Mar 1, 2016

Copyright © 2016, American Chemical Society

Logged in as:
Alexander Kronast
Account #:
3001072711

[LOGOUT](#)

PERMISSION/LICENSE IS GRANTED FOR YOUR ORDER AT NO CHARGE

This type of permission/license, instead of the standard Terms & Conditions, is sent to you because no fee is being charged for your order. Please note the following:




- Permission is granted for your request in both print and electronic formats, and translations.
- If figures and/or tables were requested, they may be adapted or used in part.
- Please print this page for your records and send a copy of it to your publisher/graduate school.
- Appropriate credit for the requested material should be given as follows: "Reprinted (adapted) with permission from (COMPLETE REFERENCE CITATION). Copyright (YEAR) American Chemical Society." Insert appropriate information in place of the capitalized words.
- One-time permission is granted only for the use specified in your request. No additional uses are granted (such as derivative works or other editions). For any other uses, please submit a new request.


[BACK](#)

[CLOSE WINDOW](#)

Copyright © 2016 [Copyright Clearance Center, Inc.](#) All Rights Reserved. [Privacy statement.](#) [Terms and Conditions.](#)
Comments? We would like to hear from you. E-mail us at customercare@copyright.com

6.3.2 2-Methoxyethylamino-bis(phenolate) yttrium catalysts for the synthesis of highly isotactic poly(2-vinylpyridine) by rare-earth metal-mediated group transfer polymerization

  [Home](#) [Account Info](#) [Help](#) 

 **ACS Publications** Most Trusted. Most Cited. Most Read. **Title:** 2-Methoxyethylamino-bis(phenolate)yttrium Catalysts for the Synthesis of Highly Isotactic Poly(2-vinylpyridine) by Rare-Earth Metal-Mediated Group Transfer Polymerization

Author: Alexander Kronast, Dominik Reiter, Peter T. Altenbuchner, et al

Publication: Macromolecules
Publisher: American Chemical Society
Date: Sep 1, 2016

Logged in as: Alexander Kronast
Account #: 3001072711

[LOGOUT](#)

Copyright © 2016, American Chemical Society

PERMISSION/LICENSE IS GRANTED FOR YOUR ORDER AT NO CHARGE

This type of permission/license, instead of the standard Terms & Conditions, is sent to you because no fee is being charged for your order. Please note the following:

- Permission is granted for your request in both print and electronic formats, and translations.
- If figures and/or tables were requested, they may be adapted or used in part.
- Please print this page for your records and send a copy of it to your publisher/graduate school.
- Appropriate credit for the requested material should be given as follows: "Reprinted (adapted) with permission from (COMPLETE REFERENCE CITATION). Copyright (YEAR) American Chemical Society." Insert appropriate information in place of the capitalized words.
- One-time permission is granted only for the use specified in your request. No additional uses are granted (such as derivative works or other editions). For any other uses, please submit a new request.

[BACK](#)[CLOSE WINDOW](#)

Copyright © 2016 [Copyright Clearance Center, Inc.](#) All Rights Reserved. [Privacy statement](#). [Terms and Conditions](#).
Comments? We would like to hear from you. E-mail us at customercare@copyright.com

6.3.3 Gated Channels and Selectivity Tuning of CO₂ over N₂ Sorption by Post-Synthetic Modification of a UiO-66-type MOF

JOHN WILEY AND SONS LICENSE TERMS AND CONDITIONS

Nov 04, 2016

This Agreement between Alexander Kronast ("You") and John Wiley and Sons ("John Wiley and Sons") consists of your license details and the terms and conditions provided by John Wiley and Sons and Copyright Clearance Center.

License Number	3981941200555
License date	Nov 04, 2016
Licensed Content Publisher	John Wiley and Sons
Licensed Content Publication	Chemistry - A European Journal
Licensed Content Title	Gated Channels and Selectivity Tuning of CO ₂ over N ₂ Sorption by Post-Synthetic Modification of a UiO-66-Type Metal–Organic Framework
Licensed Content Author	Alexander Kronast, Sebastian Eckstein, Peter T. Altenbuchner, Konrad Hindelang, Sergei I. Vagin, Bernhard Rieger
Licensed Content Date	Aug 2, 2016
Licensed Content Pages	8
Type of use	Dissertation/Thesis
Requestor type	Author of this Wiley article
Format	Print and electronic
Portion	Full article
Will you be translating?	No
Title of your thesis / dissertation	Novel Single-Site Catalysts for the Polymerization of Polar Monomers – From Aliphatic Poly(esters) to Poly(vinylpyridine)
Expected completion date	Jan 2017
Expected size (number of pages)	120
Requestor Location	Alexander Kronast Schellingstraße 78 Munich, Bavaria 80799 Germany Attn: Alexander Kronast
Publisher Tax ID	EU826007151
Billing Type	Invoice
Billing Address	Alexander Kronast Schellingstraße 78 Munich, Germany 80799 Attn: Alexander Kronast
Total	0.00 USD

7. Literature

- [1] *The European Chemical Industry - Facts & Figures 2016*, Cefic **2016**.
- [2] O. Schulz, T. Rings, R. Forest, J. von Hoyningen-Huene, *Chemical Industry Vision 2030: A European Perspective*, AT Kearney **2012**.
- [3] T. Gellrich, *Shale Gas - Reshaping the US Chemical Industry*, PWC **2012**.
- [4] J. Friese, S. Gerlein, A. Gocke, F. Plaschke, H. Schönberg, Y.-P. Willers, *The 2012 Chemical Industry Value Creators Report*, The Boston Consulting Group **2013**.
- [5] A. Kreimeyer, P. Eckes, C. Fischer, H. Lauke, P. Schuhmacher, *Angew. Chem. Int. Ed.* **2015**, *54*, 3178-3195.
- [6] M. Morawietz, J. Gotpagar, V. Sarathy, V. Ratta, **2015**.
- [7] *The New Plastic Economy*, Ellen Macarthur Foundation **2016**.
- [8] K. O. Siegenthaler, A. Künkel, G. Skupin, M. Yamamoto, in *Synthetic Biodegradable Polymers* (Eds.: B. Rieger, A. Künkel, G. W. Coates, R. Reichardt, E. Dinjus, T. A. Zevaco), Springer Berlin Heidelberg, Berlin, Heidelberg, **2012**, pp. 91-136.
- [9] K. Ziegler, E. Holzkamp, H. Breil, H. Martin, *Angew. Chem.* **1955**, *67*, 541-547.
- [10] G. Natta, *Angew. Chem.* **1956**, *68*, 393-403.
- [11] M. Ringel, A. Taylor, H. Zablit, *Innovation in 2015*, The Boston Consulting Group **2015**.
- [12] C. Zhang, in *Biodegradable Polyesters*, Wiley-VCH Verlag GmbH & Co. KGaA, **2015**, pp. 1-24.
- [13] P. A. Holmes, *Physics in Technology* **1985**, *16*, 32.
- [14] M. Okada, *Prog. Polym. Sci.* **2002**, *27*, 87-133.
- [15] W. Amass, A. Amass, B. Tighe, *Polym. Int.* **1998**, *47*, 89-144.
- [16] O. Dechy-Cabaret, B. Martin-Vaca, D. Bourissou, *Chem. Rev.* **2004**, *104*, 6147-6176.
- [17] N. Berezina, S. M. Martelli, in *Renewable Resources for Biorefineries*, The Royal Society of Chemistry, **2014**, pp. 1-28.
- [18] J. Ahmed, S. K. Varshney, *International Journal of Food Properties* **2011**, *14*, 37-58.
- [19] B. H. A. Rehm, in *Biodegradable Polyesters*, Wiley-VCH Verlag GmbH & Co. KGaA, **2015**, pp. 47-72.
- [20] M. L. Di Lorenzo, R. Androsch, in *Biodegradable Polyesters*, Wiley-VCH Verlag GmbH & Co. KGaA, **2015**, pp. 109-130.
- [21] J. Odent, J.-M. Raquez, P. Dubois, in *Biodegradable Polyesters*, Wiley-VCH Verlag GmbH & Co. KGaA, **2015**, pp. 235-274.
- [22] R. Das, K. M. Karumbaiah, in *Biodegradable Polyesters*, Wiley-VCH Verlag GmbH & Co. KGaA, **2015**, pp. 321-340.
- [23] R. W. Lenz, R. H. Marchessault, *Biomacromolecules* **2005**, *6*, 1-8.
- [24] R. Reichardt, B. Rieger, in *Synthetic Biodegradable Polymers*, Vol. 245, 1 ed., Springer-Verlag Berlin Heidelberg, **2011**, pp. 49-90.
- [25] N. Tanahashi, Y. Doi, *Macromolecules* **1991**, *24*, 5732-5733.
- [26] S. Kusaka, T. Iwata, Y. Doi†*, *Journal of Macromolecular Science, Part A* **1998**, *35*, 319-335.
- [27] S. Philip, T. Keshavarz, I. Roy, *Journal of Chemical Technology & Biotechnology* **2007**, *82*, 233-247.

-
- [28] Y. Kumagai, Y. Doi, *Die Makromolekulare Chemie, Rapid Communications* **1992**, *13*, 179-183.
- [29] H. Abe, I. Matsubara, Y. Doi, Y. Hori, A. Yamaguchi, *Macromolecules* **1994**, *27*, 6018-6025.
- [30] A. García, D. Segura, G. Espín, E. Galindo, T. Castillo, C. Peña, *Biochem. Eng. J.* **2014**, *82*, 117-123.
- [31] E. Grothe, M. Moo-Young, Y. Chisti, *Enzyme Microb. Technol.* **1999**, *25*, 132-141.
- [32] P. T. Altenbuchner, A. Kronast, S. Kissling, S. I. Vagin, E. Herdtweck, A. Pöthig, P. Deglmann, R. Loos, B. Rieger, *Chem. Eur. J.* **2015**, *21*, 13609-13617.
- [33] L. R. Rieth, D. R. Moore, E. B. Lobkovsky, G. W. Coates, *J. Am. Chem. Soc.* **2002**, *124*, 15239-15248.
- [34] E. T. H. Vink, K. R. Rábago, D. A. Glassner, P. R. Gruber, *Polym. Degrad. Stab.* **2003**, *80*, 403-419.
- [35] P. Gruber, M. O'Brien, in *Biopolymers Online*, Wiley-VCH Verlag GmbH & Co. KGaA, **2005**.
- [36] P. Degée, P. Dubois, R. Jérôme, S. Jacobsen, H.-G. Fritz, *Macromolecular Symposia* **1999**, *144*, 289-302.
- [37] F. Chabot, M. Vert, S. Chapelle, P. Granger, *Polymer* **1983**, *24*, 53-59.
- [38] G. Schwach, J. Coudane, R. Engel, M. Vert, *Polym. Int.* **1998**, *46*, 177-182.
- [39] H. R. Kricheldorf, D.-O. Damrau, *Macromol. Chem. Phys.* **1997**, *198*, 1753-1766.
- [40] M. J. L. Tschan, E. Brulé, P. Haquette, C. M. Thomas, *Polym. Chem.* **2012**, *3*, 836-851.
- [41] M. S. Islam Mozumder, L. Garcia-Gonzalez, H. D. Wever, E. I. P. Volcke, *Biochem. Eng. J.* **2015**, *98*, 107-116.
- [42] G. Swift, *Acc. Chem. Res.* **1993**, *26*, 105-110.
- [43] D. Jendrossek, R. Handrick, *Annual Review of Microbiology* **2002**, *56*, 403-432.
- [44] D. Jendrossek, in *Biopolymers Online*, Wiley-VCH Verlag GmbH & Co. KGaA, **2005**.
- [45] B. M. Bachmann, D. Seebach, *Macromolecules* **1999**, *32*, 1777-1784.
- [46] T. Tsuge, Y. Kikkawa, Y. Doi, *Science and Technology of Advanced Materials* **2004**, *5*, 449-453.
- [47] A. Rodriguez-Contreras, M. Koller, M. Miranda-de Sousa Dias, M. Calafell-Monfort, G. Braunegg, M. S. Marques-Calvo, *Journal of applied microbiology* **2013**, *114*, 1378-1387.
- [48] N. Ajellal, M. Bouyahyi, A. Amgoune, C. M. Thomas, A. Bondon, I. Pillin, Y. Grohens, J.-F. Carpentier, *Macromolecules* **2009**, *42*, 987-993.
- [49] Y. Wang, W. Zhao, D. Liu, S. Li, X. Liu, D. Cui, X. Chen, *Organometallics* **2012**, *31*, 4182-4190.
- [50] C. M. Thomas, *Chem. Soc. Rev.* **2010**, *39*, 165-173.
- [51] M. J. Stanford, A. P. Dove, *Chem. Soc. Rev.* **2010**, *39*, 486-494.
- [52] B. M. Chamberlain, M. Cheng, D. R. Moore, T. M. Ovitt, E. B. Lobkovsky, G. W. Coates, *J. Am. Chem. Soc.* **2001**, *123*, 3229-3238.
- [53] K. Fukushima, Y. Kimura, *Polym. Int.* **2006**, *55*, 626-642.
- [54] A. Amgoune, C. M. Thomas, T. Roisnel, J. F. Carpentier, *Chem. Eur. J.* **2005**, *12*, 169-179.
- [55] A. Amgoune, C. M. Thomas, S. Ilinca, T. Roisnel, J.-F. Carpentier, *Angew. Chem. Int. Ed.* **2006**, *45*, 2782-2784.
-

-
- [56] N. Spassky, M. Wisniewski, C. Pluta, A. Le Borgne, *Macromol. Chem. Phys.* **1996**, *197*, 2627-2637.
- [57] E. D. Cross, L. E. N. Allan, A. Decken, M. P. Shaver, *J. Polym. Sci., Part A: Polym. Chem.* **2013**, *51*, 1137-1146.
- [58] C. Agatemor, A. E. Arnold, E. D. Cross, A. Decken, M. P. Shaver, *J. Organomet. Chem.* **2013**, *745-746*, 335-340.
- [59] P. T. Altenbuchner, B. S. Soller, S. Kissling, T. Bachmann, A. Kronast, S. I. Vagin, B. Rieger, *Macromolecules* **2014**, *47*, 7742-7749.
- [60] O. W. Webster, W. R. Hertler, D. Y. Sogah, W. B. Farnham, T. V. RajanBabu, *J. Am. Chem. Soc.* **1983**, *105*, 5706-5708.
- [61] D. Y. Sogah, W. R. Hertler, O. W. Webster, G. M. Cohen, *Macromolecules* **1987**, *20*, 1473-1488.
- [62] O. W. Webster, in *New Synthetic Methods*, Springer Berlin Heidelberg, Berlin, Heidelberg, **2004**, pp. 1-34.
- [63] R. P. Quirk, J. Ren, *Macromolecules* **1992**, *25*, 6612-6620.
- [64] A. D. Jenkins, *Eur. Polym. J.* **1991**, *27*, 649.
- [65] A. H. E. Müller, G. Litvinenko, D. Yan, *Macromolecules* **1996**, *29*, 2346-2353.
- [66] A. H. E. Müller, G. Litvinenko, D. Yan, *Macromolecules* **1996**, *29*, 2339-2345.
- [67] P. M. Mai, A. H. E. Müller, *Die Makromolekulare Chemie, Rapid Communications* **1987**, *8*, 99-107.
- [68] P. M. Mai, A. H. E. Müller, *Die Makromolekulare Chemie, Rapid Communications* **1987**, *8*, 247-253.
- [69] A. H. E. Mueller, *Macromolecules* **1994**, *27*, 1685-1690.
- [70] S. Collins, D. G. Ward, *J. Am. Chem. Soc.* **1992**, *114*, 5460-5462.
- [71] H. Yasuda, H. Yamamoto, K. Yokota, S. Miyake, A. Nakamura, *J. Am. Chem. Soc.* **1992**, *114*, 4908-4910.
- [72] H. Yasuda, H. Yamamoto, M. Yamashita, K. Yokota, A. Nakamura, S. Miyake, Y. Kai, N. Kanehisa, *Macromolecules* **1993**, *26*, 7134-7143.
- [73] E. Y. X. Chen, *Chem. Rev.* **2009**, *109*, 5157-5214.
- [74] B. S. Soller, S. Salzinger, C. Jandl, A. Pöthig, B. Rieger, *Organometallics* **2015**, *150129130938007*.
- [75] H. Yasuda, H. Tamai, *Prog. Polym. Sci.* **1993**, *18*, 1097-1139.
- [76] E. Kirillov, C. W. Lehmann, A. Razavi, J.-F. Carpentier, *Organometallics* **2004**, *23*, 2768-2777.
- [77] M. H. Lee, J.-W. Hwang, Y. Kim, J. Kim, Y. Han, Y. Do, *Organometallics* **1999**, *18*, 5124-5129.
- [78] C. Qian, W. Nie, J. Sun, *Organometallics* **2000**, *19*, 4134-4140.
- [79] H. Yasuda, E. Ihara, *Macromol. Chem. Phys.* **1995**, *196*, 2417-2441.
- [80] K. Tanaka, M. Furo, E. Ihara, H. Yasuda, *J. Polym. Sci., Part A: Polym. Chem.* **2001**, *39*, 1382-1390.
- [81] E. Ihara, M. Morimoto, H. Yasuda, *Proceedings of the Japan Academy, Series B* **1995**, *71*, 126-131.
- [82] E. Ihara, M. Morimoto, H. Yasuda, *Macromolecules* **1995**, *28*, 7886-7892.
- [83] B. S. Soller, S. Salzinger, B. Rieger, *Chem. Rev.* **2016**, *116*, 1993-2022.
- [84] U. B. Seemann, J. E. Dengler, B. Rieger, *Angew. Chem. Int. Ed. Engl.* **2010**, *49*, 3489-3491.
- [85] S. Salzinger, B. S. Soller, A. Plikhta, U. B. Seemann, E. Herdtweck, B. Rieger, *J. Am. Chem. Soc.* **2013**, *135*, 13030-13040.
-

-
- [86] N. Zhang, S. Salzinger, B. Rieger, *Macromolecules* **2012**, *45*, 9751-9758.
- [87] N. Zhang, S. Salzinger, B. S. Soller, B. Rieger, *J. Am. Chem. Soc.* **2013**, *135*, 8810-8813.
- [88] L. Zhang, Z. Zhang, P. Wang, *NPG Asia Materials* **2012**, *4*, e8.
- [89] C.-X. Cai, L. Toupet, C. W. Lehmann, J.-F. Carpentier, *J. Organomet. Chem.* **2003**, *683*, 131-136.
- [90] H. Kaneko, H. Nagae, H. Tsurugi, K. Mashima, *J. Am. Chem. Soc.* **2011**, *133*, 19626-19629.
- [91] T. K. Panda, H. Kaneko, K. Pal, H. Tsurugi, K. Mashima, *Organometallics* **2010**, *29*, 2610-2615.
- [92] P. T. Altenbuchner, P. D. L. Werz, P. Schöppner, F. Adams, A. Kronast, C. Schwarzenböck, A. Pöthig, C. Jandl, M. Haslbeck, B. Rieger, *Chem. Eur. J.* **2016**, *22*, 14576-14584.
- [93] F. Adams, P. T. Altenbuchner, P. D. L. Werz, B. Rieger, *RSC Advances* **2016**, *6*, 78750-78754.
- [94] P. T. Altenbuchner, F. Adams, A. Kronast, E. Herdtweck, A. Pöthig, B. Rieger, *Polym. Chem.* **2015**.
- [95] J. M. Longo, M. J. Sanford, G. W. Coates, *Chem. Rev.* **2016**, *116*, 15167-15197.
- [96] A. M. DiCiccio, J. M. Longo, G. G. Rodríguez-Calero, G. W. Coates, *J. Am. Chem. Soc.* **2016**, *138*, 7107-7113.
- [97] K. Sumida, D. L. Rogow, J. A. Mason, T. M. McDonald, E. D. Bloch, Z. R. Herm, T. H. Bae, J. R. Long, *Chem. Rev.* **2012**, *112*, 724-781.
- [98] M. Cokoja, C. Bruckmeier, B. Rieger, W. A. Herrmann, F. E. Kühn, *Angew. Chem. Int. Ed.* **2011**, *50*, 8510-8537.
- [99] P. T. Altenbuchner, S. Kissling, B. Rieger, in *Transformation and Utilization of Carbon Dioxide* (Eds.: M. B. Bhanage, M. Arai), Springer Berlin Heidelberg, Berlin, Heidelberg, **2014**, pp. 163-200.
- [100] M. Hammann, D. Castillo, C. Anger, B. Rieger, *Journal of Materials Chemistry A* **2014**, *2*, 16389-16396.
- [101] K. Hindelang, A. Kronast, S. I. Vagin, B. Rieger, *Chem. Eur. J.* **2013**, *19*, 8244-8252.
- [102] K. Hindelang, S. I. Vagin, C. Anger, B. Rieger, *Chem. Commun.* **2012**, *48*, 2888.